691 Y

INDC - 17/G

PAPERS PRESENTED AT TOPICAL SESSION ON GAMMA RAYS FROM NUCLEAR REACTIONS

Held during the 7th International Nuclear Data Committee Meeting

at Lucas Heights, Sydney, Australia, on October 9, 1974

Edited by M. J. Kenny

Australian Atomic Energy Commission Research Establishment

Several of these papers have been, or will be submitted to international journals. Until such time as they are published the data presented here should not be quoted without prior permission of the authors.

PAPERS PRESENTED AT TOPICAL SESSION ON

GAMMA RAYS FROM NUCLEAR REACTIONS

Held during the 7th International Nuclear Data Committee Meeting

at Lucas Heights, Sydney, Australia, on October 9, 1974

Edited by M. J. Kenny

Australian Atomic Energy Commission Research Establishment

PREFACE

The 7th International Nuclear Data Committee meeting was held at Lucas Heights, Sydney, Australia, in October 1974. During the meeting, a topical session was held entitled, "Gamma Rays from Nuclear Reactions". Papers were presented by a number of INDC delegates and by participants from the Australian Atomic Energy Commission, the Australian National University and the University of Melbourne.

This report contains the text of the papers as submitted by the authors without further editing. The paper presented by Professor G. B. Yankov (USSR) was delivered in Russian and translated into English by an interpreter. Since the full text is not available in English, only the abstract is presented here. The papers submitted by Dr. B. Rose (UKAEA) and Professor B. Spicer (University of Melbourne) were not orally presented and only the abstracts are included in this publication.

Several of the papers have been submitted, or will be submitted, to international journals. Until such time as they are published, data presented here should not be quoted without prior permission from the authors.

In the Table of Contents, the name of the person who presented each paper is given. At the commencement of each paper, the names of all authors and their affiliation are given.

CONTENTS

SECOND INTERNATIONAL SYMPOSIUM ON NEUTRON CAPTURE GAMMA RAY SPEGTROSCOPY - PETTEN, SEPTEMBER 2-6, 1974

J. R. BIRD

This symposium concentrated on a specific topic and provided quite a thorough review of progress since the first symposium in 1969. Some of the material presented was already well known, but a number of new developments and trends were also evident - from the papers and from private discussions.

There was considerable emphasis on reaction mechanisms with only one third, or less, of the time being spent on nuclear spectroscopy and structure. This meant that there was also more emphasis on epithermal rather than thermal capture. This presumably arose, in part at least, from the fact that there was to be an International Conference on Nuclear Structure in Amsterdam the following week.

Some of the more significant (and recent) work reported was as follows.

Direct Capture

This is variously defined, but the picture given by Lane is that:

(i) At energies close to thermal we observe on-resonance and between-resonance capture. The latter may be considered as the sum of contributions of local resonances and background capture which is the contribution of all distant levels (including hard-sphere interactions).

(ii) When resonances overlap we have a strongly fluctuating cross section (Ericsson fluctuations).

(iii) At high energies the fluctuations become small and direct or hard-sphere capture dominates.

Attempts to observe background capture from the interference shape of isolated levels is recognised to be rendered extremely difficult by level-level interference. The only case discussed was the 91 keV resonance in ^{53}Cr (γ,n) (98 keV resonance in (n,γ)). This is quite broad and very asymmetric (Jackson) and although a second broad bump may be superimposed on the low energy tail a value of $\sigma_{non\text{-}res} = 200$ μb is derived. This asymmetry has also

been observed in σ_c measurements at Karlsruhe (Beer et al.) and the high resolution ORELA data should be studied to throw more light on this reaction. Jackson's results for ^{61}Ni (γ,n) give $\sigma_{non-res} \leq 13$ b and this was claimed as confirmation of theoretical predictions that $\sigma_{non-res}$ should drop dramatically from below to above the peak of the 3s strength function maximum.

The mass dependence of $\sigma_{non-res}$ was discussed theoretically by both Lane and Mahaux. The latter, using an optical model approach, calculated a number of shapes varying in maximum to minimum ratio, but all calculations produce a drop when going from A = 50 to A = 60. Chrien appealed for similar calculations in the region of the 4s strength function maximum.

Work at Brookhaven, described by Chrien, has involved a careful study of partial cross sections from below 1 eV to about 20 eV. in a number of nuclei in the region A = 150-170. The between resonance cross section is fitted by multilevel calculations with all known resonances including any just above or below the interval measured. In about three cases an additional $\sigma_{non-res}$ is needed to fit the observations. Random signs of the phases of the resonances are needed. Chrien is confident that when this work is completed there will be definite evidence for $\sigma_{non-res}$.

A new approach to the search for direct capture has been taken in the analysis of thermal capture spectra of RCN. Results for (^{37}Cl+n) are found to give a much improved correlation with (d,p) results when (I_γ/E_γ) is used rather than (I_γ/E_γ^3) or (I_γ/E_γ^5). Mughabghab reviewed thermal results for many nuclei and concluded that 12 nuclei from ^{27}Al to ^{46}Ca give the best correlation using E_γ^{11}. These, he concludes, have $\sigma_{thermal}$ dominated by direct capture. From ^{48}Ti to ^{57}Fe an exponent of 2 to 3 gives the best correlation and this is attributed to the dominance of valence capture. For Ni and Zn an exponent of 4 to 5 is needed and this is attributed to the dominance of the tail of the giant resonance. This is a neat picture, but in fact an exponent of 0 to 3 give the same correlation coefficients in the Ti to Fe region so that definite conclusions are barely warranted. Further comparison of thermal and resonance spectra should help to clarify this situation.

In reviewing high neutron energy capture, Bergqvist pointed out that direct capture seems to provide only a relatively small part of the cross section (~10%) up to E_n = 14 MeV which is the region of the giant dipole resonance.

Lane reviewed the development of evidence and ideas since the 1950's on simple interactions and described them as "the most exciting anomaly on the nuclear physics scene for some time: that resonance states which can have 1000 or more components show such simple behaviour".

The importance of single particle transitions comes from correlations between $\Gamma_{\gamma f}$ and (2J+1)S (i.e. partial radiative widths and stripping spectroscopic factors), from correlations between $\Gamma_{\gamma i}$ and Γ_n; and from comparison of observed and calculated values of $\Gamma_{\gamma i}$. As mentioned above, a characteristic exponent of E_γ may also apply.

Mughabghab reviewed the now considerable body of evidence for occurrence of these effects in the mass regions A = 24-60 and A = 90-142 and even higher. In doing so, he provided a considerable amount of new evidence from comparison of calculated valence model strengths with experimental results (for example in ^{24}Mg, ^{36}Ar and ^{54}Fe). Three other papers to the conference reported new evidence for correlations in Nb and Mo. Jackson also reported (γ,n) results in Cr and Ni giving $\Gamma_{\gamma i}$-Γ_n correlations of ~0.7. Thus the importance of single particle effects and the range of non-statistical nuclei is well-established, the valence model often underestimates the transition rates and overestimates the correlation coefficients. It is thus generally not the only process contributing to resonant capture in these nuclei.

Valence capture is going through a honeymoon period in which many signs of its importance are appearing. The next step must be to take full account of effects such as the errors in (d,p), Γ_n and $\Gamma_{\gamma i}$ results, and to fully map the energy and mass regions in which it occurs.

The success of the valence neutron model implies that the giant dipole resonance does not steal all the single particle strength for s,p and possible d-states as is assumed in normal photonuclear treatments of the giant resonance. This problem was discussed by Lane in a review of ideas which are being applied to establish a compromise.

It is clearly important to investigate d-wave effects further to find out whether they are single particle or giant dipole in character.

Semi-direct Capture

Bergqvist and co-workers continue with NaI measurements of spectra from fast neutron capture and comparisons with calculations from theories of semi-direct capture. The fits are qualitatively satisfactory at the high energy end of the spectra. The cross sections do not confirm the presence of destructive interference below the giant dipole resonance (as mentioned in the previous paragraph).

Bergqvist also stressed the importance of new data on 14 MeV capture cross sections which agree with results obtained by integrating spectra. All previous activation-type measurements are now suspected to have been in error because of the effects of secondary neutrons.

Lucas Heights experiments provide data in the region linking valence capture effects at low energies to semi-direct effects at high energies and are thus an important addition to other neutron capture work. A new group using the Karlsruhe 3 MeV accelerator reported their first measurements of spectra in the keV energy range (on nickel).

M1 Giant Resonance

Electron scattering at 180° preferentially observes magnetic transitions and recent experiments at NRL and IKO report the systematic appearance of a giant M1 resonance in many nuclei. The centroid occurs at $63/A^{\frac{1}{3}}$ MeV and the width is approximately one-fifth of the centroid energy. For example, in ^{197}Au, the resonance is centred on approximately 8 MeV with a width of several MeV.

The electron scattering experiments are subject to uncertainties in the shape of the radiative tail of the elastic peak and it is to be hoped that neutron capture results can be obtained to confirm the observed M1 properties.

E2 Giant Resonance

Electron scattering also provides evidence for an E2 giant resonance below the E1 giant resonance. Angular distributions for gamma rays from 14 MeV neutron capture in ^{12}C show an anisotropy suggesting the presence of E2 transitions, but ^{10}B, ^{29}Si and ^{40}Ca do not show this effect.

Nuclear Spectroscopy

The study of nuclear levels is now assisted by the use of polarised thermal beams and targets; the use of filtered beams at ½ keV (boron), 2 keV (scandium), 24 keV (iron), and the very intense and pure beams provided by guide tubes at the Grenoble reactor. Thus level energies can be obtained to ±100 eV or better (±10 eV with the best bent crystal spectrometer) and spin determinations can be made with the polarisation facilities. Very little interest seems to exist at the moment in angular correlation work. Work with (n,γ) sources for resonance fluorscence show that Γ_γ values are similar for bound levels and neutron resonances.

Heavy Nuclei

An experiment at Munich reported two gamma rays at 700 and 718 keV associated with but preceding delayed fission by 1 to 2 μs. Their intensity is rather high and further work is needed to confirm whether these are from (n, γf) reactions.

Applications

A number of papers were presented on materials analysis using neutron capture, the most active program of this kind being at Karlsruhe, where plans are in hand for using a californium source and a Ge(Li) detector for studying manganese nodules on the floor of the Pacific Ocean.

General Situation

It is quite apparent that a lot of current work in neutron capture spectra is being fitted in between other work which is often programmatic in nature. This is particularly true at electron linacs and is even more obvious because of the reduction in number of these which are active. In contrast, there is a lot of interest in measuring gamma ray strength functions using inelastic scattering of electrons, ^{3}He, ^{4}He, etc. (using the wide range of intermediate energy facilities currently in operation). Work with reactor beams has a new lease of life using the new techniques and facilities listed earlier.

The Petten symposium was a well organised and cohesive event and it was agreed that a third such symposium would be organised - if possible at Brookhaven in October 197 or possibly at Grenoble.

NON-STATISTICAL EFFECTS IN GAMMA RAYS FROM keV NEUTRON CAPTURE

M. J. KENNY, B. J. ALLEN, J. W. BOLDEMAN, A. R. de L. MUSGROVE

Australian Atomic Energy Commission

Neutron capture gamma ray spectra for many nuclei do not follow statistical model predictions, but exhibit a broad bump for gamma ray energies around 5 MeV ($126 < A < 142$, $181 < A < 206$). This bump has been found to be due to primary E1 radiation. Other non-statistical effects, e.g. partial width correlations at (n,γ) resonances between neutron and gamma widths have been observed in these mass regions and also for $40 < A < 70$ and $90 < A < 112$. These are all regions close to closed neutron shells where the initial and final states in the (n,γ) process occur in the vicinity of single particle states.

Through collaborative experiments with ORNL we have access to neutron capture cross section data obtained on the ORELA facility. By combining the capture gamma ray spectra obtained at Lucas Heights with the ORELA data, we are in a position to obtain a better understanding of the capture process. Of particular interest at the present time are valence effects, doorway states and correlations. The nuclei for which we have the strongest information on non-statistical effects are Ca, Fe and Zr, with some information on silicon and barium. Our neutron energy range extends to 1 MeV.

We have used a NaI detector to study gross features of the gamma ray spectrum following capture of neutrons with energies 50, 150, 250, 460 and 1000 keV. In all thirty elements have been studied spanning the mass range 40 to 240. In many cases a qualitative estimate can immediately be made of the presence of non-statistical decay. A computer program containing the known response functions of the detector at various energies has been

used to unfold the spectra so that the intensities of gamma rays in bin widths of 0.25 MeV have been obtained. Figure 1 shows 9 typical spectra at energies of 250 and 450 keV where there are examples of both statistical and non-statistical decay. In some cases spectra which have at first sight appeared to be statistical have been shown, after unfolding, to have a non-statistical component. The major survey has been supplemented by more detailed measurements with a high resolution Ge(Li) detector.

In silicon the capture cross section data shows a broad asymmetric resonance at a neutron energy of 55 keV and a very sharp narrow resonance at 67.7 keV. The asymmetric resonance is the only such case that has been observed in the series of ORELA measurements on over 40 nuclei and is indicative of a direct capture component. Figure 3 shows the asymmetry. Detailed spectra measurements at Lucas Heights have shown that the 55 keV resonance is followed only by transitions to negative parity states at several MeV excitation and is assigned s-wave The 67.7 keV resonance is followed by strong transitions to low lying positive parity states and is presumed p-wave with $J_c^{\pi} = {}^3/_2^-$. A further asymmetric resonance is observed at 180 keV and inverse (γ,n) experiments point to a doorway state at E_n = 800 keV. Further analysis of existing spectra and exgension to higher neutron energies is currently under way. However it is already apparent that strong valence effects occur in ^{28}Si.

For capture by ^{41}Ca a correlation coefficient of 0.74 is observed between Γ_n^o and Γ_γ for 10 s-wave resonances. The average value $\langle\Gamma_\gamma\rangle_s$ is 3.7 eV which is about three times the value expected in this mass region. Strong single particle effects do occur, but are not sufficient to account for all of this increase. The spectra show transitions to the $^7/_2^-$ ground state of ^{41}Ca for neutron energies above 50 keV. This is interpreted as being due to d-wave resonances. At energies above 200 keV,

the ground state transition would account for ~10 per cent of the observed strength. Analysis of the cross section data confirms the increasing prominence of d-wave resonances above 150 keV and the d-wave cross section is comparable with s-wave and in excess of p-wave.

The most detailed spectra measurements have been made for iron, where NaI data extends to 1 MeV and Ge(Li) data to 0.5 MeV. Figure 2 shows the unfolded spectra at various energies and it is seen that they are similar in shape up to 460 keV. At 1000 keV the high energy component broadens considerably without any real reduction in strength. The neutron energy spread is about 50 keV in each case and since the s-wave level spacing is ~25 keV in ^{56}Fe, only 2 to 3 resonances would contribute to each spectrum and substantial fluctuations in capture spectra might be expected. The data are therefore conspicuous by their overall similarity over a wide energy range. The increasing p- (and d-) wave cross sections relative to the s-wave component make no apparent change to the spectra.

Figure 4 shows the high energy end (E_γ > 3 MeV) of the spectra obtained with a Ge(Li) detector for energies up to 460 keV. The energies of the primary γ-rays shift with increasing neutron energy. Transitions are observed to all low lying states up to 706 keV ($^1/_2^-$ $^3/_2^-$, $^5/_2^-$) and to other higher states. While the ground state doublet is always prominent, transitions to other states become more significant at higher energies.

Estimates of the intensity ratios of γ-ray transitions to the four lowest energy states, relative to the summed intensities for E_γ > 3 MeV are shown in the table (Figure 5). The behaviour is consistently similar from thermal to 1 MeV. It is possible that unresolved gamma rays may produce normalisation errors, the maximum possible effect of which would be to reduce the relative values of the high energy component by about one fifth.

At 460 keV, the NaI spectrum has been analysed for both statistical and valence model components. When normalised to the observed intensity at 3 MeV, insufficient strength was predicted at high γ-ray energies. Then the valence model as applied by Mughabghab was used to calculate expected partial radiative widths to strong single particle final states. Calculations were also made for the 27.7 keV s-wave resonance whose parameters are well known. The observed high energy strengths at both 27 and 460 keV are about twice the calculated value for the valence model. This discrepancy is too large to be accounted for by normalisation errors. To obtain a higher valence component would require lowering Γ_n which in this case is unlikely. It appears then that the valence model does not on its own account for the observed high energy strength. This is in line with the observations of Bhat et al. who calculated ground state valence components for s-wave resonances up to 220 keV and found them to fall well below the ground state widths ($\Gamma_{\gamma o}$) measured in the inverse $^{57}Fe(\gamma,n)$ reaction.

For capture by ^{90}Zr, detailed analysis of the capture cross section data has shown strong correlations between Γ_n and Γ_γ over an energy range of 200 keV. The correlation coefficient for 37 assigned $p^3/_2$ resonances is (0.59 ± 0.12). The sample size of 37 produces a high statistical probability of valence effects being present. Theoretical studies of the theory of valence capture in conjunction with R. F. Barrett have eliminated a number of major problems such as the consistency of channel radius for the normalisation of the single particle wave functions and the form of the Wigner limit. The theory has managed to reproduce the observed capture gamma ray spectrum for a neutron energy averaged over 10 to 70 keV with surprising accuracy. An interesting feature of zirconium is a strong

uncorrelated ground state transition which is approximately equal to the averaged valence component.

A brief mention can also be made for capture by ^{138}Ba where a correlation of 0.49 is observed between Γ_n and Γ_γ for 9 s-wave resonances. The average $\langle\Gamma_\gamma\rangle$ is 340 meV which once again is larger than expected for the mass region and is not explained purely by single particle effects.

In summary, non-statistical effects have been observed for a number of nuclei close to closed neutron shells. While valence capture calculations give reasonable agreement in the case of zirconium (closed shell N = 50), they do not give an adequate explanation for iron (near closed shell N = 28 + 2). The apparent failure of the statistical and valence capture models to adequately account for the observed strength to the low lying states leads to the consideration of semi-direct theory in which the incoming neutron scatters in the target nucleus creating a 2p-1h state.

The authors acknowledge valuable assistance in the ORELA measurements from R. L. Macklin of ORNL and in the AAEC measurements from R. F. Barrett and K. H. Bray of the Australian National University.

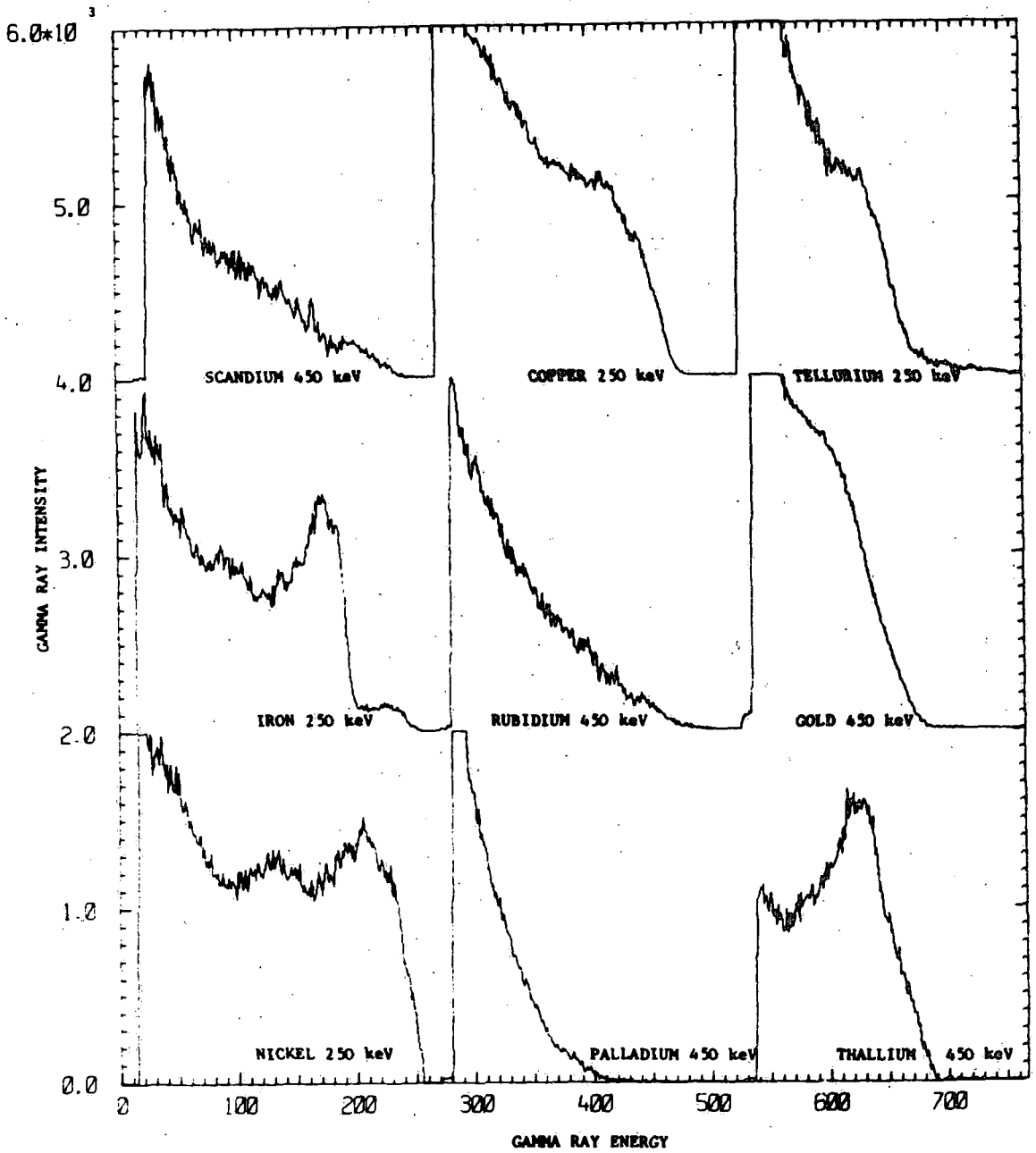

FIGURE 1: Sodium iodide spectra for various elements at 250 and 450 keV neutron energies showing both statistical and non-statistical decay.

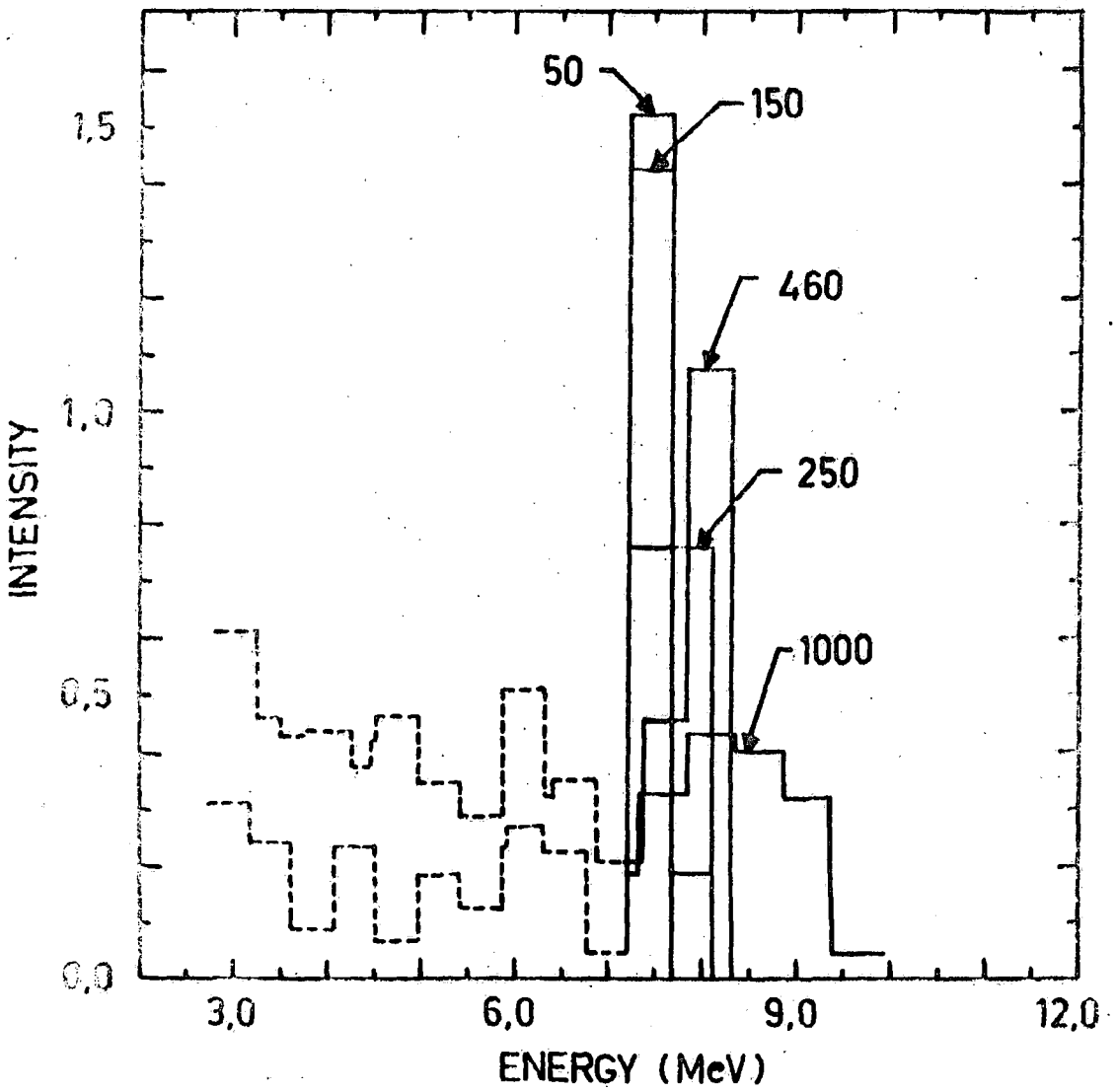

Fig. 2 γ-ray intensity distributions for Fe(n,γ) at E_n = 50, 150, 250, 460 and 1000 keV. The data are normalised to equal area. Dashed lines are the upper and lower bounds of the low γ-ray energy data.

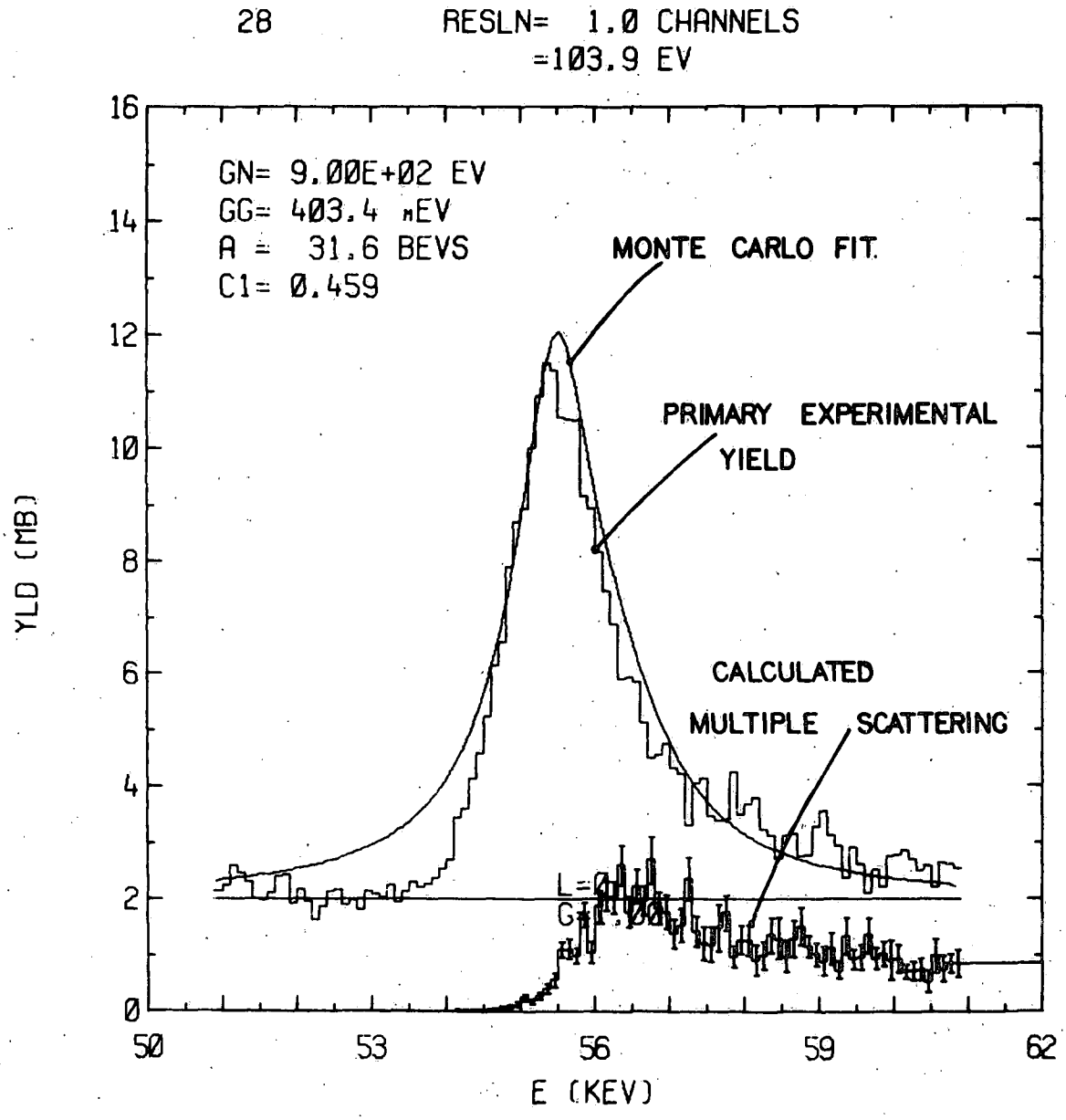

FIGURE 3: Capture cross section data for ^{28}Si showing asymmetry in 55 keV resonance

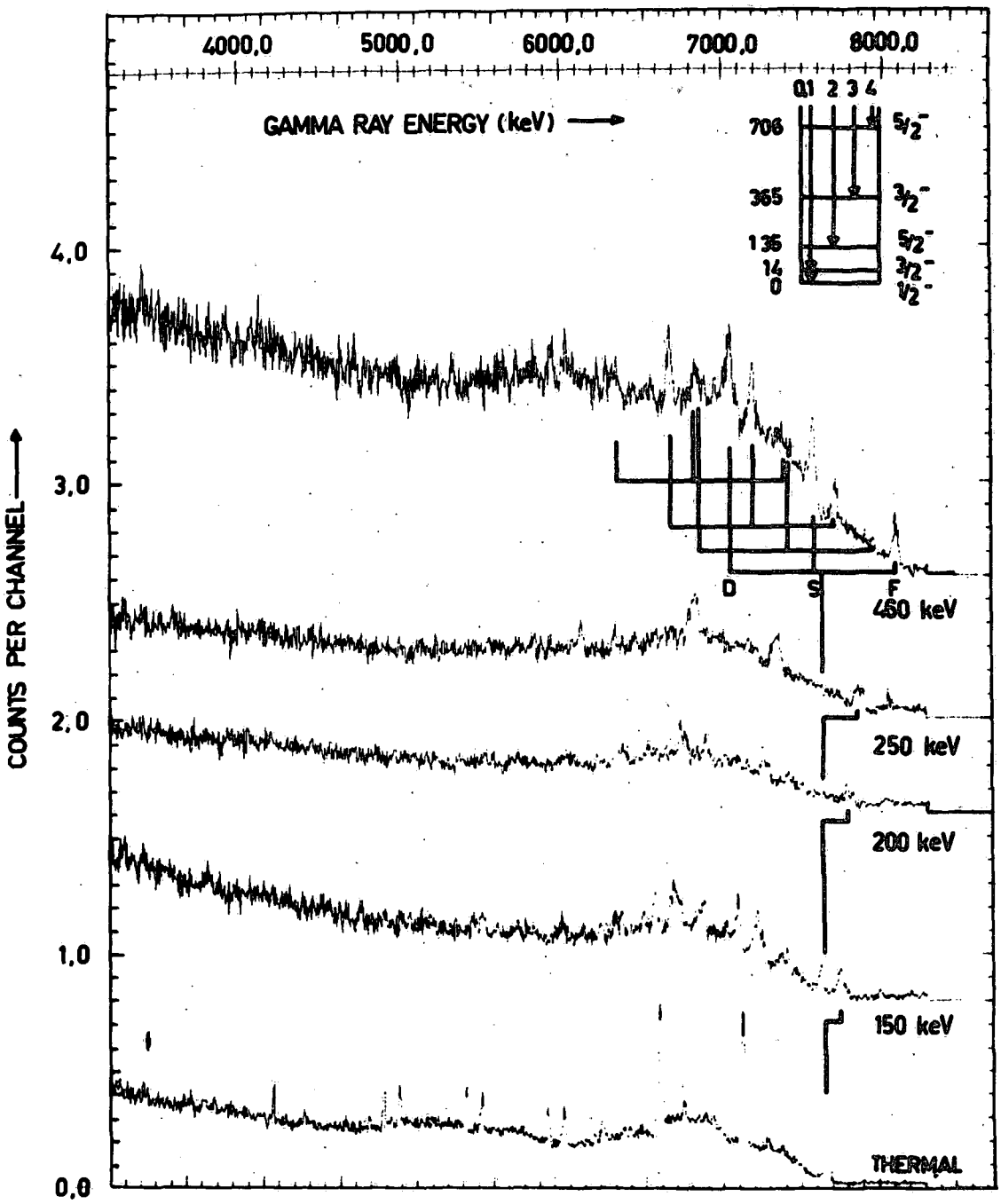

FIGURE 4: Gamma-ray spectra for Fe(n,γ) measured with a Ge(Li) detector. Inset shows low lying states in ^{57}Fe.

Energy keV	ℓ	Det.	$\gamma_n^2 . 10^3$ MeV	Γ_γ eV	I %	I_1 %	Γ_o^v eV	Γ_1^v eV	Γ_3^v eV	I^v %
Thermal		Ge(Li)			63	63				
1.167	1	Ge(Li)		0.6	68	66				
27.7	0	Ge(Li)	3.64	1.45 $\pm$0.15	54	53	0.125	0.08	0.06	23
(5-90)		NaI			42	32				
50		NaI			42					
150		NaI			41	29				
250		NaI			44	44				
460		NaI	2.15	1.0 $\pm$0.5	43	38	0.088	0.056	0.040	23
1000		NaI			39*					

*Includes I_4

FIGURE 5: Observed and calculated relative intensities for transitions to low lying states in ^{57}Fe

GAMMA-RAY PRODUCTION CROSS SECTION OF OXYGEN

C Nordborg, L G Strömberg and H Condé, Research Institute of National Defense, Stockholm
L Nilsson, Tandem Accelerator Laboratory, Uppsala

Abstract:

The gamma-ray production cross section of Oxygen have been measured between 6.5 and 10.5 MeV. The measurement has been made in two parts covering the energy regions from 6.5 to 8.2 MeV and from 7 to 10.5 MeV, respectively. The gamma-rays were detected with a large NaI crystal using time-of-flight techniques. The differential cross sections at 90^{o} were measured together with angular distributions at three different energies. Spins for the involved levels in the compound nucleus are proposed and the shapes of the angular distributions are compared with calculations based on the compound nucleus model. The results are also compared with previous reported measurements.

Introduction

The differential cross sections for gamma-ray production from non-elastic neutron reactions in Oxygen have been measured between 6.5 and 10.5 MeV. The measurement was performed in two parts. The incident neutron energy region from 6.5 to 8.2 MeV was measured at the 5.5 MeV van de Graaff at Studsvik (1) while the higher neutron energy region from 7 to 10.5 MeV has recently been measured at the EN tandem accelerator in Uppsala.

The measurments have been performed with water as the scattering sample using a large NaI crystal for gamma-ray detection at 90^{o} relative to the incident neutrons.

At these neutron energies only a limited number of gamma-rays are produced in $(n,n'\gamma)$ and $(n,\alpha\gamma)$-reactions on ^{16}O, the most prominent one being the 6.13 MeV gamma-ray transition from the 3^{-} level in ^{16}O to the 0^{+} ground state. The excitation function for the 6.13 MeV gamma-ray transition has been studied through-out the whole energy region in steps of about 50-100 keV. The data, which are preliminary for the higher energy part, reveal a prominent structure of the cross-section with energy and are compared with previous reported measurements. In the higher energy region the cross sections for the production of the 6.92 and 7.12 MeV gamma-rays in the $^{16}O(n,n'\gamma)$-reaction and the 3.09, 3.68 and 3.85 MeV gamma-rays in the $^{16}O(n,\alpha\gamma)$-reaction have also been measured.

The angular distributions of the 6.13 MeV gamma-ray transition have been measured at 6.9, 7.8 and 8.9 MeV. The angular distributions at 6.9 and 7.8 MeV have a pronounced structure and are compared with distributions calculated from the compound nucleus model assuming different spin and parities of the levels in the compound nucleus ^{17}O.

Experimental arrangements

A schematic lay-out of the experimental arrangement is shown in figure 1..

Neutrons in the energy range 6.5 - 8.2 MeV were produced at the 5.5 MeV pulsed van de Graaff at Studsvik using the $^{2}H(d,n)^{3}He$ reaction (1). The neutron energy range 7 - 10.5 MeV was studied at the EN tandem accelerator at Uppsala using the $^{2}H(d,n)^{3}He$ and the $^{3}H(p,n)^{3}He$ reactions. The neutron flux was in both cases monitored by a plastic scintillator which was run in a time-of-flight arrangement. The monitor was calibrated against a proton recoil telescope (figure 2).

The scattering sample (figure 1) was a thin-walled cylindrical holder of plexiglass (diameter 4 cm, height 5 cm) filled with water, situated at a distance of about 15 cm from the target.

The gamma-ray spectrometer consisted of a NaI crystal with a diameter of 22.6 cm and a length of 20.8 cm, viewed by seven RCA 8054 photomultipliers. The detector was placed in a heavy shield, which could be rotated around the sample position (figure 1). Time-of-flight techniques were used to improve the signal-to-background ratio.

Data handling

The background was subtracted by means of a computer program and the resulting pulse-height spectrum was grouped into 50 keV intervals. The statistical errors were also calculated. In order to determine the intensities of the gamma-ray lines an unfolding calculation was performed by normalisation of the response functions of the NaI spectrometer to the experimental pulse-height spectrum.

The cross sections were determined by using the area under the normalised response function. The integrated neutron flux on the sample area was calculated using the neutron peak in the time-of-flight spectrum measured with the neutron monitor.

In the energy region below 8.2 MeV the data have been corrected for neutron and gamma-ray attenuations and multiple scattering of neutrons while for the energy region above 8.2 MeV the calculation of the corrections have not yet been completed.

The estimated total error in the cross sections is about ± 15% where the main contribution to the error comes from the uncertainties in the neutron flux measurement (± 10%).

Results

The differential cross sections at 90^{o} for the production of the 6.13, 6.92 and 7.12 MeV gamma-rays from the $^{16}O(n,n'\gamma)^{16}O$ reaction are shown in figure 3 and 4. The data above 8.2 MeV neutron energy are not fully corrected for multiple scattering and are just tentative.

In the same figure the recent data by Dickens and Perey (2) are also shown. Below 8 MeV the two measurements agree while above 8 MeV the data for E_{γ}= 6.13 MeV by Dickens and Perey are systematically higher than the present preliminary data.

The angular distributions of the 6.13 MeV gamma-ray at the incident neutron energies of 6.9 and 7.8 MeV have a pronounced structure (figure 5) and the preliminary data at 8.9 MeV show rough agreement with the distribution at 7.8 MeV.

The angular distributions of the 6.13 MeV gamma-ray have been calculated at 6.9 and 7.8 MeV neutron energy using the compound nucleus formalism by Sheldon and van Patten (1, 3). The best agreement between the experiment and the calculations was obtained by assuming a $7/2^-$ assignment for the level at 10.6 MeV and a 3/2 or 5/2 assignment for the 11.5 MeV level in ^{17}O (figure 6) in accordance with previous spin determinations for these levels (1).

References

1. Lundberg, B., Strömberg, L.G. and Condé, H., Physica Scripta 2, 273 (1970).

2. Dickens, J.K. and Perey, F.G., Nucl. Sci. Eng. 40, 283 (1970).

3. Sheldon, E. and van Patten, D.M., Revs. Mod. Phys. 38, 143 (1966).

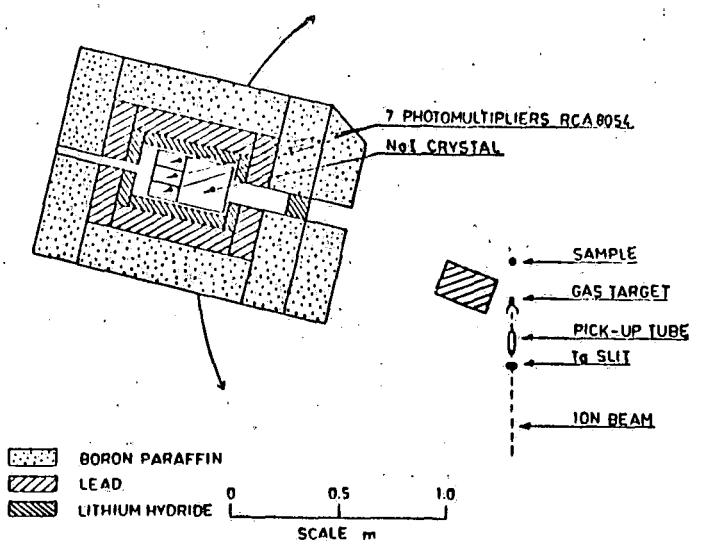

Fig. 1. Lay-out of the target-sample-detector arrangement.

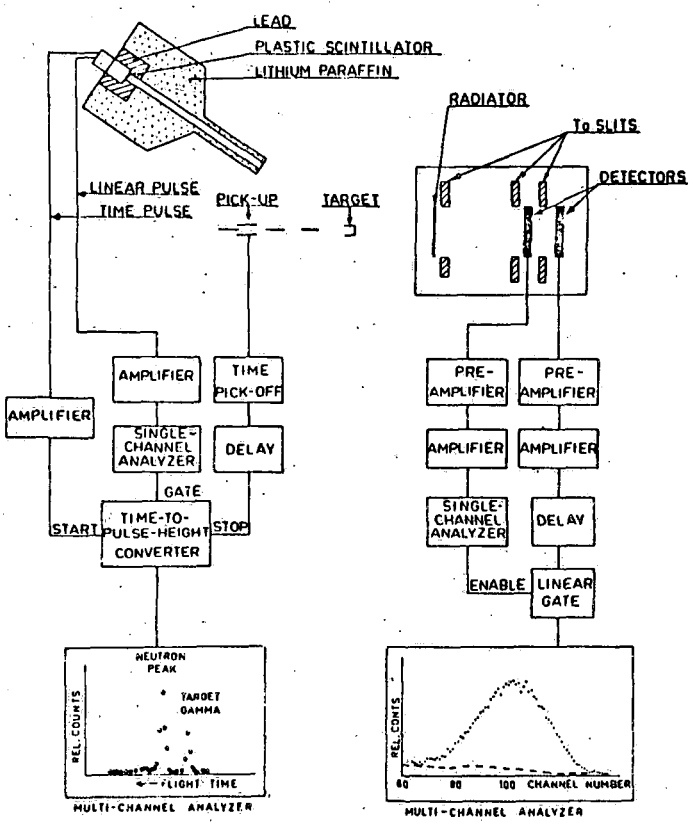

Fig. 2. Schematic diagram of the experimental arrangements and the electronic circuits used in the neutron flux calibration measurement. Time-of-flight spectrum from the neutron monitor and proton spectrum from the proton recoil telescope counter are shown. The dashed curve in the proton spectrum indicates background without radiator.

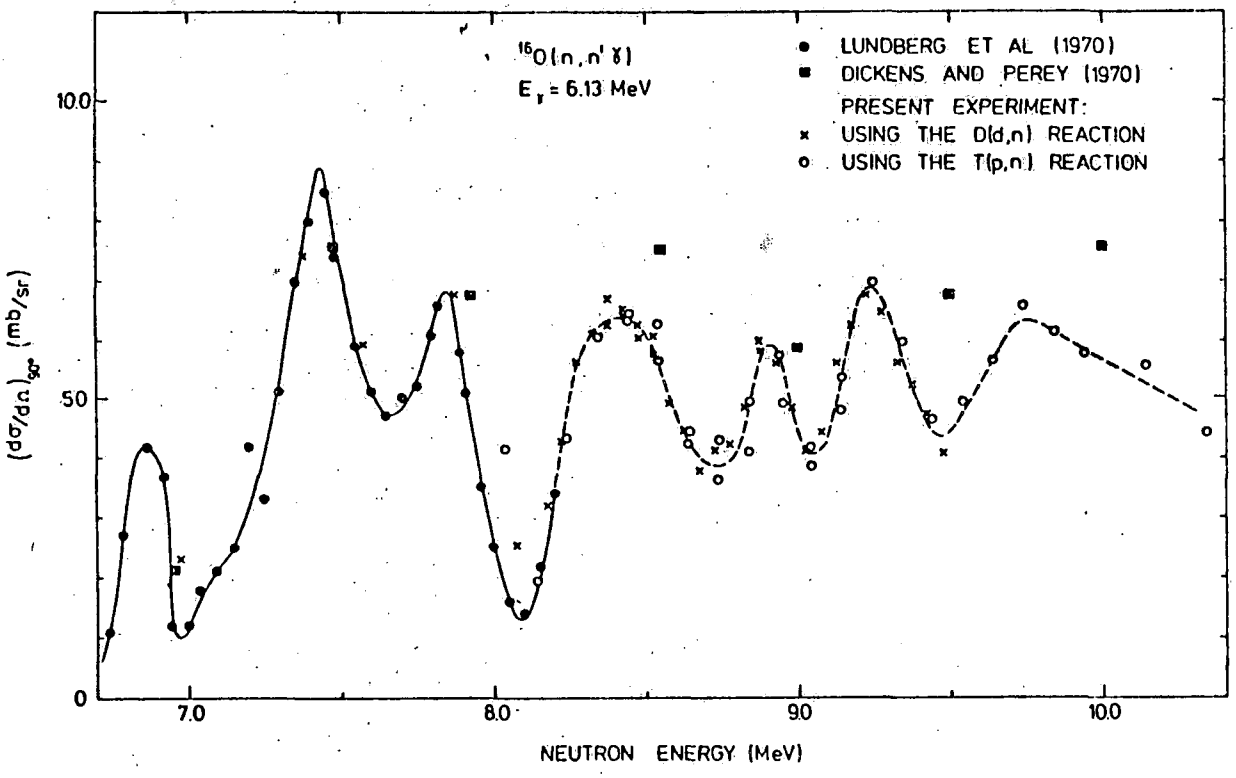

Fig. 3. Cross-section for the production of the 6.13 MeV gamma-rays in the $^{16}O(n,n'\gamma)^{16}O$ reaction. Data above 8 MeV neutron energy are preliminary.

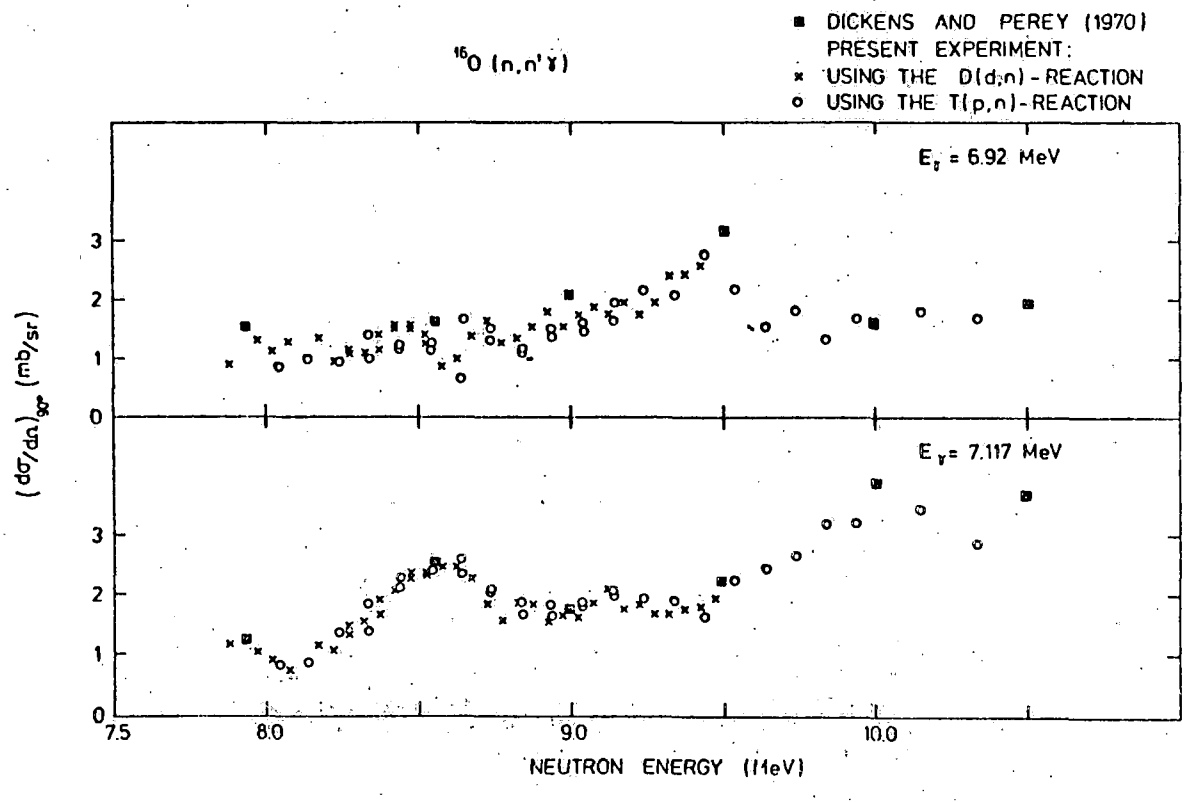

Fig. 4. Cross section for the production of the 6.92 and 7.12 MeV gamma-rays in the $^{16}O(n,n'\gamma)^{16}O$ reaction (Preliminary data)

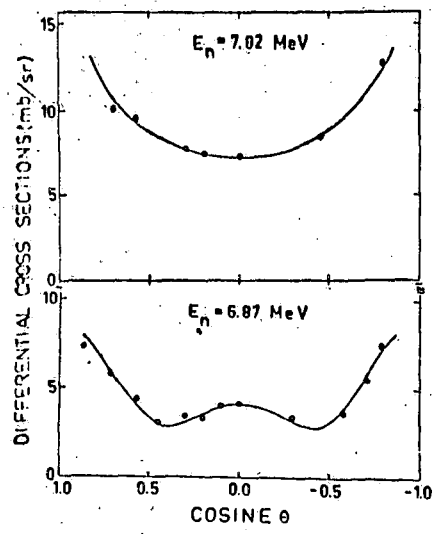

Fig. 5. Differential cross sections for the 6.13 MeV gamma-ray from the $^{16}O(n,n'\gamma)^{16}O$ reaction at a neutron energy of 6.87 MeV and 7.82 MeV.

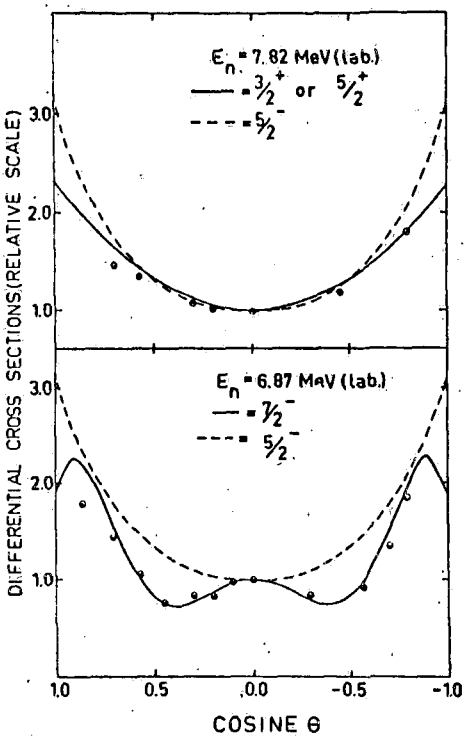

Fig. 6. Relative angular distributions calculated for incident neutron energies of 6.87 and 7.82 MeV and different spin and parity assignment. Measured data points are indicated by solid circles.

GAMMA RAYS FROM FAST NEUTRON CAPTURE IN SILICON AND SULPHUR

L Nilsson and A Lindholm, Tandem Accelerator Laboratory, Uppsala and
I Bergqvist, Department of Physics, University of Lund, Lund.

Submitted to Second int.symp. of neutron capture gamma-ray spectra, Petten, Sept 1974.

ABSTRACT:

Gamma-ray spectra from neutron capture in natural samples of silicon and sulphur have been measured at incident neutron energies between 4.7 and 10.9 MeV as well as at 15 MeV. A large NaI(Tl) scintillator was used as gamma-ray detector and time-of-flight technique was employed to reject undesirable background. The experimental results are compared with theoretical predictions of the semi-direct model.

Introduction

Studies of neutron capture in 2sld-shell nuclei have previously been performed mostly at low energies (below 100 keV) and around 14 MeV. In the low-energy region the compound-nucleus process is expected to be dominant, whereas at 14 MeV semi-direct capture processes[1], involving the excitation of the giant dipole resonance, account for the main features of the observed shapes and intensities of gamma-ray spectra[2]. In the intermediate energy region, one might expect a competition between compound-nucleus processes and reactions of direct and semi-direct type. In fact, estimates of Lane and Lynn[3] indicate compound-nucleus cross sections as high as those expected from direct and semi-direct reactions. This would imply a more complicated situation for light nuclei as compared with heavy nuclei, for which the compound-nucleus cross sections at ~ 10 MeV are expected to be orders of magnitude lower than the direct and semi-direct ones.

The photo-nuclear cross sections for light nuclei show, in general, considerable structure. One would then expect that the neutron-capture excitation functions for high-energy transitions also exhibit structure and that the gamma-ray spectra varies with neutron energy in a way which does not resemble the systematic variation of the spectra from heavy nuclei. Furthermore, the effects of isospin selection rules should be of importance in neutron capture in light nuclei.

This work reports experimental gamma-ray spectra from neutron capture in natural samples of silicon and sulphur at several incident neutron energies between 4.7 and 10.9 MeV as well as at 15 MeV. Shapes of gamma-ray spectra and cross sections for transitions to individual final levels (or group of levels) are compared with predictions based on the semi-direct capture model.

Experimental arrangement

The experiments were performed at the 5.5 MeV van de Graaff accelerator at Studsvik and at the FN tandem accelerator at Uppsala. The accelerators were adjusted to give ion pulses of less than 5 ns duration at frequencies of 1 MHz and 2 MHz, respectively. The $^{2}H(d,n)^{3}He$ reaction was used to produce monoenergetic neutrons in the energy range 4.5 to 8.5 MeV, the $^{3}H(p,n)^{3}He$ reaction in the energy range 8.9 to 10.9 MeV and the $^{3}H(d,n)^{4}He$ reaction for 15 MeV neutrons. In the

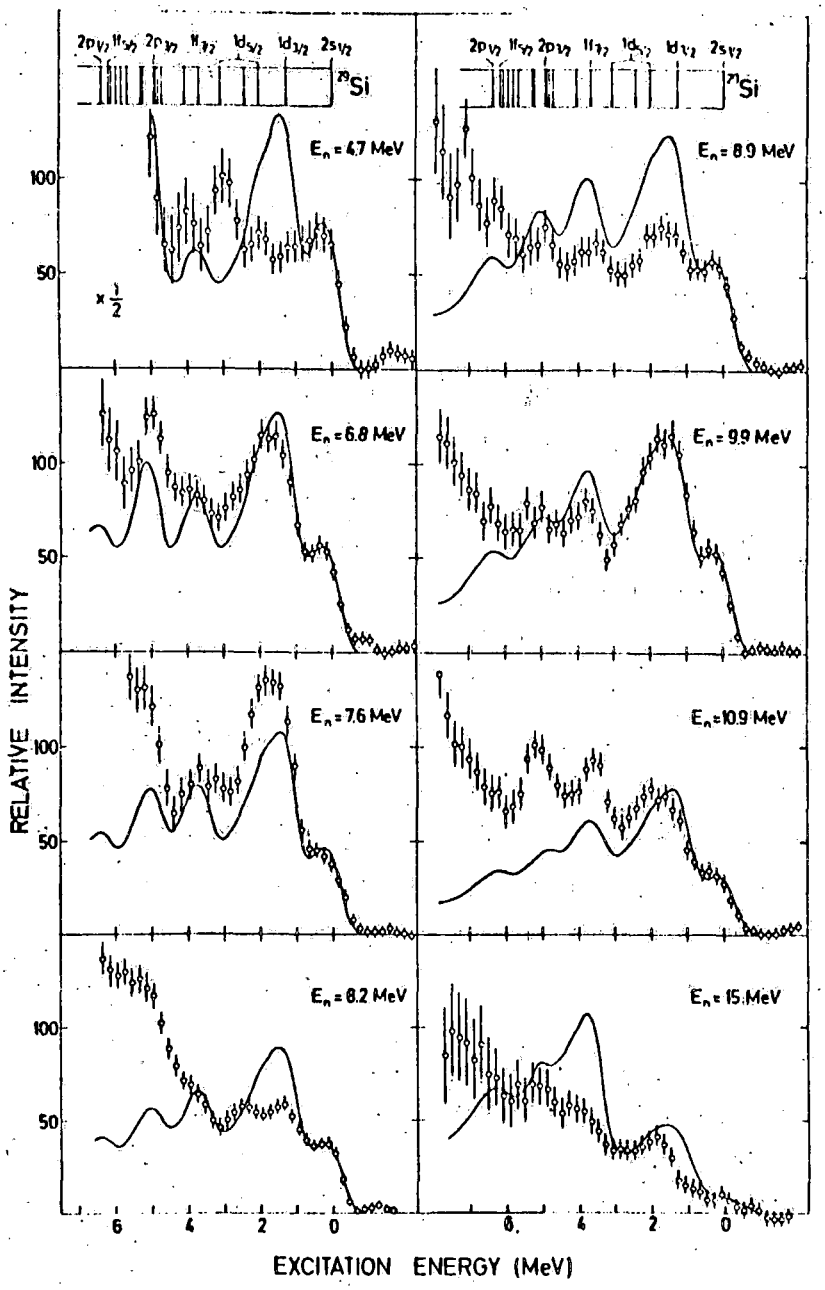

Fig. 1. Gamma-ray spectra from neutron capture in ^{28}Si at various neutron energies normalized to the same neutron flux and plotted versus excitation energy of the final nucleus. The single-particle structure of ^{29}Si is given on top of the figure. The curves represent spectra calculated from the semi-direct capture model with complex particle-vibration coupling[6]. The theoretical spectra are normalized to reproduce the intensity of the transition to the $2s_{1/2}$ ground state.

former two cases gas-target systems were used, in the latter one a tritiated titanium target. The neutron flux monitored using time-of-flight techniques by a plastic scintillation counter placed at 135° to the incident ion beam direction. The monitor counter was calibrated against a polyethylene telescope placed in the forward direction. The gamma-ray detector, a NaI(Tl) crystal, 22,6 cm in diameter and 20.8 cm long, was placed in a heavy shielding consisting of lithium hydride, lead and boron paraffin. Gamma radiation from the sample was

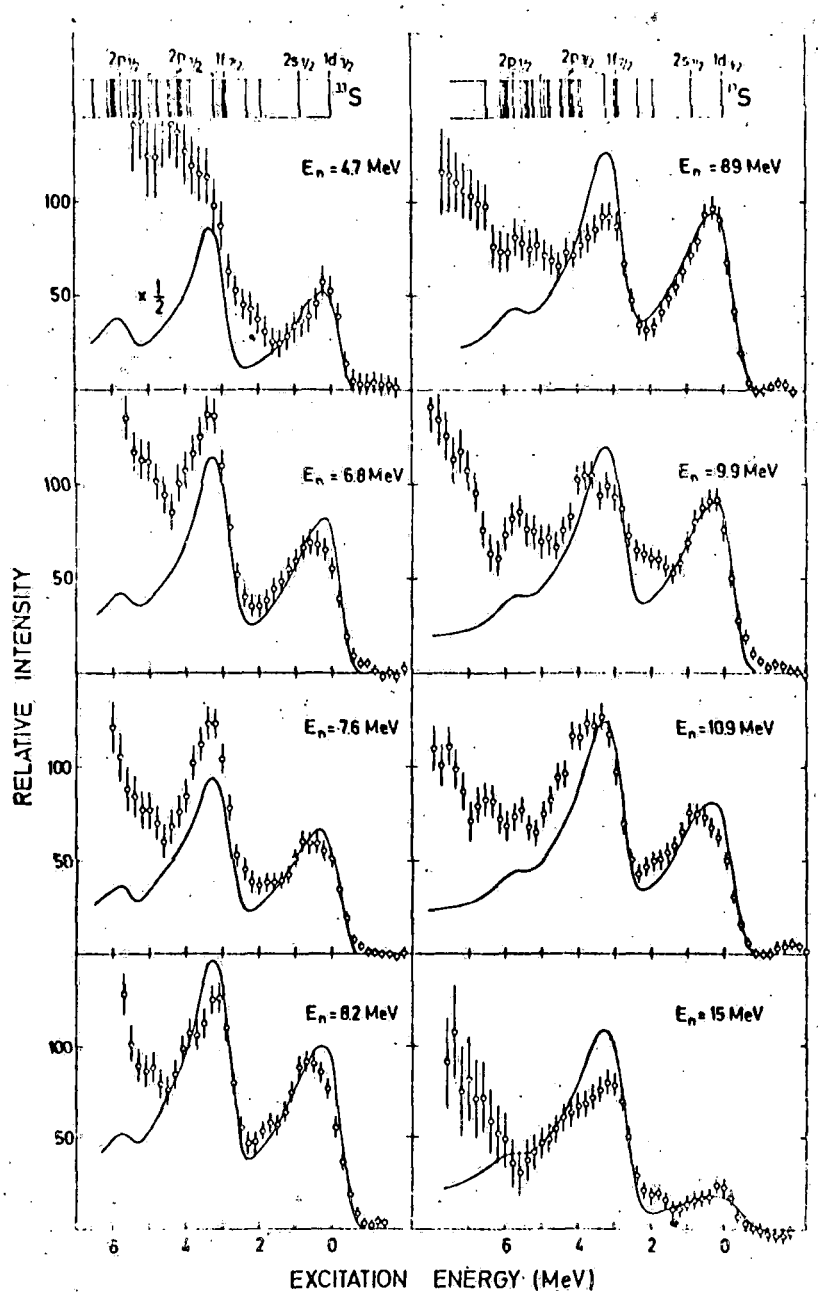

Fig. 2. Gamma-ray spectra from neutron capture in ^{32}S at various neutron energies normalized to the same neutron flux and plotted versus excitation energy of the final nucleus. The single-particle structure of ^{33}S is given on top of the figure. The curves represent spectra calculated from the semi-direct capture model with complex particle-vibration coupling[6]. The theoretical spectra are normalized to reproduce the sum of the intensities to the $1d_{3/2}$ and $2s_{1/2}$ states at 0 and 0.84 MeV.

collimated through a lead collimator, 10 cm in diameter and 1 m long, which was plugged with 40 cm of lithium hydride for neutron attenuation. Time-of-flight technique was used to distinguish gamma radiation from target neutrons and neutrons scattered from the sample.

Calculations

Semi-direct capture cross section for the reactions $^{28}Si(n,\gamma)^{29}Si$ and $^{32}S(n,\gamma)^{33}S$ are calculated according to the scheme described in ref. 4, the only difference being that the parameters of the $T_<$ component of the giant dipole resonance (E_R=19.0 MeV and Γ=5.0 MeV for ^{29}Si; E_R=19.0 Mev and Γ=6.0 MeV for ^{33}S) are used in the cross section formula[5]. The particle-vibration coupling strength parameters are adjusted to roughly reproduce the 15 MeV cross sections of the ground state transitions. This procedure requires for both reactions v_1=100 MeV with real surface coupling[1] and v_1=50 MeV and w_1=45 MeV with complex coupling[6].

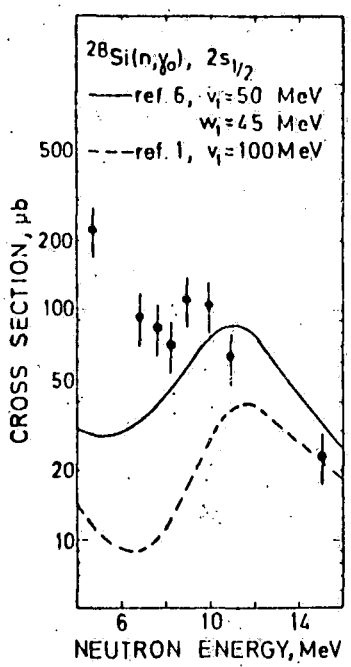

Fig. 3. Cross section of the $^{28}Si(n,\gamma)^{29}Si$ reaction for transitions to the $2s_{1/2}$ ground state in ^{29}Si. The curves represent cross sections calculated from the semi-direct capture model with complex (full curve) and real surface (dashed curve) particle-vibration coupling interaction.

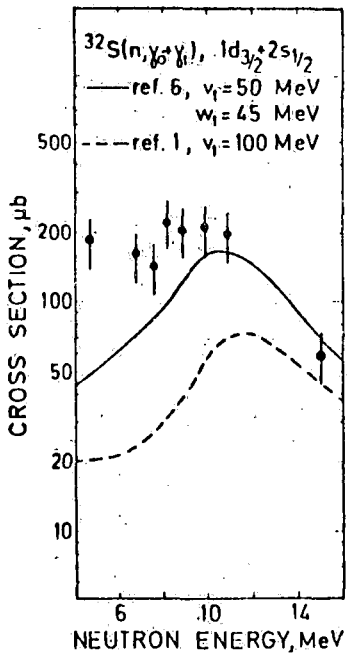

Fig. 4. Cross section of the $^{32}S(n,\gamma)^{33}S$ reaction for transitions to the $1d_{3/2}$ and $2s_{1/2}$ states at 0 and 0.84 MeV in ^{33}S. The curves represent cross sections calculated from the semi-direct capture model with complex (full curve) and real surface (dashed curve) particle-vibration coupling interaction.

Results

The gamma-ray spectra at a number of neutron energies for the reactions $^{28}Si(n,\gamma)^{29}Si$ and $^{32}S(n,\gamma)^{33}S$ are given in figs. 1 and 2, respectively. Also shown in the figure are spectra calculated from the semi-direct model with complex particle-vibration coupling as proposed by Potokar[6]. For the $^{28}Si(n,\gamma)^{29}Si$ reaction the intensity of the transition to the $2s_{1/2}$ ground state varies slowly with neutron energy and passes through a weak maximum around 9 MeV neutron energy. The intensity of the transition to the $1d_{3/2}$ state at 1.28 MeV, on the other hand, fluctuates strongly with neutron energy. The model predicts a strong transitions to the $1d_{3/2}$ state, but cannot account for the observed fluctuations.

The spectra from the $^{32}S(n,\gamma)^{33}S$ reaction are dominated by two groups of transitions; to the $1d_{3/2}$ and $2s_{1/2}$ states at 0 and 0.84 MeV and to the $1f_{7/2}$ and $2p_{3/2}$ states at 2.93 and 3.22 MeV. These four levels contain large single-particle strengths. It can also be observed, that the intensities to the $J^{\pi}=5/2^{+}$ and $3/2^{+}$ levels at 1.97 and 2.31 MeV, with small single-particle strengths, are weak. Thus the shapes of the spectra indicate that the reaction process selects levels in the final nucleus with single-particle character, i.e. that a direct-type mechanism contributes considerably to the reaction process.

The energy dependence of the cross section for the ground state transition of the $^{28}Si(n,\gamma)^{29}Si$ reaction is illustrated in fig. 3. The experimental cross sections are compared with predictions of the semi-direct capture model. A similar comparison for the $^{32}S(n,\gamma)^{33}S$ reaction is shown in fig. 4. It is evident, that the model fails to account for the observed excitation functions and that additional reaction processes are required. It seems plausible that the compound nucleus process contributes appreciably to the cross sections at least at low neutron energies.

References

1. C.F. Clement, A.M. Lane and J.R. Rook, Nucl. Phys. 66 (1965) 273, 293
2. F. Rigaud et al., Nucl. Phys. A154 (1970) 243
   F. Cvelbar et al., Nucl. Phys. A130 (1969) 401; A138 (1969) 412
   H. Dinter, Nucl. Phys. A111 (1968) 360
3. A.M. Lane and J.E. Lynn, Nucl. Phys. 11 (1959) 646
4. A. Lindholm et al., contribution 42 to this conference
5. L. Nilsson and J. Eriksson, Phys. Letters 49B (1974) 165
6. M. Potokar, Phys. Letters 46B (1973) 346

GAMMA RAYS FROM FAST NEUTRON CAPTURE IN ^{89}Y AND ^{140}Ce

A. Lindholm and L. Nilsson, Tandem Accelerator Laboratory, Uppsala, Sweden and I. Bergqvist and B. Pålsson, Department of Physics, University of Lund, Lund, Sweden.

Submitted to Second int.symp. of neutron capture gamma-ray spectra, Petten, Sept 1974.

ABSTRACT:

Gamma-ray spectra from the reactions $^{89}Y(n,\gamma)^{90}Y$ and $^{140}Ce(n,\gamma)^{141}Ce$ have been recorded with a large NaI(Tl) scintillator for incident neutron energies between 6.2 and 10.9 MeV. Time-of-flight technique was used to reject undesirable background. The experimental results are compared with theoretical predictions of the semi-direct capture model.

Introduction

Studies of neutron capture gamma-ray spectra in the giant-resonance region have been performed mainly with 14 MeV neutrons. Excitation functions for individual transitions over the entire giant-resonance have been recorded only for the reactions $^{208}Pb(n,\gamma)^{209}Pb$ [1] and $^{40}Ca(n,\gamma)^{41}Ca$ [2]. The comparison of these data with the semi-direct capture model shows that for the $^{208}Pb(n,\gamma)^{209}Pb$ reaction the model accounts for the shapes of the gamma-ray spectra as well as the neutron energy dependence of the cross sections. For $^{40}Ca(n,\gamma)^{41}Ca$ on the other hand, the model fails to describe the shapes of the spectra at least in the low-energy part of the resonance. Furthermore the observed excitation functions disagree with the semi-direct capture model predictions. This situation motivates further experiments preferably on nuclei at intermediate closed neutron shells.

The present paper reports studies of the reactions $^{89}Y(n,\gamma)^{90}Y$ and $^{140}Ce(n,\gamma)^{141}Ce$ in the neutron energy range 6.2 - 10.9 MeV. Gamma-ray spectra and capture cross sections are compared with predictions based on the semi-direct capture model.

Experimental arrangements

Neutrons in the energy range 6.2 - 8.2 MeV were produced at the 5.5 MeV pulsed van de Graaff at Studsvik using the $^{2}H(d,n)^{3}He$ reaction. The neutron energy range 8.9 - 10.9 MeV was studied at the EN tandem accelerator at Uppsala. Time-of-flight techniques were used to improve the signal-to-background ratio. The samples were cylinders of Y_2O_3 and CeO_2 powder, 8 cm in diameter and 6 cm long. The sample was placed with its axis along the direction of the incident beam. Background gamma-ray spectra were recorded with a water sample containing the same amount of oxygen atoms. The signal-to-background ratios in the high-energy part of the spectra are typically 10:1. Further details of the experimental procedure and data handling are described elsewhere [3].

Calculations

Capture cross sections for individual gamma-ray transitions have been calculated using the semi-direct model derived by Clement, Lane and Rook[4]. The model has been modified to include spin-orbit coupling in the initial and final channels, contribution from direct capture and interference between the direct and collective capture amplitudes. To evaluate the matrix elements between the initial and final states, calculations of the incident and bound-state wave functions are required. The incident wave functions have been computed by means of a version of the

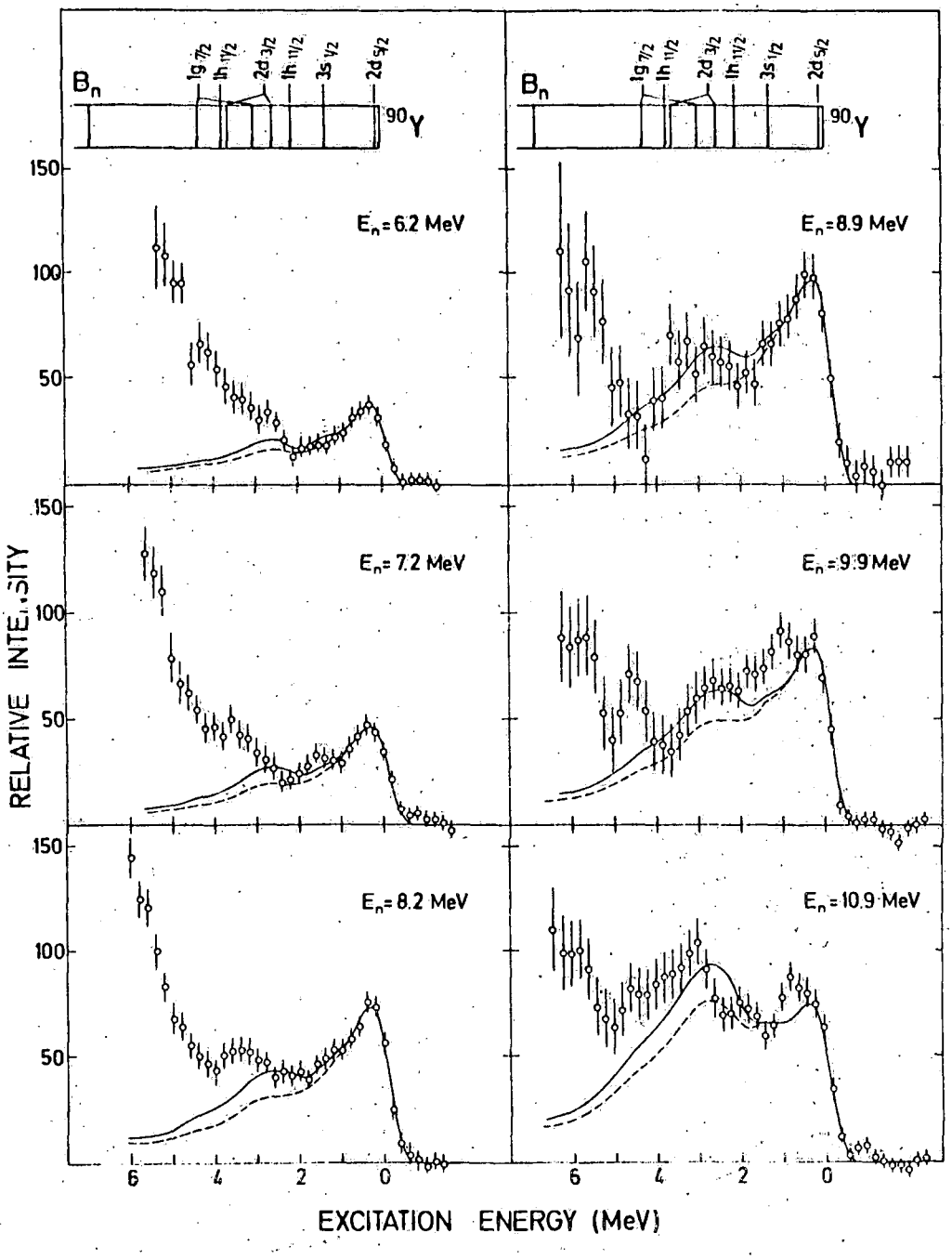

Fig. 1. Gamma-ray spectra from neutron capture in ^{89}Y at various neutron energies normalized to the same neutron flux and plotted versus excitation energy of the final nucleus. The single-particle structure of ^{90}Y is given on top of the figure. The curves represents spectra calculated from the semi-direct capture model with complex (full curve) and real surface (dashed curve) particle-vibration coupling interaction.

ABACUS-2 code[5] with an optical potential of the form derived by Rosen et al[6]. The bound-state wave functions have also been calculated by the ABACUS-2 code using a real Saxon-Wood potential and a spin-orbit potential of Thomas form. The depth of the Saxon-Wood potential was adjusted to give the experimental binding energy of the single-particle states.

The calculations for the reaction $^{89}Y(n,\gamma)^{90}Y$ have been performed as for an even-even ($j^{\pi}=0^{+}$) target nucleus. The single-particle strengths and binding energies were obtained from (d,p) experiments on ^{89}Y[7]. Some information has been derived by comparison with (d,p) studies on ^{90}Zr[8]. Single-particle structure of

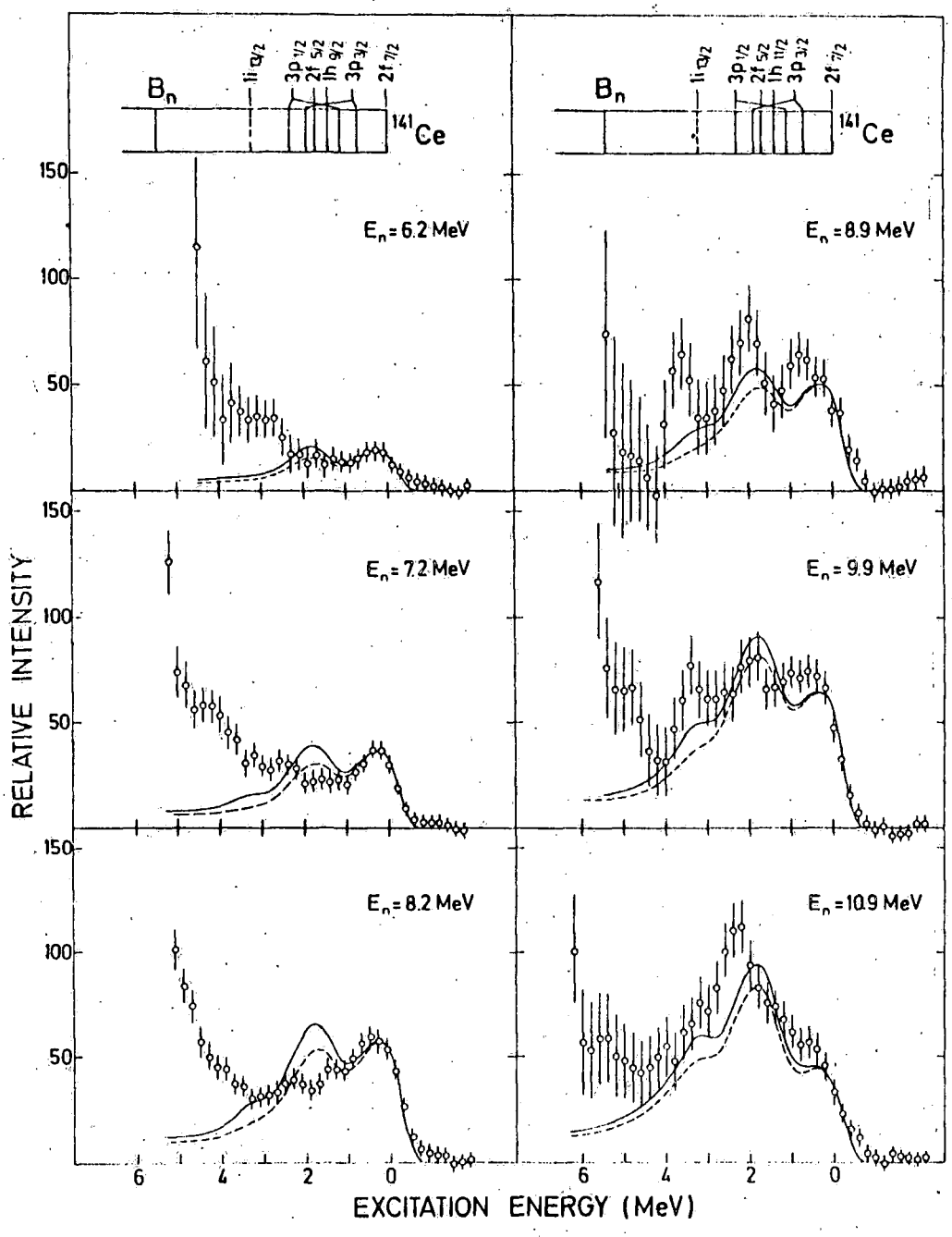

Fig. 2. Gamma-ray spectra from neutron capture in ^{140}Ce at various neutron energies normalized to the same neutron flux and plotted versus excitation energy of the final nucleus. The single-particle structure of ^{141}Ce is given on top of the figure. The curves represents spectra calculated from the semi-direct capture model with complex (full curve) and real surface (dashed curve) particle-vibration

^{141}Ce is similarly given by (d,p) experiments on ^{140}Ce[9] and other nuclei near the closed neutron shell N=82. The energy (E_R) and width (Γ) of the giant dipole resonance, which are parameters in the semi-direct capture formula, have been taken from photonuclear work[10] (for $^{89}Y(n,\gamma)^{90}Y$; E_R = 16.7 MeV and Γ = 4.2 MeV and for $^{140}Ce(n,\gamma)^{141}Ce$; E_R = 15.3 MeV and Γ = 4.7 MeV).

Two different types of coupling between the incident neutron and the vibration of the target nucleus have been applied; the real surface form used by Clement, Lane and Rook[4] and the complex form proposed by Potokar[11]. The coupling strength was used as a parameter adjusted to reproduce the observed cross sections close to the peak of the giant dipole resonance. In the case of real surface coupling strength parameters, v_1, of 270 and 340 MeV were required for $^{89}Y(n,\gamma)$ and $^{140}Ce(n,\gamma)$ respectively. With complex coupling the strength parameters were taken to be v_1= 90 MeV and w_1=140 MeV for both reactions. v_1 and w_1 represents the real and imaginary strenghts of the isospin part of the optical potential.

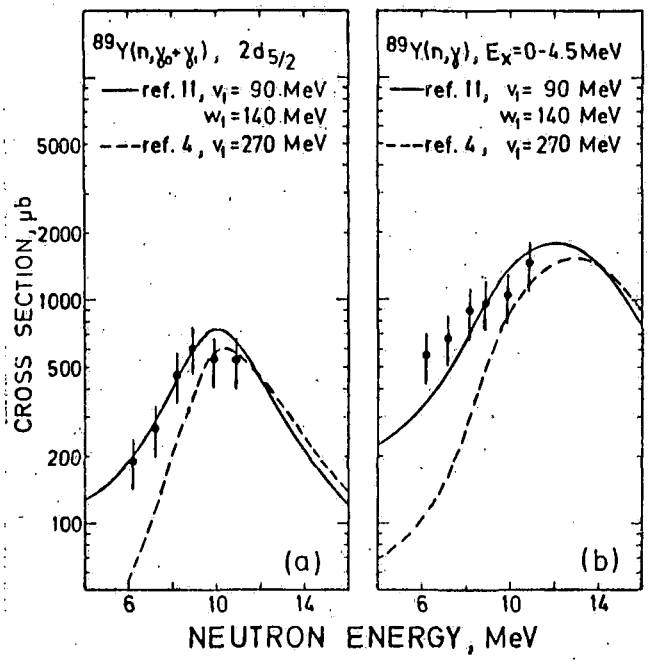

Fig. 3. Cross sections of the $^{89}Y(n,\gamma)^{90}Y$ reaction for transitions to the two $2d_{5/2}$ levels at 0 and 203 keV in ^{90}Y (a) and for transitions to levels below 4.5 MeV in ^{90}Y (b). The curves represent cross sections calculated from the semi-direct capture model with complex (full curve) and real surface (dashed curve) particle-vibration coupling interaction.

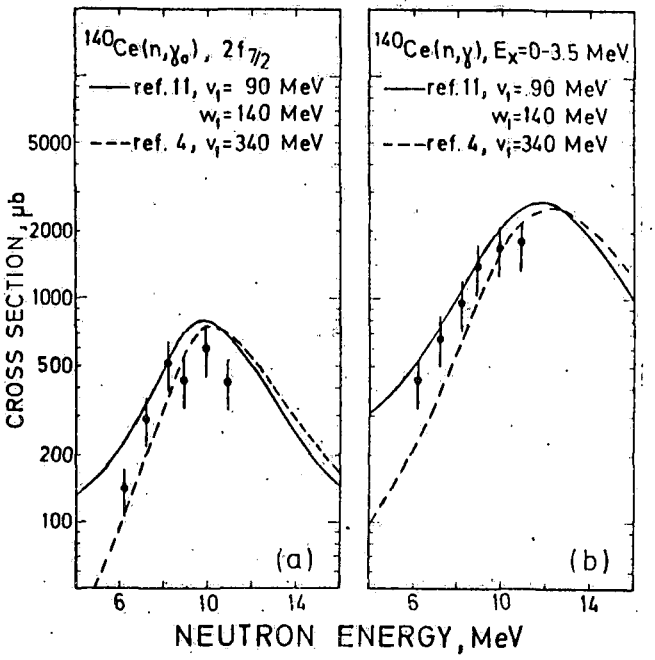

Fig. 4. Cross sections of the $^{140}Ce(n,\gamma)^{141}Ce$ reactions for transitions to the $2f_{7/2}$ ground state of ^{141}Ce (a) and for transitions to levels below 3.5 MeV in ^{141}Ce (b). The curves represent cross sections calculated from the semi-direct capture model with complex (full curve) and real surface (dashed curve) particle-vibration coupling interaction.

Results

Gamma-ray spectra calculated from the semi-direct capture model are shown in figs. 1 and 2 by full curves (complex particle-vibration coupling) and dashed curves (real particle-vibration coupling) together with the experimental data.

The calculated intensity of each individual transition has been multiplied by the response function of the gamma-ray detector and the resulting distributions have been added to give the "theoretical" spectra. The theoretical spectra have been normalized to reproduce the observed intensity of the ground-state transition

It is evident from figs. 1 and 2 that the semi-direct model accounts for the essential features of the gamma-ray spectra. The two types of coupling interaction give roughly the same shape for the gamma-ray spectra over the neutron energy range covered in this work.

The cross sections of the $^{89}Y(n,\gamma)^{90}Y$ reaction for transitions to the two $2d_{5/2}$ levels and for transitions to levels below 4.5 MeV in ^{90}Y are given in fig. 3 together with calculations based on the semi-direct capture model. A similar comparison for the $^{140}Ce(n,\gamma)^{141}Ce$ reaction is shown in fig. 4

The semi-direct model with complex particle-vibration coupling interaction gives a satisfactory description of the energy dependence of the cross sections, whereas the model with real surface particle-vibration coupling interaction fails to account for the observed energy variation of the cross sections.

References

1. I. Bergqvist, D.M. Drake and D.K. McDaniels, Nucl. Phys. A191 (1972) 641
2. I. Bergqvist, D.M. Drake and D.K. McDaniels, to be published in Nucl. Phys.
3. L. Nilsson, A. Lindholm and I. Bergqvist, contribution 61 to this conference
4. C.F. Clement, A.M. Lane and J.R. Rook, Nucl. Phys. 66 (1965) 273, 293
5. E.H. Auerbach, KAPL-M-EHA-1 (1960)
6. L. Rosen et al., Ann. of Phys. 34 (1965) 96
7. R.E. Goans and C.R. Bingham, Phys. Rev. C5 (1972) 914
8. C.R. Bingham and M.L. Halbert, Phys. Rev. C2 (1970) 2297
9. R.H. Fulmer, A.L. McCarthy and B.L. Cohen, Phys. Rev. 128 (1962) 1302
10. B.L. Berman et al., Phys. Rev. 162 (1967) 1098
    A. Lepretre et al., Nucl. Phys. A175 (1971) 609
    R. Bergere et al., Nucl. Phys. A133 (1969) 417
    H. Beil et al., Nucl. Phys. A172 (1971) 437
11. M. Potokar, Phys. Letters 46B (1973) 346

The Level Structure of ^{50}V and the 5.255 MeV Isobaric Analog Resonance in ^{51}V Studied by the $^{50}Ti(p,n)$ and $(p,n\gamma)$ Reactions

Yoshiaki Tomita and Shigeya Tanaka

Nuclear Physics Laboratory

Japan Atomic Energy Research Institute

Tokai-mura, Ibaraki-ken, Japan

Abstract

The $^{50}Ti(p,n)$ and $(p,n\gamma)$ reactions have been studied at proton energies between 3.8 and 5.4 MeV. Excitation functions and angular distributions have been measured for both neutrons and γ-rays. The results have been analyzed by the statistical theories. For most of the levels in ^{50}V below 1.9 MeV spins and parities have been determined. The branching ratios and the mixing ratios for the γ-rays deexciting these levels have also been obtained. The 5.255 MeV analog resonance has been observed in the (p,n) reaction and has been assigned to be 9/2+.

E

NUCLEAR REACTIONS $^{50}Ti(p,n)$, $(p,n\gamma)^{50}V$, E_p=3.8-5.4; measured $\sigma(E_p;E_n,\theta)$, $(E_p;E_\gamma,\theta)$; ^{50}V deduced levels, J, π, branching ratios; ^{51}V analog resonance, J, π; enriched target.

1. Introduction

The structure of low-lying levels of ^{50}V has been studied by various reactions, i.e. $^{51}V(p,d)$[1], $^{50}Ti(p,n\gamma)$[2], $^{49}Ti(^{3}He,d)$[3], $^{51}V(d,t)$[4] and $^{52}Cr(d,\alpha)$[4,5], and has been shown to be qualitatively consistent with the shell model calculation by McCullen, Bayman and Zamick[6]. However, the spin assignments have not been made for most of the levels above 1 MeV, and the existing γ-ray data are only for the lowest five levels studied by means of the $^{50}Ti(p,n\gamma)$ reaction by Blasi et al.[2]

In the present investigation, level and decay scheme below 1.9 MeV has been studied by the $^{50}Ti(p,n)$ and $(p,n\gamma)$ reactions, and spin (parity) assignments have been made for most of the levels investigated by means of the statistical theories for average cross sections. Especially the 4_2^+ level predicted by McCullen et al.[6] was located at 0.910 MeV, the same energy where a 7+ level had been observed by DelVecchio et al.[4] and Bachner et al.[5], and a doublet is proposed for the 0.910 MeV level.

It has been well known[7] that (p,n) reaction cross sections are enhanced at isobaric analog resonances. Analog resonances in ^{51}V have been studied in the $^{50}Ti(p,p)$ and (p,p') reactions by Cosman, Slater and Spencer[8]. The analog resonance at E_p=5.255 MeV has also been observed in the present investigation, and has been assigned to be 9/2+.

2. Experimental procedure and results

2.1. procedure

The experiment was performed using pulsed proton beams of about 2 ns widths produced by the JAERI 5.5 MV Van de Graaff at a repetition rate of 1 MHz. The ^{50}Ti target was prepared by evaporating TiO_2 (enriched to 83.2% in ^{50}Ti) onto a thick tantalum backing, and had a thickness of about 1 keV for a 5 MeV proton beam. Neutron spectra were measured by

the time-of-flight method. Three neutron detectors were used, each of which consisted of a liquid scintilator, 12.5 cm in diameter and 10.2 cm thick, and a photomultiplyer. They were separated from each other by 10° and were placed at 7.9 m from the target. The γ-ray detector was a 30 cm^3 Ge(Li) detector and was placed at 14 cm from the target.

Excitation functions for $^{50}Ti(p,n)^{50}V$ were measured at lab angles of 45°, 55° and 65° in the proton energy ranges 3.8-4.0 MeV and 4.5-5.4 MeV. Angular distributions were also measured at nine angles between 10° and 95° in the energy range 5.15-5.4 MeV. Since the cross section fluctuation was expected to be very large and the target used was very thin, the measurements were made at intervals of 2.5 keV, and counts for four proton energies were accumulated into a single spectrum. Neutrons due to other isotopes of titanium were not seen in the spectra except those from the ground state of ^{48}V.

Gamma ray spectra were taken at 50° in the proton energy range 4.1-5.0 MeV. Angular distributions of γ-rays were measured at 0°, 30°, 50°, 70° and 90° at two proton energy ranges 4.6-4.695 and 4.7-4.795 MeV. The proton energy were varied in steps of 5 keV in each of the ranges. For some cases, only prompt γ-rays were detected within about 20 ns after the arrival of the incident protons in order to reduce background. Gamma ray spectra from a natural titanium target were also taken at several proton energies, and were used to identify γ-rays originating from other titanium isotopes than ^{50}Ti.

2.2. level and γ-ray energies

Typical spectra are shown in fig. 1 for neutrons and in fig. 2 for γ-rays. Since the time-to-height converters were not calibrated precisely, the level energies were determined with uncertainties of about 10 keV from the neutron spectra alone using the Q-value[9] of -2.999 MeV

for the $^{50}Ti(p,n)^{50}V$ reaction. Most of the γ-ray energies were determined with uncertainties of 1 keV. From the results of the thershold measurements shown in fig. 3, the origins of significant γ-rays were easily identified. Then using the known energies of the first five levels, the level energies of most of the levels were determined with uncertainties of 1 keV. These level energies were in turn used to recalibrate the energy scale of the neutron spectra, and the energies of the rest of the levels were determined with uncertainties of 3-5 keV. The results are summarized in table 1 together with the results of previous studies[1-5]. The γ-ray energies and branching ratios determined in the present investigation are listed in table 2, and the decay scheme determined is presented in fig. 10, the details of which are discussed in sect. 5.

2.3. excitation functions and angular distributions

Since the cross section fluctuation was very large, the measured excitation functions were averaged over the proton energy ranges of 100 keV widths. The results for neutron data at 55° are shown in figs. 4 and 5 by rectangles. When the 55° data were not available because of overlapping with the γ-ray peaks etc., the averages of the 45° and 65° data were used. Since both the cross sections at 55° obtained from neutrons and those at 50° from γ-rays were almost same as those averaged over the solid angle as are seen in figs. 6 and 7, excitation functions obtained from the γ-ray data at 50° are also shown in fig. 5 by ellipses. In the figures the horizontal and the vertical sizes of the symbols represent the energy width of averaging and "uncertainties" in the cross sections, respectively. The "uncertainties" shown here are not the experimental uncertainties, which are generally smaller, but the expected deviations of the averaged cross sections from the statistical model

predictions due to the cross section fluctuations. They were estimated from the observed fluctuations of the cross sections about their averages in each energy interval as follows:

$$\Delta\sigma = \frac{v}{\sqrt{N}},$$
$$v^2 = \frac{1}{N}\sum_{n=1}^{N}(\sigma_n - \langle\sigma\rangle)^2, \qquad (1)$$
$$\langle\sigma\rangle = \frac{1}{N}\sum_{n=1}^{N}\sigma_n,$$

where σ_n indicates a cross section at the n-th energy and N is the total number of energies in an energy interval. The absolute values of the cross sections were not determined experimentally since the thickness of the target was not accurately known. The scaling indicated were made assuming a thickness with which the cross sections for the lowest five levels were best reproduced by the statistical model calculation described in sect. 3.

The neutron angular distributions were averaged over the energy range 5.15 - 5.4 MeV. However, for levels which were appreciably influenced by the analog resonance at Ep = 5.255 MeV, the energy range 5.3 - 5.4 MeV was taken. The relative angular distributions thus obtained are shown in fig. 6. The relative γ-ray angular distributions are shown in fig. 7 for the two energy regions investigated.

2.4. isobaric analog resonance

The observed cross sections of some of the levels are plotted in figs. 8 and 9 in the energy range 5.1 - 5.4 MeV. A rather sharp peak is seen at about 5.26 MeV selectively in several levels which have relatively small cross sections. This peak can be identified as due to the isobaric analog resonance observed[8] in ^{50}Ti(p,p')^{50}Ti(2_1^+) at Ep = 5.264 MeV.

3. Analysis

The method of the analysis and the general aspect of the results are described here. The analysis of the analog resonance is presented in sect. 4, and the detailed discussion on the spin-parity assignment for each level is given in sect. 5. The (p,n) reactions in the energy region investigated here are considered to proceed through compound nuclear processes, and the analysis presented here is based on the Hauser-Feshbach theory[10] for neutrons and on Sachler's theory[11] for γ-rays. The modification proposed by Moldauer[12] is not used, because the present reaction includes rather many channels and the effect of this modification is very small. Transmission coefficients were calculated by a computer code TRANCE[13] using the optical-potential parameters by Perey[14] for proton channels and the equivalent local potential parameters by Engelbrecht and Fiedeldy[15] for neutron channels.

3.1. excitation functions

Since the spin-parities of the lowest five levels have been known well[2,4,5], comparison between the experimental and the calculated cross sections were first made for these levels and the absolute values of the measured cross sections were normalized to the calculated values. This normalization is only for the convenience of the comparison between the experimental and the calculated cross sections, and is not very important, since the conclusion of the analysis can be deduced only from the relative values of the various cross sections. The fits for the five levels are shown in fig. 4. The very good fits seen here support the assignment of the spin-parity sequence of 6+, 5+, 4+, 3+ and 2+. The breaks at 5.25 MeV in the calculated cross section lines are the effect of the enhancement due to the analog resonance, which is discussed in sect. 4. The excitation functions of other levels are shown

in fig. 5 for various choices of the spin-parities. Calculated cross section of a level somewhat depends on the choices of the spin-parities of other levels. The effects of this dependence are indicated in the figure by hatched areas. This dependence was especially large for negative parity levels. The spin dependence of the cross section $\sigma(J)$ resulted in the sequence of magnitude of

$$\sigma(1) > \sigma(2) \approx \sigma(0) > \sigma(3) > \sigma(4) > \sigma(5) > \sigma(6), \quad (2)$$

and enabled to unambiguously assign spins greater than or equal to 3.

A characteristic feature in the mass region $A \sim 50$ is that the neutron transmission coefficients for s and d waves are quite larger than those for p and f waves at low energies. In the present case at En = 2.0 MeV, for instance, the values of the transmission coefficients are as follows: $Ts_{\frac{1}{2}} = 0.999$, $Td_{\frac{3}{2}} = 0.606$ and $Td_{\frac{5}{2}} = 0.658$, while $Tp_{\frac{1}{2}} = 0.147$, $Tp_{\frac{3}{2}} = 0.122$, $Tf_{\frac{5}{2}} = 0.009$ and $Tf_{\frac{7}{2}} = 0.029$. Therefore, crudely speaking, the levels with positive (negative) parity are mainly populated through the compound states with positive (negative) parity. This fact causes some differences between the cross sections of levels with different parity. Especially, $\sigma(4-)$ is considerably larger than $\sigma(4+)$ as is seen in fig. 5.

3.2. angular distributions

The measured neutron angular distributions had large uncertainties, and were not very useful in determining the spin-parities except for a few cases. The calculated angular distributions are shown in fig. 6, and are generally consistent with the spin-parity assignment from the excitation functions and the γ-ray angular distributions. Rather different angular distributions are predicted between the opposite parities

for levels with J = 4 or 5.

The γ-ray angular distributions were well determined experimentally and could resolve most of the ambiguities in the spin assignments from the excitation functions, though nothing could be said as to the parities. In calculating the angular distributions, the mixing ratios were so determined as to best fit the experimental angular distributions. The best fits obtained are shown in fig. 7 by different curves for various choices for the spins of the levels. The mixing ratios thus obtained are listed in table 2.

4. Isobaric analog resonance

The enhancement of (p,n) cross sections at analog resonances has been explained by Robson et al[16] as due to the mixing of the analog states with the background T< compound states. According to their theory, the enhanced (p,n) cross sections at an analog resonance are calculated by the enhanced transmission coefficient in the entrance channel, which is expressed as

$$\tilde{T}_{p^*} = T_{p^*} \frac{(E-E_0+\Delta)^2}{(E-E_0)^2+\frac{1}{4}\Gamma^2}, \qquad (3)$$

where p^* denotes the proton channel responsible for the analog resonance, T_{p^*} is the transmission coefficient in the absence of the analog resonance, and E_0, Γ and Δ are the energy, width and level shift of the resonance, respectively, and are treated as parameters. Since the energy steps of the present measurement were not narrow enough to determine Γ, the value of 20 keV by Cosman et al[8] was taken. The resonance energy E_0 was found to be 5.255 ± 0.010 MeV and was consistent with the value of 5.264 ± 0.020 MeV obtained by Cosman et al.[8]

Then the value of Δ was varied in order to fit the cross sections of the ground 6+ and the first 5+ levels. The value of Δ has a permissible maximum imposed by the condition

$$\widetilde{T}_{p^*} \leqq 1 . \qquad (4)$$

The best values of Δ obtained for various spin-parity assignments J^π for the resonance are as follows:

$$\begin{aligned} J^\pi &= \tfrac{5}{2}- & \Delta &= -64\,\mathrm{keV}, \\ J^\pi &= \tfrac{7}{2}- & \Delta &= -48\,\mathrm{keV}, \\ J^\pi &= \tfrac{7}{2}+ & \Delta &= -140\,\mathrm{keV}, \\ J^\pi &= \tfrac{9}{2}+ & \Delta &= -85\,\mathrm{keV}. \end{aligned} \qquad (5)$$

Here the values for $J^\pi = \frac{5}{2}-$ and $\frac{7}{2}-$ are the maximums given by (4). The fits obtained are shown in fig. 8 by various curves, where the cross sections calculated for the sum of the second, third and fourth excited levels are also shown. The spin-parities $\frac{5}{2}-$ and $\frac{7}{2}-$ cannot reproduce the observed enhancement in the 6+ and 5+ levels, and $J^\pi = \frac{7}{2}+$ exhibit too large peak in the summed cross section for the 4+, 3+ and 2+ levels. Only $J^\pi = \frac{9}{2}+$ explains all the data and the spin-parity of the analog resonance is assigned to be $\frac{9}{2}+$.

The assignment does not agree with the value of $(\frac{5}{2}-)$ by Cosman et al.[8] They concluded this result from the proton angular distribution for the first 2+ level of ^{50}Ti at a incident proton energy close to the peak of the resonance. But the cross section fluctuation is too large to draw a definite conclusion from the shape of the angular distribution at a single incident energy with a small energy spread. In assigning

$J^\pi = (\frac{5}{2}-)$ they had to consider this resonance to be analog to the 4.012 MeV $\frac{5}{2}-$ level of ^{51}Ti. This correspondence has a difficulty, as was alluded by themselves. The Coulomb energy differences obtained from the resonance energies of other resonances by them are in the range ΔE_c = 7.700 - 7.793 MeV, while the above correspondence gives ΔE_c = 7.622 MeV, which seems too small. The present assignment of $\frac{9}{2}+$ relates the 5.255 MeV resonance to the 3.759 MeV $\frac{9}{2}+$ level in ^{51}Ti and gives ΔE_c = 7.772 MeV in agreement with other resonances.

The above mentioned inadequacy of negative parity for this resonance can be qualitatively understood from the fact that positive parity levels in ^{50}V are populated mainly through compound states with positive parity, as is mentioned in sect. 3.1, and that the cross section of the 6+ ground state is strongly enhanced at this resonance.

Using the values of J^π and Δ thus obtained, the cross sections of higher levels can be calculated. The results are shown in fig. 9 for three levels whose cross sections are enhanced at this resonance and for other four levels, which are considered to have spins J = 1 - 4, for comparison. The theoretical lines for energy-averaged excitation functions shown in figs. 4 and 5 also include the enhancement due to this resonance. The calculation shows that levels with negative parity or with $J \leq 3$ have not enhanced yields at the resonance. Thus the 0.836 MeV level is assigned to be 5+ and the 1.702 and 1.753 MeV levels to be 4+ or 5+.

5. Level and decay scheme of ^{50}V

5.1. the 0.0, 0.226, 0.320, 0.355 and 0.388 MeV levels

Excitation function of these levels are consistent with the assignment[2,4,5] of 6+, 5+, 4+, 3+ and 2+. The 0.226 MeV level cannot be other than 5+ from the enhancement at the analog resonance and from the

neutron angular distribution. The 0.320 MeV level is assigned to be 4+ from the excitation function, since a 4- level has a larger cross section as is seen in an example for the 0.910 MeV level in fig. 5. The 0.320 MeV level has been reported to decay to the 0.226 MeV level by Blasi et al.[2] They did not observe the 320 keV γ-transition to the ground state and set an upper limit of 2% to the branching ratio. In the present investigation, 320 keV peaks were clearly seen in all the γ-ray spectra as is seen in fig. 2. Since the 0.320 MeV level decays mainly to the 0.226 MeV level, and other γ-ray which feeds the latter is the 684 keV γ-ray alone as is shown in fig. 10, the population of this level is expressed as

$$P(0.320\,\mathrm{MeV\ level}) = \sigma(226\,\mathrm{keV}\,\gamma) - \sigma(0.226\,\mathrm{MeV\ level}) - \sigma(684\,\mathrm{keV}\,\gamma). \quad (6)$$

If the 320 keV γ-ray is emitted by the 0.320 MeV level, the excitation function of this γ-ray should be proportional to P(0.320 MeV level). This hold very well as is seen in fig. 3, where the energy dependence of P(0.320 MeV level) is shown to closely follow the excitation function of the 320 keV γ-ray. The ratio of the two quantities gives a branching ratio of 2.6 ± 0.3% for this γ-ray.

5.2. the 0.836 and 0.910 MeV levels

The 0.836 MeV level is assigned to be 5+ from the excitation function and the enhancement at the analog resonance. This level seems to decay to the ground state by emitting a 836 ± 2 keV γ-ray, the existence of which could not be ascertained firmly because of the overlap with the 834 keV γ-rays from ^{72}Ge in the spectra. There was found no other γ-ray which could be considered to decay from this level. The excitation function and the neutron angular distribution of the 0.910 MeV level are

consistent only with a 4+ assignment. The 684 keV γ-ray was ascribed to this level, because the excitation function of the 684 keV γ-ray was nearly the same with that of this level and there was found no other γ-ray deexciting this level. The γ-ray angular distributions are also consistent with 4+. A 7+ level has been observed[4,5] at this energy. This disagreement is discussed in sect. 5.8.

5.3. the 1.301 and 1.332 MeV levels

The excitation function of the 1.301 MeV level favours an assignment of J = 2, and the angular distribution of the 913 keV γ-ray, which deexcites this level to the 0.388 MeV level, definitely supports this assignment rejecting other choices of J = 0 or 1. The excitation function and the neutron angular distribution of the 1.332 MeV level can be explained only with a J = 1 assignment. The only γ-ray which can be ascribed to this level is the 944 keV γ-ray. However, the yield of this γ-ray gives considerably larger cross section than that of this level though there is no cascade γ-ray to this level. On the other hand, the yield of the 913 keV γ-ray amounts to only 70 ± 6% of the cross section of the 1.301 MeV level. Furthermore at Ep = 4.40 MeV, which is between the thresholds of the two levels, a 946 keV γ-ray was observed. The relative yield of the 913 and 946 keV γ-rays was 72 ± 4 and 28 ± 4%, respectively. This 946 keV γ-ray can be considered to deexcites the 1.301 MeV level to the 0.355 MeV level, and the missing γ-ray yield of 30 ± 6% for the 1.301 MeV level is just compensated by the 946 keV γ-ray. Since the energy resolution of the γ-ray detector was not good, the 944 and 946 keV γ-ray peaks were not resolved in the spectra. With the branching ratio given above the yield of the 946 keV γ-ray was calculated from the yield of the 913 keV γ-ray in order to determine the yield of the 944 keV γ-ray. Excitation function of this γ-ray thus obtained is shown in fig. 5 and is con-

sistent with that of the 1.332 MeV level obtained from the neutron data.

5.4. the 1.401 MeV level

This level is assigned to be $J^{\pi} = 3(+)$ from the excitation function and the γ-ray angular distributions, and decays mainly to the 0.388 MeV level by the 1013 keV transition and with a weaker intensity to the 0.320 MeV level by the 1081 keV transition.

5.5. the 1.495 and 1.519 MeV levels

The 1.495 MeV level is assigned to be J = 1 from the excitation function and the neutron angular distribution. This level decays to the 0.388 MeV level by the 1107 keV transition. As to the 1.519 MeV level, the excitation function indicates J = 0 or 2. This level decays to the 0.388 and 0.355 MeV levels by the 1131 and 1164 keV transitions, and the angular distributions of these γ-rays choose J = 2 definitely. On the other hand, the neutron angular distribution favours J = 0. This may be due to the fact that this level only barely separate from the 1.495 MeV level in the neutron spectra in the energy range where the angular distribution was measured and the cross section may have large error due to the peeling-off procedure. In any case the quality of the data is by far better for the 1131 keV γ-ray angular distributions than for the neutron angular distribution, and the assignment of J = 2 should be taken.

5.6. the 1.562 and 1.676 MeV levels

The 1.562 MeV level decays to the 0.388 and 0.355 MeV levels by the 1174 and 1207 keV transitions. All the data indicate the assignment of J = 2. Especially the angular distributions of the 1174 keV γ-ray reject other choices. The 1.676 MeV level is assigned to be J = 3 from the excitation function. The 375 keV γ-ray deexcites this level to the

1.301 MeV level. Weak 1288 keV γ-ray peaks were observed above the threshold of this level. This γ-ray may be the transition from this level to the 0.388 MeV level.

5.7. the 1.702, 1.753 and 1.810 MeV levels

The 1.702 and 1.753 MeV levels are assigned in sect. 4 to be 4+ or 5+ from the enhancement at the analog resonance. The 1.810 MeV decays to the 0.388 MeV 2+ level by the 1422 keV transition. The γ-ray excitation function suggests this level to be $J \leq 2$.

5.8. comparison with previous experiments and the shell model prediction

The spin-parity assignments from the present experiment are summarized in table 1 together with the results of other experiments[2-5]. The last second column is the assignments from the present experiment. They are consistent with the results of the previous works except the 0.910 MeV level. The last column is the assignments proposed from all the data. The proposed level scheme is also shown in fig. 10 together with the γ-transitions. Here we considered the 0.910 level to be a doublet of 4+ and 7+ levels. As is mentioned before, this level has been assigned [4,5] to be 7+ from the $^{52}Cr(d,\alpha)^{50}V$ reaction, while the present assignment is 4+. There seems little ambiguity in both assignments, and the unique solution of this disagreement is a doublet of 4+ and 7+. This is also consistent with the fact that in the present (p,n) study a 7+ level cannot be excited with apreciable intensity and that the above (d,α) reaction mainly picks up a $(f7/2)^2$ pair and the excitation of J = even levels is forbidden[17].

The main configuration of the low-lying levels of ^{50}V is considered to be $(f7/2)_p^3(f7/2)_n^{-1}$. A shell model calculation confined to the $(f7/2)^n$ configurations was made by McCullen, Bayman and Zamick (M.B.Z)[6]. In

this model, the cross conjugate nuclei ^{50}V and ^{46}Sc have the same level structure. The ^{50}V level scheme proposed here, the ^{46}Sc level scheme proposed by Guichard et al[18] and the shell model prediction by M.B.Z. are compared in fig. 11. The correspondence between the three are nearly complete for low-lying levels, if the 0.835 MeV level of ^{46}Sc is 4+. This good correspondence also supports the above proposal of a doublet for the 0.910 MeV level.

6. Summary

The low-lying level and decay scheme of ^{50}V has been well established in the present investigation. The present results show that the study of both the (p,n) and (p,nγ) reactions are very efficient in the spin assignment. In fact the spins of most of the levels of ^{50}V observed below 1.9 MeV in previous experiments have been determined here.

The 5.255 MeV analog resonance in ^{51}V has been assigned to be 9/2+. Analog resonances with spins as large as this are difficult to study by (p,p) reactions masked by the predominant partial waves with low l values in the medium mass nuclei. The present results shows that such resonances can be studied by observing neutron yields for levels with relatively high spins. A characteristic feature in the A $\gtrsim$ 50 mass region that the parity change in the neutron emission process is approximately forbidden has enabled the parity assignment of the analog resonance and in turn the parity assignments of levels enhanced by the resonance.

After the present manuscript had been written, the authors noticed the work by Smith et al.[19] They reported two 1+ level at 1.333 and 1.490 MeV which are consistent with our results.

We wish to thank Messrs. Y. Sato and T. Yoshida for their assistence in the experiment. We are also indebted to Drs. K. Harada, M. Maruyama and Y. Sugiyama for careful reading of the manuscript and for discussions.

Table 1. Experimental data on the level structure of ^{50}V

Level No.	Ex(keV) ref. 2,4)	Ex(keV) present	$(p,n\gamma)$[2] J^π	$^{51}V(d,t)$[3] l_n	$^{52}Cr(d,\alpha)$ ref. 4)	$^{52}Cr(d,\alpha)$ ref. 5)	Adopted J^π in ref. 5)	J^π (p,n), (p,nγ) present	Adopted J^π
0	0	0	6+	3	6	(6)	6+	6+	6+
1	226.2	226±1	(5+)	3+(1)	4	4+6	5+	5+	5+
2	320.1	320±3	(4+)	3+(1)	(0,2,4)		(4+)	4+	4+
3	355.2	355±3	(3+)	3	2	2+4	3+	(3+)	3+
4	387.9	388±3	(2+)	(3)	(2)		(2+)	(2+)	2+
5	837±2	836±2		3	4	4+6	5+	5+	5+
6		910±1						4+	4+
	910±2			3	6	6	7+		7+
7	1305±3	1301±1		3	(0,2,4)		(2+)	2	2+
8	1332±2	1332±1		3	0+2(4)	0+2	1+	1	1+
9	1404±2	1401±1		(1+3)	0,(2)			3(+)	3+
10	1497±3	1495±1		3				1	1+
11	1520±4	1519±1		3				2	2+
12	1564±4	1562±1						2	2
13	1680±4	1676±1		3+(1)	2			3	3+
14	1703±4	1702±4		3+1	(2,4)			4+ or 5+	4+ or 5+
	1725±4			3					

Table 1. (continued)

Level No.	Ex(keV) ref. 2,4)	Ex(keV) present	$(p,n\gamma)^{2)}$ J^π	$^{51}V(d,t)^{3)}$ l_n	$^{52}Cr(d,\alpha)$ ref. 4)	$^{52}Cr(d,\alpha)$ ref. 5)	Adopted J^π in ref. 5)	J^π (p,n),(p,nγ) present	Adopted J^π
15	1760±4	1753±4		(3+1)	4			4+ or 5+	4+ or 5+
	1766±8			3+(1)					
16	1805±4	1810±1			2			0,1,2	(1+)
17	1935±6	1936±5		3	(4 or 0)				
18	1956±4	1953±5		3	(4 or 0)				
19	2038±4	2037±5		(3,2,0)	4				

Table 2. Gamma-ray energies, branching ratios and mixing ratios

E_i (MeV)	E_f (MeV)	E_γ (keV)	J_i^π	J_f^π	branching ratio(%)	mixing ratio
0.320	0	320	4+	6+	2.6 ± 0.3	
0.910	0.226	684	4+	5+	100^{+0}_{-10}	$-0.44 \leq \delta \leq 0.17$ or $-11.2 \leq \delta \leq -1.7$
1.301	0.355	946	2+	3+	28 ± 4	
	0.388	913		2+	72 ± 6	0.09 ± 0.09
1.332	0.388	944	1+	2+	100^{+0}_{-5}	
1.401	0.320	1081	3+	4+	12 ± 3	
	0.388	1013		2+	88 ± 5	0.08 ± 0.03
1.495	0.388	1107	1+	2+	100^{+0}_{-5}	-0.58 ± 0.03
1.519	0.355	1164	2+	3+	17 ± 3	$-0.17 \leq \delta \leq 0.36$ or $\delta \leq -1.7$
	0.388	1131		2+	83 ± 5	$-0.12 \leq \delta \leq 0.05$ or $1.0 \leq \delta \leq 1.4$
1.562	0.355	1207	2	3+	45 ± 3	$-1.37 \leq \delta \leq -0.32$
	0.388	1174		2+	55 ± 3	$-0.36 \leq \delta \leq 2.2$
1.676	1.301	375	3+	2+	100^{+0}_{-20}	
	0.388	1288		2+	< 15	
1.810	0.388	1422	(1+)	2+	100^{+0}_{-10}	

References

1) J. B. Ball and R. F. Sweet, Phys. Rev. 140 (1965) B904

2) P. Blasi, P. R. Maurenzig, N. Taccetti and R. A. Ricci, Phys. Lett. 28B (1969) 555

3) J. N. Bishop, D. J. Pullen and B. Rosner, Phys. Rev. C2 (1970) 550

4) R. DelVecchio, W. W. Daenick, D. L. Dittmer and Y. S. Park, Phys. Rev. C3 (1971) 1989

5) D. Bachner, G. Van der Giet and D. Lancè, Nucl. Phys. A209 (1973) 373

6) J. D. McCullen, B. F. Bayman and L. Zamick, Phys. Rev. 134 (1964) B515

7) J. D. Fox, C. F. Moore and D. Robson, Phys. Rev. Lett 12 (1964) 198

8) E. R. Cosman, D. C. Slater and J. E. Spencer, Phys. Rev. 182 (1969) 1131

9) N. B. Gove and A. H. Wapstra, Nuclear Data Tables 11 (1972) 127

10) W. Hauser and H. Feshbach, Phys. Rev. 87 (1952) 366

11) G. R. Satchler, Phys. Rev. 94 (1954) 1304; 104 (1956) 1198

12) P. A. Moldauer, Phys. Rev. 135 (1964) B642

13) S. Igarashi, private comunication

14) F. G. Perey, Phys. Rev. 131 (1963) 745

15) C. A. Engelbrecht and H. Fiedelday, Ann. of Phys. 42 (1967) 262

16) D. Robson, J. D. Fox, P. Richard and C. F. Moore, Phys. Lett. 18 (1965) 86

17) N. K. Glendenning, Phys. Rev. 137 (1965) B102

18) A. Guichard, M. Bedjidian, J. Y. Grossiord, M. Gusakow, J. R. Pizzi and C. Ruhla, Nucl. Phys. A192 (1972) 125

19) J. W. Smith, L. Meyer-Schützmeister, T. H. Braid, P. P. Singh and G. Hardie, Phys. Rev. C7 (1973) 1099

Figure captions

Fig. 1 Neutron spectra for the $^{50}Ti(p,n)^{50}V$ reaction observed at 45°. Level numbers correspond to those given in table 1.

Fig. 2 A typical γ-ray spectrum for the $^{50}Ti(p,n\gamma)^{50}V$ reaction observed at 50°. Gamma-ray energies are given in keV. Asterisks indicate γ-rays due to other isotopes of titanium than ^{50}Ti.

Fig. 3 Excitation functions for γ-rays observed at 50°. Numbers indicate γ-ray energies in keV. The quantity P(320) is the population of the 0.320 MeV level obtained from eq. (6).

Fig. 4 Excitation functions of the lowest five levels measured at 55° averaged over each 100 keV interval. Experimental values are shown by rectangles, the vertical sizes of which indicate "uncertainties" obtained from eqs. (1). Symbols connected by lines refer to the statistical model calculations described in sect. 3.1.

Fig. 5 Excitation functions of the levels other than the lowest five levels. Rectangles and symbols connected by lines have the same meaning as in fig. 4. Excitation functions obtained from the γ-ray data at 50° are also shown by ellipses. Hatched areas indicate the range of variation in the calculated values due to the different choices of the spin-parities of other levels.

Fig. 6 Normalized angular distributions of neutrons for different levels averaged over the energy ranges shown in the figure. Different lines refer to the statistical model calculations for different choices of the spin-parities.

Fig. 7 Normalized angular distributions of various γ-rays. Different lines refer to the statistical model calculations for different choices of the spin-parities.

Fig. 8 The measured cross sections for the lowest five levels are shown by closed circles for energies around the 5.255 MeV analog resonance. Different lines represent the theoretical values for different choices of the spin-parity of each levels.

Fig. 9 Behaviour of the cross sections for various levels around the 5.255 MeV analog resonance. Defferent lines represent the theoretical values for different choices of the spin-parity of each levels.

Fig.10 Level and decay scheme of ^{50}V determined in this work. Gamma-rays for which energies are not shown were not observed in the present measurement.

Fig.11 Comparison of the low-lying levels of ^{50}V with those of ^{46}Sc and the shell model prediction by MBZ. Only levels with positive parity are shown for ^{46}Sc.

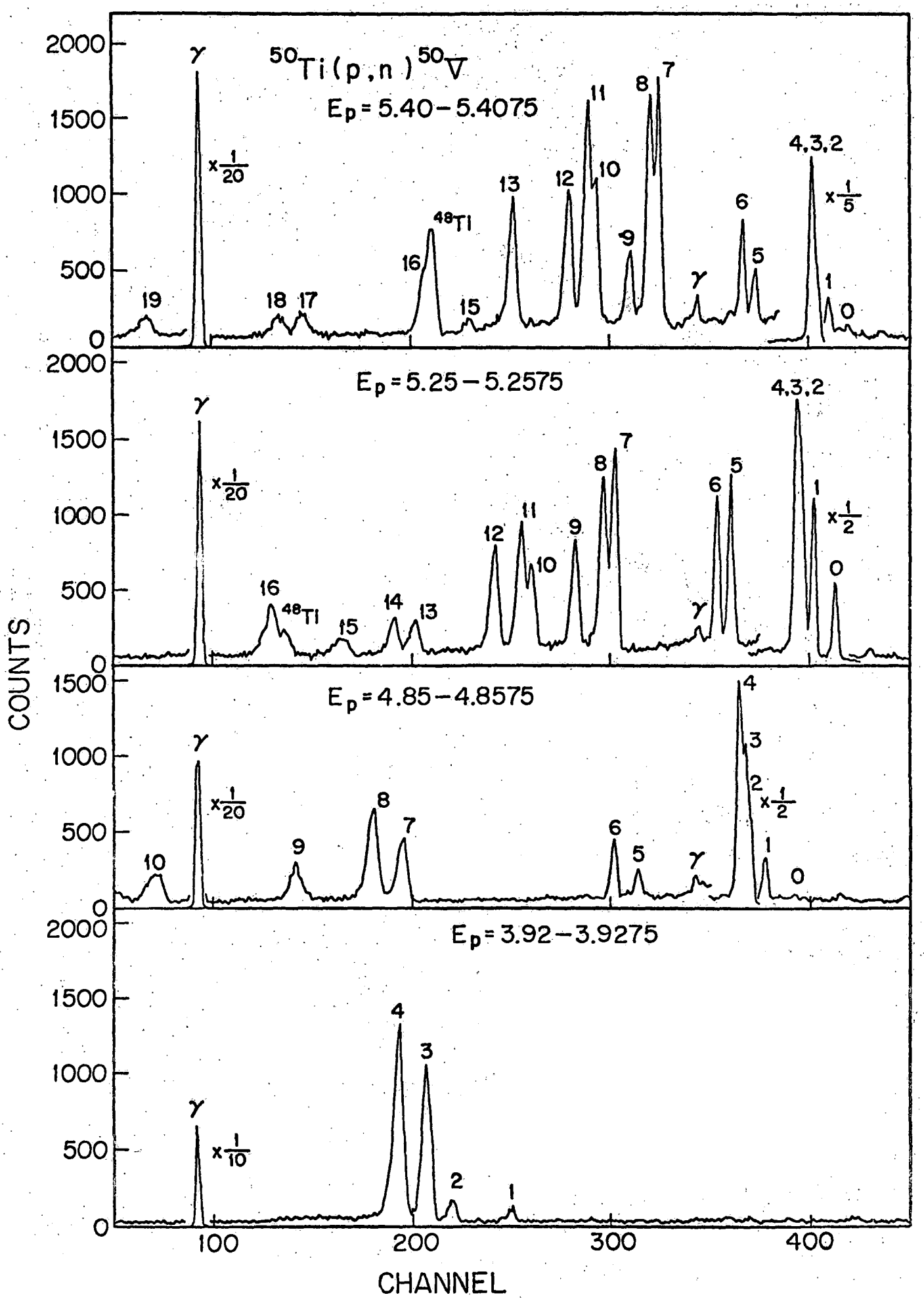
$^{50}Ti(p,n)^{50}V$
$E_p = 5.40 - 5.4075$
$E_p = 5.25 - 5.2575$
$E_p = 4.85 - 4.8575$
$E_p = 3.92 - 3.9275$
COUNTS
CHANNEL
100
200
300
400
2000
1500
1000
500
0
γ
^{48}Ti
$\times\frac{1}{20}$
$\times\frac{1}{5}$
$\times\frac{1}{2}$
$\times\frac{1}{10}$
19
18
17
16
15
14
13
12
11
10
9
8
7
6
5
4,3,2
4
3
2
1
0

Fig 1

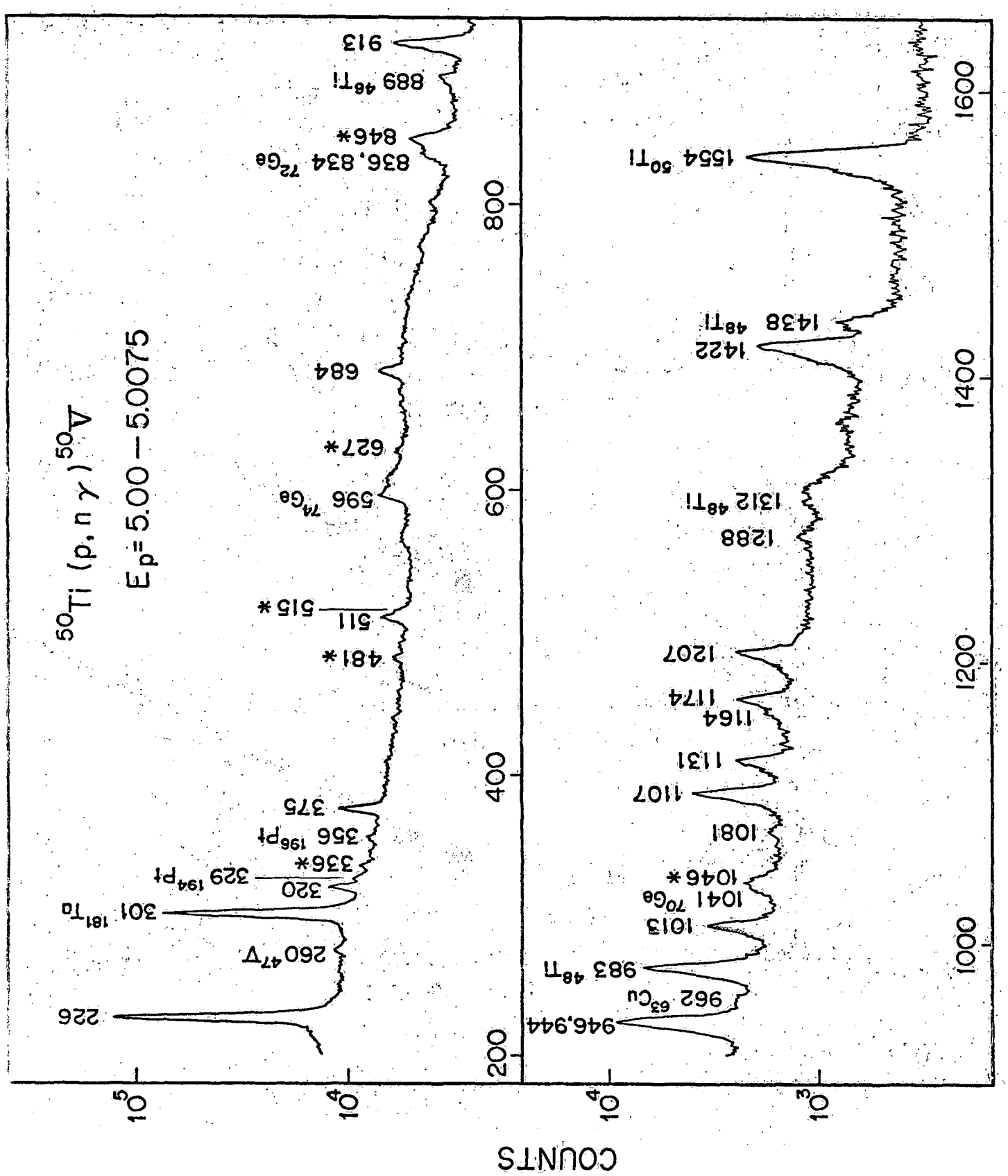
^{50}Ti (p, n γ) ^{50}V
E_p= 5.00 – 5.0075
COUNTS
CHANNEL
226
260 ^{47}V
301 ^{181}Ta
320
329 ^{194}Pt
336*
356 ^{196}Pt
375
481*
511
515*
596 ^{74}Ge
627*
684
836, 834 ^{72}Ge
846*
889 ^{46}Ti
913
946, 944
962 ^{63}Cu
983 ^{48}Ti
1013
1041 ^{70}Ge
1046*
1081
1107
1131
1164
1174
1207
1288
1312 ^{48}Ti
1422
1438 ^{48}Ti
1554 ^{50}Ti

Fig 2

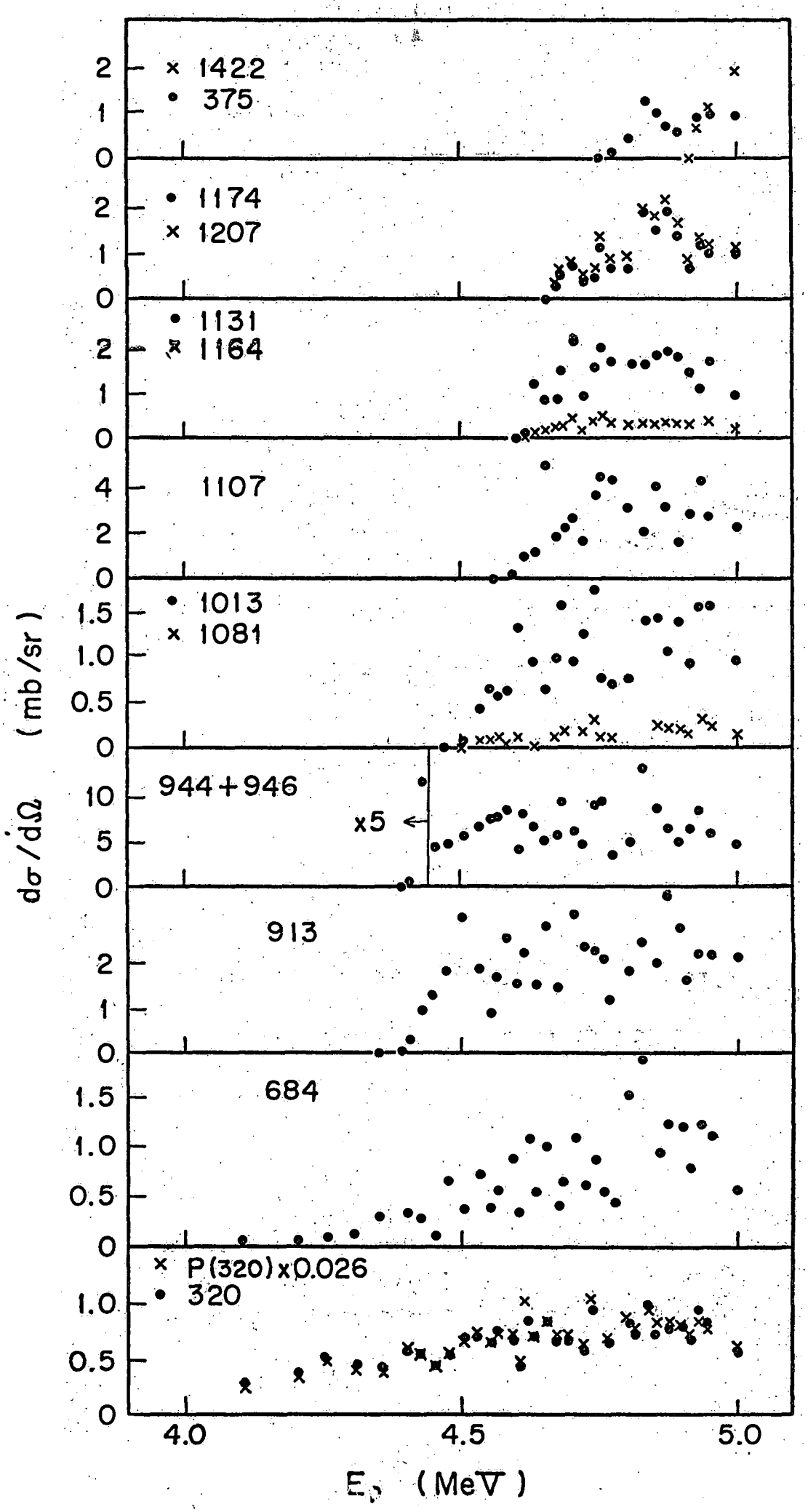
× 1422
• 375
• 1174
× 1207
• 1131
× 1164
1107
• 1013
× 1081
944+946
x5
913
684
× P(320)x0.026
• 320
dσ/dΩ (mb/sr)
4.0
4.5
5.0
E, (MeV)

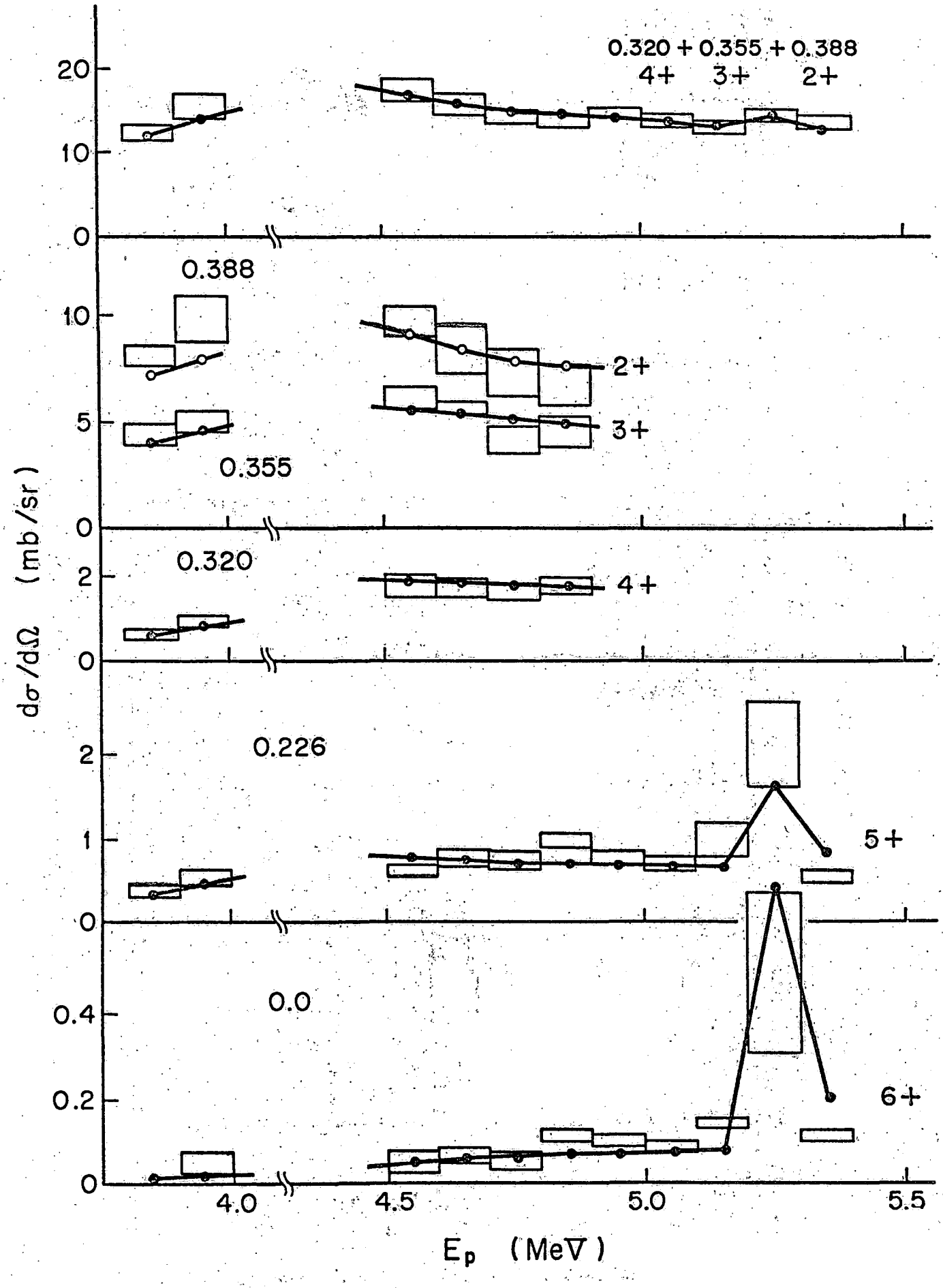
0.320 + 0.355 + 0.388
4+ 3+ 2+
0.388
2+
3+
0.355
0.320
4+
0.226
5+
0.0
6+
dσ/dΩ (mb/sr)
Ep (MeV)
4.0
4.5
5.0
5.5

Fig 4

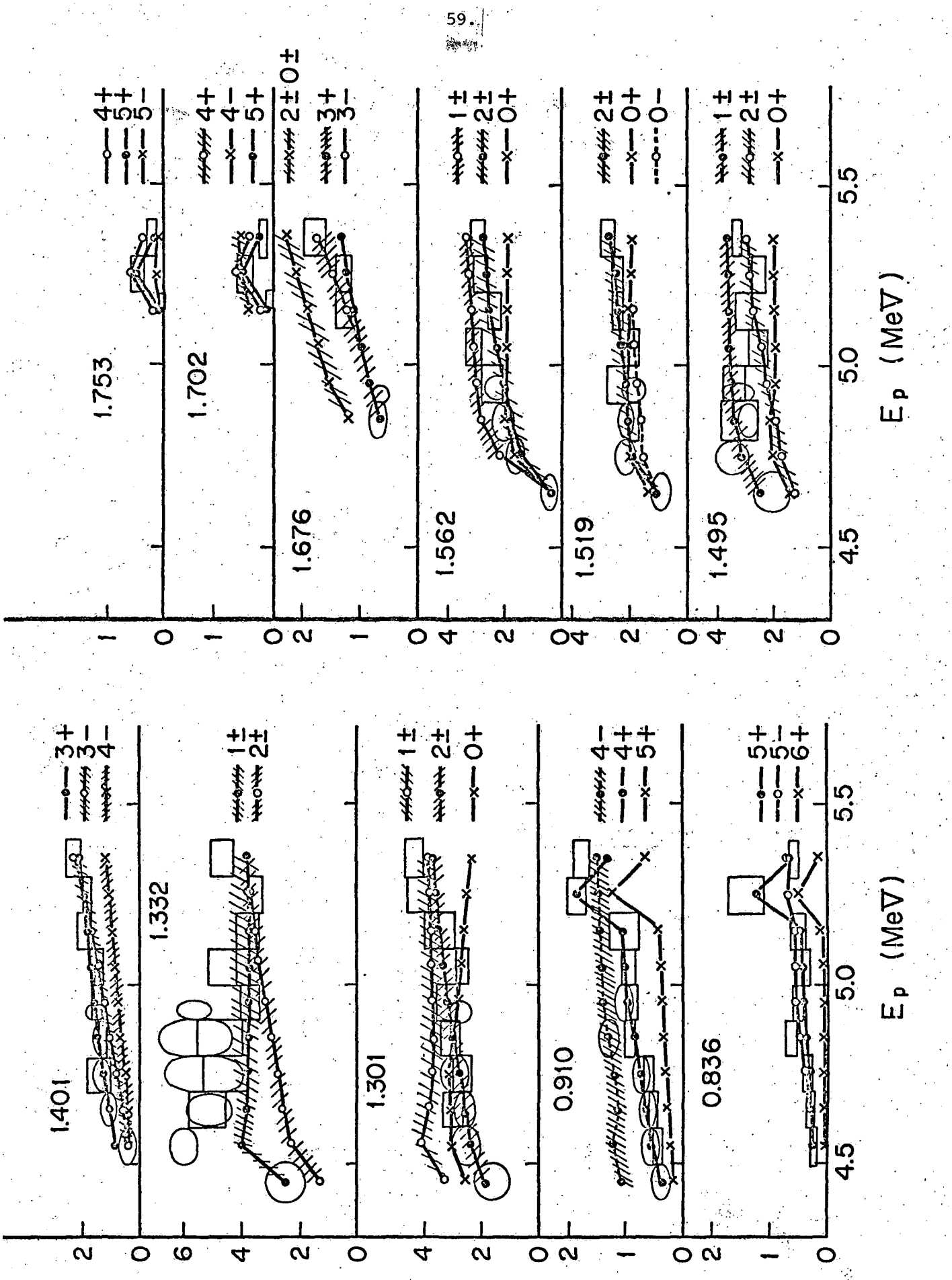
dσ/dΩ (mb/sr)
Ep (MeV)
1.401
1.332
1.301
0.910
0.836
1.753
1.702
1.676
1.562
1.519
1.495
3+ 3− 4−
1± 2±
1± 2± 0+
4− 4+ 5+
5+ 5− 6+
4+ 5+ 5−
4+ 4− 5+
2± 0± 3+ 3−
1± 2± 0+
2± 0+ 0−
1± 2± 0+

Fig 5

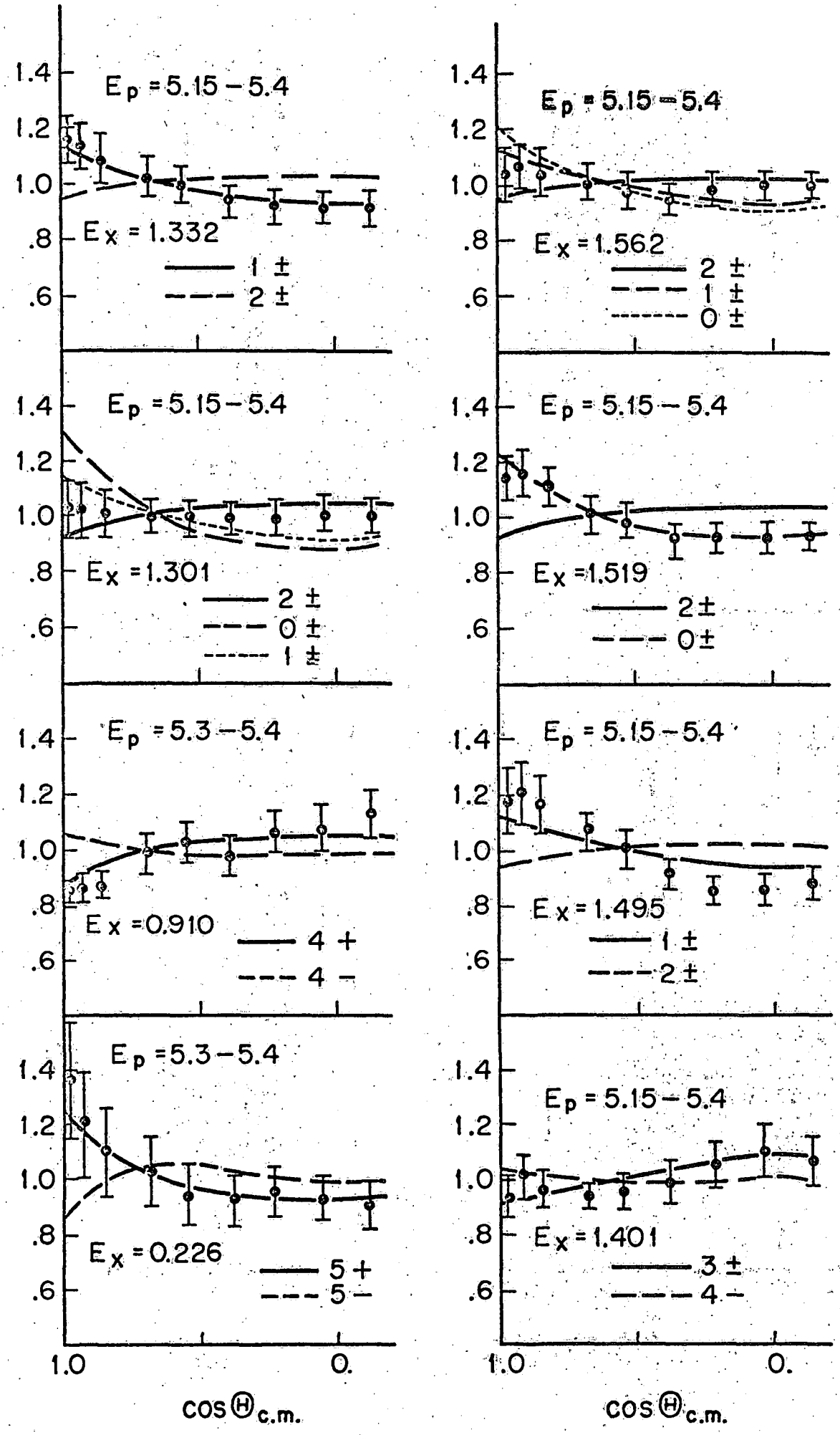
Ep = 5.15 – 5.4
Ex = 1.332
1 ±
2 ±
Ep = 5.15 – 5.4
Ex = 1.562
2 ±
1 ±
0 ±
Ep = 5.15 – 5.4
Ex = 1.301
2 ±
0 ±
1 ±
Ep = 5.15 – 5.4
Ex = 1.519
2±
0±
Ep = 5.3 – 5.4
Ex = 0.910
4 +
4 –
Ep = 5.15 – 5.4
Ex = 1.495
1 ±
2 ±
Ep = 5.3 – 5.4
Ex = 0.226
5 +
5 –
Ep = 5.15 – 5.4
Ex = 1.401
3 ±
4 –
1.4
1.2
1.0
.8
.6
1.0
0.
cos Θc.m.

Fig 6

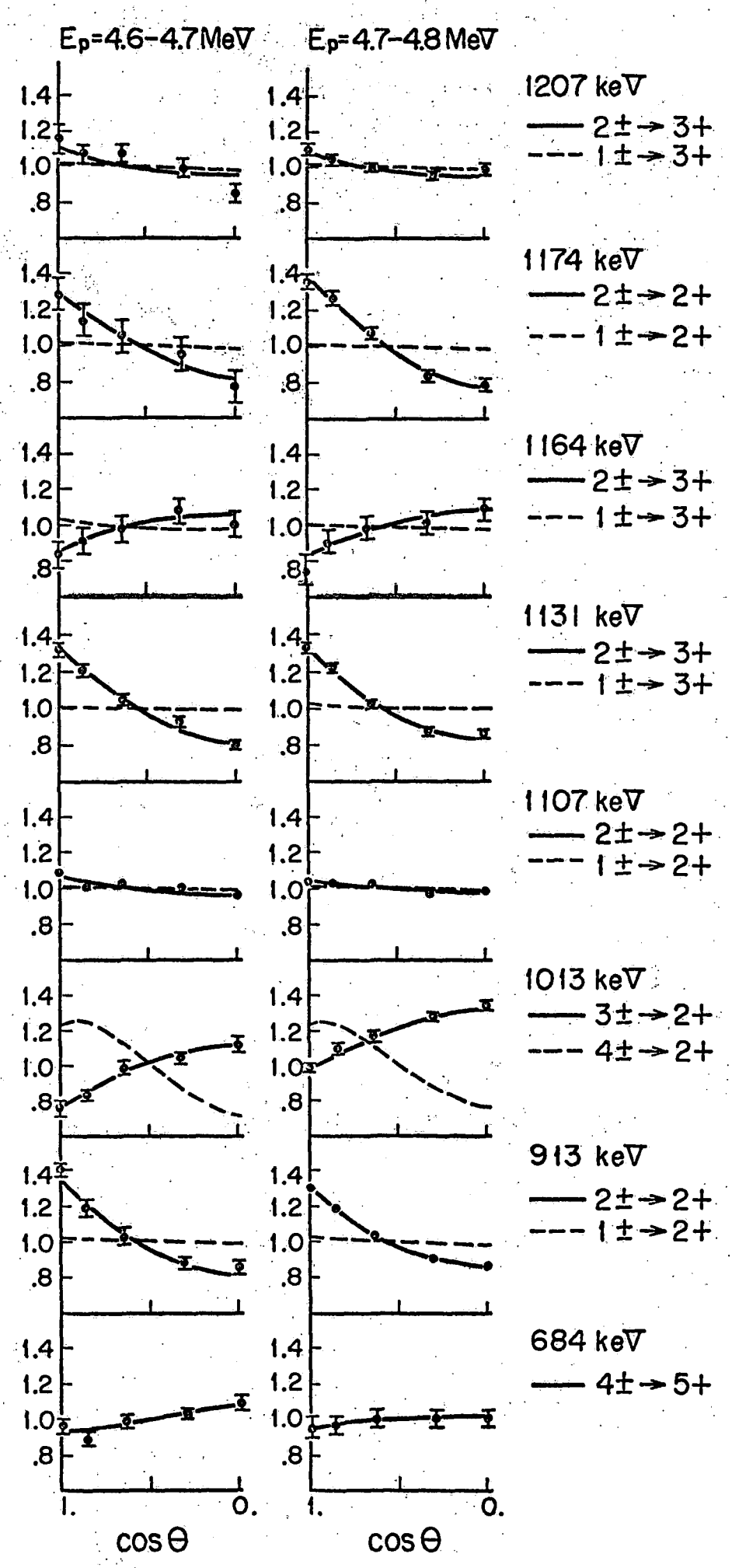
Ep=4.6-4.7MeV
Ep=4.7-4.8MeV
1207 keV
2±→3+
1±→3+
1174 keV
2±→2+
1±→2+
1164 keV
2±→3+
1±→3+
1131 keV
2±→3+
1±→3+
1107 keV
2±→2+
1±→2+
1013 keV
3±→2+
4±→2+
913 keV
2±→2+
1±→2+
684 keV
4±→5+
1.4
1.2
1.0
.8
1.
0.
cos θ

Fig 7

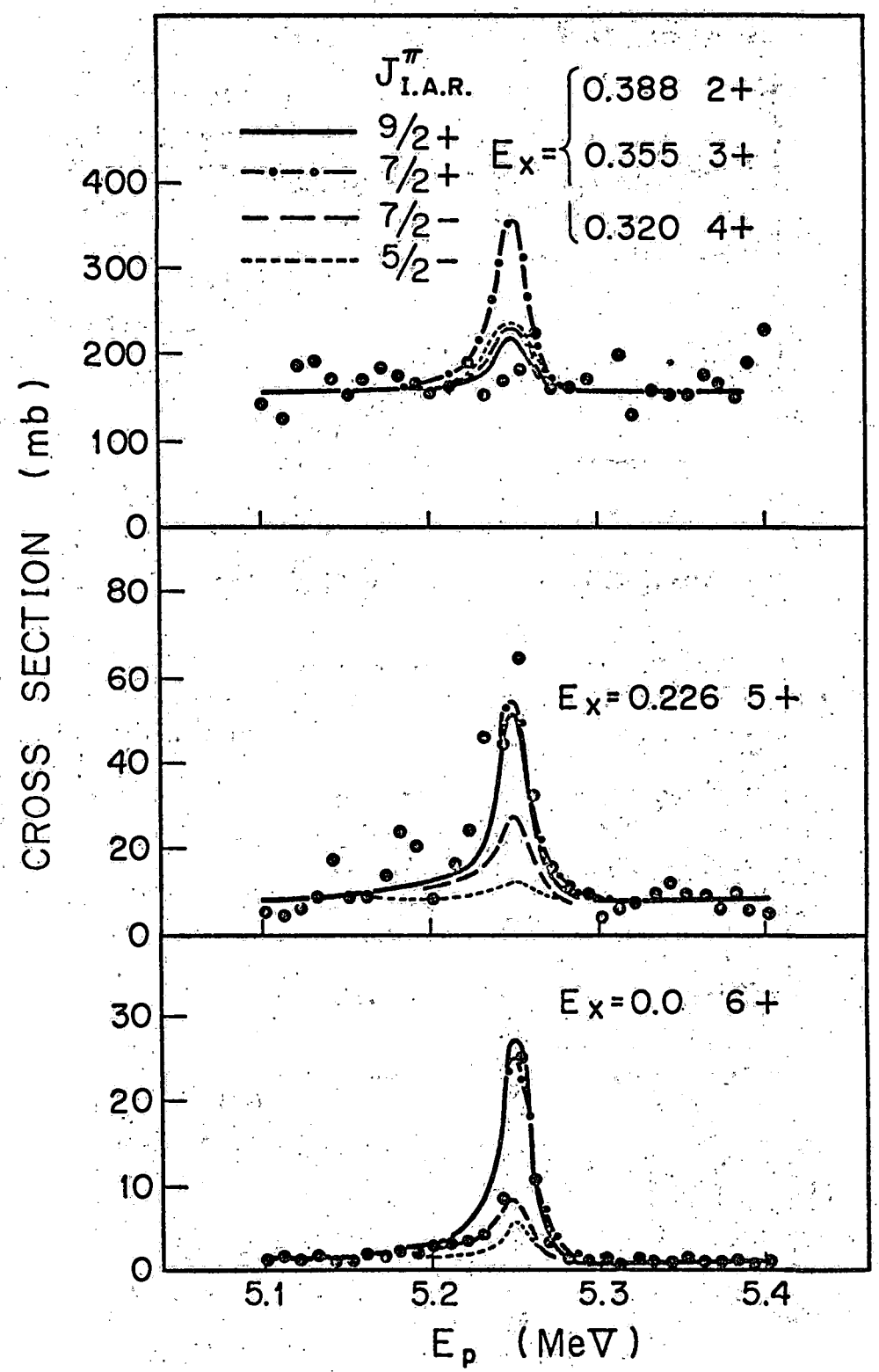
$J^{\pi}_{I.A.R.}$
9/2+
7/2+
7/2−
5/2−
E_x = 0.388 2+
0.355 3+
0.320 4+
E_x = 0.226 5+
E_x = 0.0 6+
CROSS SECTION (mb)
E_p (MeV)
400
300
200
100
0
80
60
40
20
0
30
20
10
0
5.1
5.2
5.3
5.4

Fig 8

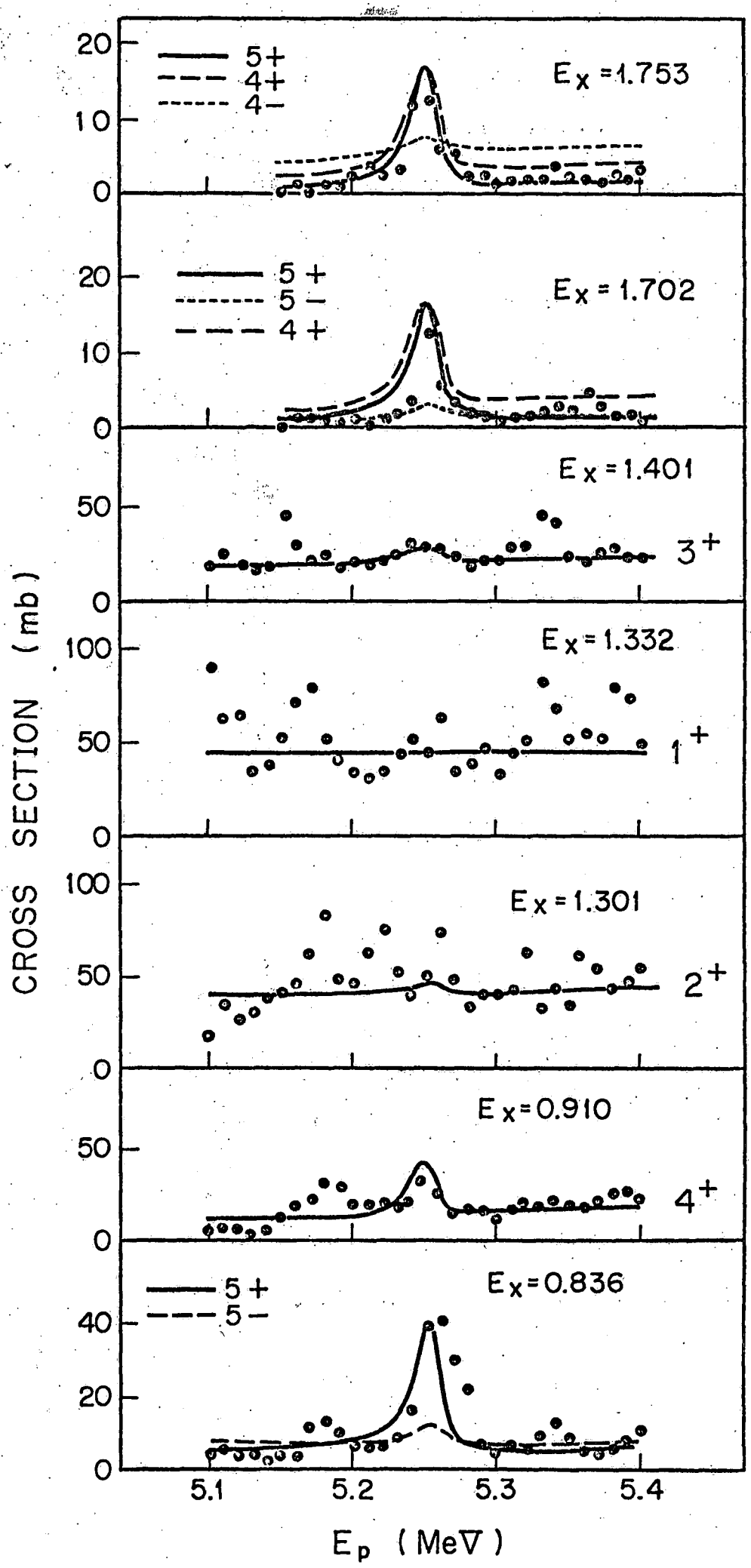
5+
4+
4−
Ex =1.753
5 +
5 −
4 +
Ex = 1.702
Ex = 1.401
3+
Ex = 1.332
1+
Ex = 1.301
2+
Ex = 0.910
4+
5 +
5 −
Ex = 0.836
CROSS SECTION (mb)
Ep (MeV)
5.1
5.2
5.3
5.4

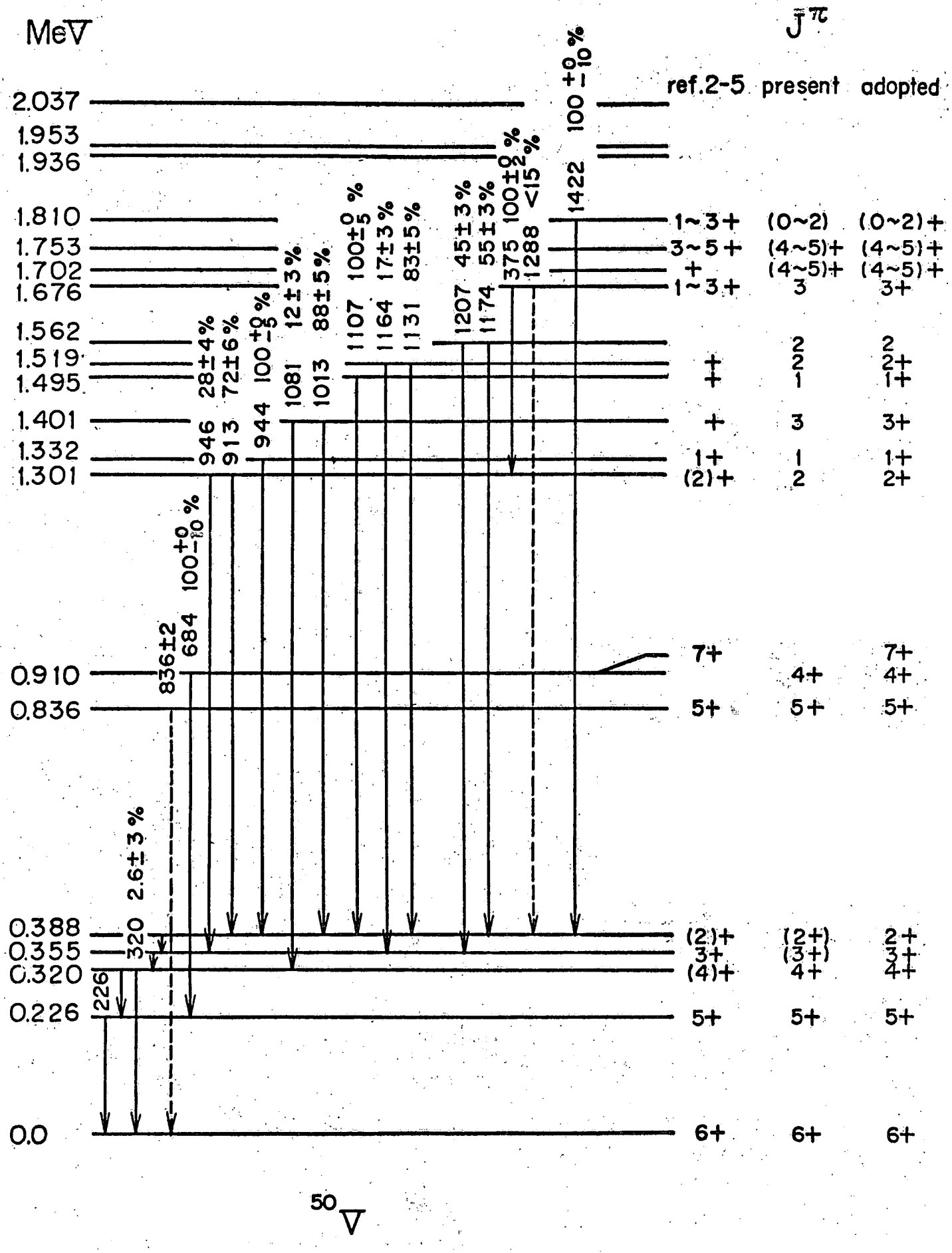
MeV
J^{π}
ref.2-5
present
adopted
2.037
1.953
1.936
1.810
1.753
1.702
1.676
1.562
1.519
1.495
1.401
1.332
1.301
0.910
0.836
0.388
0.355
0.320
0.226
0.0
100 +0 −10 %
1422
100±2 %
<15 %
1288
375
100±5 %
45±3 %
55±3 %
1207
1174
17±3 %
83±5 %
1164
1131
12±3 %
88±5 %
1107
1081
1013
100 +0 −5 %
944
28±4 %
72±6 %
946
913
100 +0 −10 %
836±2
684
2.6±3 %
320
226
1~3+ (0~2) (0~2)+
3~5+ (4~5)+ (4~5)+
+ (4~5)+ (4~5)+
1~3+ 3 3+
2 2
+ 2 2+
+ 1 1+
+ 3 3+
1+ 1 1+
(2)+ 2 2+
7+ 7+
4+ 4+
5+ 5+ 5+
(2)+ (2+) 2+
3+ (3+) 3+
(4)+ 4+ 4+
5+ 5+ 5+
6+ 6+ 6+
^{50}V

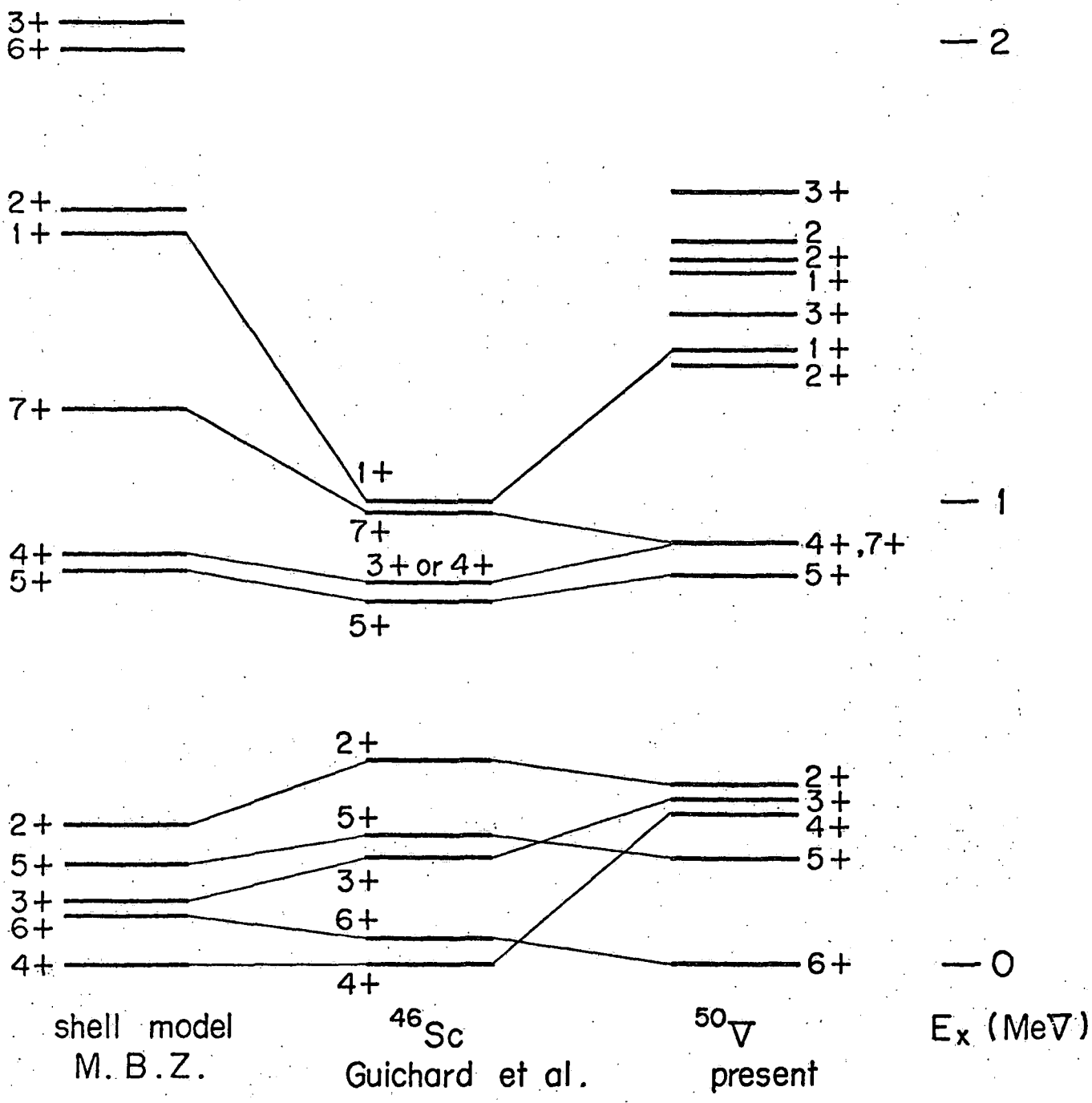
3+
6+
2+
1+
7+
4+
5+
1+
7+
3+ or 4+
5+
3+
2
2+
1+
3+
1+
2+
4+,7+
5+
2+
5+
3+
6+
4+
2+
5+
3+
6+
4+
2+
3+
4+
5+
6+
— 2
— 1
— 0
shell model
M. B. Z.
46Sc
Guichard et al.
50V
present
Ex (MeV)

Fig 11

ELECTROMAGNETIC TRANSITIONS IN ^{22}Na

R.H. Spear, R.A.I. Bell, M.T. Esat, P.R. Gardner and D.C. Kean

Department of Nuclear Physics,

Australian National University, Canberra, Australia

and

A.M. Baxter

Physics Department,

Australian National University, Canberra, Australia

NUCLEAR REACTIONS ^{23}Na(^{3}He,$\alpha\gamma$), E = 8.46 MeV; measured $\sigma(E_\alpha,E_\gamma)$. ^{22}Na level deduced γ-branching. ^{19}F(α,nγ), E = 4.7 - 6.1 MeV; measured $\sigma(E,E_\gamma)$. ^{22}Na levels deduced γ-branching. ^{19}F(α,nγ), E = 5.0 - 5.2 MeV; measured $\sigma(E_\gamma,\theta)$. ^{22}Na level deduced J, π, δ. ^{19}F(α,nγ), E = 11.2 MeV; measured $\sigma(E_n,E_\gamma,\theta_{n\gamma})$. ^{22}Na deduced levels; ^{22}Na levels deduced J, π, δ, τ.

Abstract

Electromagnetic properties of excited states of ^{22}Na below 4.6-MeV excitation energy have been studied using the $^{23}Na(^{3}He,\alpha\gamma)^{22}Na$ and $^{19}F(\alpha,n\gamma)^{22}Na$ reactions. Investigation of the decay scheme of the 4069-keV level using the $^{23}Na(^{3}He,\alpha\gamma)^{22}Na$ reaction shows a (10±3)% branch to the 1528-keV level, compared to a value of 21% reported previously. The existence of weak gamma-ray transitions from the 1983-, 2211-, and 2572-keV levels has been confirmed from gamma-ray spectra obtained above and below threshold for population of these levels via the $^{19}F(\alpha,n)^{22}Na$ reaction. A long standing controversy regarding the spin of the 1983-keV level has been resolved by gamma-ray angular distribution measurements close to threshold for the population of the 1983-keV level via the $^{19}F(\alpha,n)^{22}Na$ reaction; the results show that $J^{\pi}(1983) = 3^{+}$. Neutron-gamma correlation studies of the $^{19}F(\alpha,n\gamma)^{22}Na$ reaction, taken in conjunction with previous data, impose limitations on spins and parities of several levels and on mixing ratios of associated gamma-ray transitions. The spin-parity values are as follows, relatively unlikely assignments being bracketed: $J^{\pi}(3708) = 6^{+}(4^{\pm})$; $J^{\pi}(4069) = 4^{+}$; $J^{\pi}(4466) = 1^{-}, 2^{\pm}, 3^{-}$ or 4^{-}; $J^{\pi}(4522) = 7^{+}, 5^{\pm}(4^{-},6^{+})$.

I. INTRODUCTION

The ^{22}Na nucleus lies within a mass region where pronounced prolate deformations are known to occur. Its low-lying energy levels may be classified into a series of bands which are generally characteristic of those expected from the rotations of intrinsically deformed shapes. The large amount of experimental work devoted to this nucleus has been predominantly motivated by a desire to elucidate this classification and to extend it to higher energies.

The Brookhaven group have performed an extensive series of gamma-ray spectroscopic studies[1-6], and have interpreted their results in terms of the Nilsson model and the SU_3 classification scheme. Studies of various particle transfer reactions populating states in ^{22}Na have been made by Garrett and his collaborators[7-10]; they have considered their results in the light of the Nilsson model, and also of the extensive shell-model calculations performed by Halbert et al.[11]. The results of other experimental investigations are summarized by Endt and Van der Leun[12], and other relevant theoretical studies include the Hartree-Fock calculations by Lee and Cusson[13] and Gunye[14], the weak-coupling calculations of Wong and Zuker[15], and the Coriolis model calculations of Wasielewski and Malik[16].

A rotational-band classification for excitation energies E_x up to 5 MeV is shown in Fig. 1; it is distilled from the works of various authors[6,8,10,12,17]. Spin assignments which had not been established by model independent methods when the present work was begun are shown in parentheses. Evidence for the allocation of states to rotational bands is deduced from, for example, observation that their excitation energies follow an approximate J(J+1) dependence, the presence of enhanced intraband E2 transitions, and the values of spectroscopic factors deduced from particle transfer reactions. Many of the assignments

are quite speculative; this is particularly true for the $K^\pi = 1^-$ and 1^+ bands, and for the higher members of the other bands, whose spins have generally been deduced from model-dependent arguments. From a study of the $^{10}B(^{16}O,\alpha)^{22}Na$ reaction Del Campo et al.[17] have recently proposed extension of the $K^\pi = 3^+$, $T = 0$; $K^\pi = 0^+$, $T = 0$; and $K^\pi = 1^-$, $T = 0$ bands to spins as large as 10^+, 9^+ and 8^- respectively, at excitation energies ranging up to 13.6 MeV. It is clearly desirable that spins, parities and gamma-decay characteristics should be firmly established for all levels involved in these speculations.

In the light of these general considerations, the work described in this paper was undertaken with the following specific objectives:

I.1. Investigation of some weak gamma-ray transitions (Section II)

From studies of the reaction $^{20}Ne(^3He,p\gamma)^{22}Na$, Olness et al.[2,6] found that the 4069-keV state decays 100% to the 1983-keV state, with an upper limit of 25% on any other branches. Anttila et al.[18] studied the reaction $^{21}Ne(p,\gamma)^{22}Na$ and reported a 21% branch from the 4069-keV state to the 1528-keV 5^+ state. The only combination of spin assignments consistent with the branching-ratio and mean-lifetime ($\tau \lesssim 4$fs) results of Anttila et al., and with the restriction[12] that $J^\pi(1983) = 2^+$ or 3^+, is $J(4069) = 4$, $J^\pi(1983) = 3^+$. There appears to be no other secure experimental basis for a $J = 4$ assignment for the 4069-keV state. It has been generally conjectured[2,6] that the 4069-keV state is the 4^+ member of the $K^\pi = 0^+$, $T = 1$ band (see Fig. 1) and the analogue of the 3356-keV 4^+, $T = 1$ state of ^{22}Ne. Although the $J = 4$ assignment deduced from the results of Anttila et al. supports this conjecture, the 21% branch to the 1528-keV 5^+ state raises some problems. Assuming that the E2 component has $|M|^2 \lesssim 10$ W.u. (a conservative limit for a $\Delta K = 3$ transition as required by the classification shown in Fig. 1), the data of Anttila et al. imply

an M1 strength of greater than 0.1 W.u. for a $\Delta K = 3$ transition. The M1 strength should be doubly inhibited by the K-selection rule for interband transitions, so this result constitutes a gross violation of the K-selection rule. Because the crucial branch to the 1528-keV level was observed in complex Ge(Li) singles spectra, it was decided to check the existence of this transition by selecting the appropriate particle group in the reaction $^{23}Na(^{3}He,\alpha)^{22}Na$ and examining the spectrum of coincident gamma rays.

During their investigations of the reaction $^{19}F(\alpha,n\gamma)^{22}Na$, Baxter et al.[19] found evidence for the existence of a $(1.3 \pm 0.4)\%$ branch from the 2572-keV level to the 657-keV level. Prior to this it had been believed that the 2572-keV level decayed 81% to the ground state and 19% to the 583-keV state[1,2]. A spin assignment of 2 for the 2572-keV level is well established, but there is still some doubt about the negative parity assignment, although the weight of the evidence suggests that it is probably correct[12]. Assuming negative parity, the weak branch to the 657-keV 0^+ state would be an M2 transition of strength 0.50 ± 0.16 W.u.[19], which would be consistent with the $\Delta T = 1$ character required by the classification of Fig. 1. It was decided to study the $^{19}F(\alpha,n\gamma)^{22}Na$ reaction below and above threshold for population of the 2572-keV level in order to confirm that the gamma ray reported by Baxter et al. is in fact associated with the decay of the 2572-keV level. While this work was in progress Haas et al.[20] also reported the observation of this transition in singles spectra from the reaction $^{19}F(\alpha,n\gamma)^{22}Na$, finding a $(1.8 \pm 0.5)\%$ branch. However, there is no indication that this identification was confirmed by investigation of threshold behaviour. Haas et al. also reported previously unobserved weak branches from the 2572- and 1983-keV levels. It was decided to investigate whether these gamma rays displayed the appropriate threshold behaviour.

I.2 Measurement of the angular distribution of gamma rays from the 1983 → 583-keV transition (Section III)

The J = 3 assignment for the 1983-keV level has not been firmly established. Angular correlation measurements[1] give $J^\pi = 2^+$ or 3^+, and transfer reactions[7] indicate $J^\pi = 3^+$, 4^+, or 5^+; taken together these results give $J^\pi = 3^+$. In addition, the work of Anttila et al. (discussed in Section I.1) strongly supports $J^\pi = 3^+$. However linear polarization measurements[19] suggest $J^\pi = 2^+$. Although the accumulated evidence favours the 3^+ assignment, further investigation is desirable. For this reason, the angular distribution of gamma rays from the 1983 → 583-keV transition has been studied using the $^{19}F(\alpha,n\gamma)^{22}Na$ reaction at energies just above threshold for population of the 1983-keV state.

I.3 Angular-correlation studies of $^{19}F(\alpha,n\gamma)^{22}Na$ in collinear geometry (Section IV)

In an attempt to obtain model-independent spin assignments for some of the ^{22}Na states of interest, and multipole mixing ratios for associated gamma-ray transitions, angular-correlation measurements of the reaction $^{19}F(\alpha,n\gamma)^{22}Na$ were performed in a collinear geometry (Method II of Litherland and Ferguson[21]). Neutrons were detected at 0°, and the angular correlations of coincident gamma rays were measured for transitions from the 3708-, 4069-, 4466- and 4522-keV states. During the course of this work, Freeman et al.[22] published the results of similar measurements for the 3708-, 4466-, 4522- and 4708-keV states; however, the geometry used by these authors did not ensure good definition of nuclear alignments, and hence neither rigorous spin assignments nor accurate values of mixing ratios could be obtained.

II. INVESTIGATION OF SOME WEAK GAMMA-RAY TRANSITIONS

II.1. The $^{23}Na(^{3}He,\alpha)^{22}Na$ reaction

The decay scheme of the 4069-keV level was investigated using the $^{23}Na(^{3}He,\alpha)^{22}Na$ reaction (Q = 8161 keV). A target of approximately 300 $\mu g/cm^2$ NaBr evaporated onto a thin carbon foil was bombarded with a beam of 8.46-MeV $^{3}He^{++}$ ions from the A.N.U. EN tandem accelerator. Alpha particles emitted at 20° to the beam direction were detected with a 600 μm × 50 mm × 8 mm position-sensitive detector placed in the focal plane of a 61-cm double-focussing magnetic spectrometer[23]. The detector bias was adjusted to separate alpha and proton groups of equal magnetic rigidity. Gamma rays in coincidence with alpha particles were detected at 90° in a 12.7 cm diameter × 10.2 cm long NaI(Tl) crystal mounted with its axis vertical and its front face 4.1 cm above the target spot. Conventional fast/slow coincidence electronics were used to accumulate a two-parameter, 16-channel (position signal) × 256 channel (gamma signal), α-γ coincidence spectrum in an IBM 1800 on-line computer. Further discrimination between α-γ and p-γ coincidence events was afforded by the different transit times through the magnetic spectrometer for alphas and protons of equal energies and rigidities. The spectrometer entrance slits were set to subtend ± 2.25° vertically and ± 1.5° horizontally at the target; these settings were chosen to provide an optimum compromise between yield and resolution. The beam current was limited to 80 nA to ensure that pile-up in the gamma detector remained within acceptable limits, and also to minimise evaporation of the target material. Even so it was necessary to move to a fresh target spot every few hours.

Fig. 2 shows the spectrum of gamma rays in coincidence with alpha particles populating the 4069-keV level, obtained after running for 40 hours. The inset shows the position spectrum in coincidence with

all gamma rays, and the particle windows used to obtain the gamma-ray spectrum presented. A correction for contamination by gamma rays from the 3944-keV level was made by fitting two gaussian peaks to the position spectrum and then subtracting an appropriate fraction of the 3944-keV level spectrum from the 4069-keV level spectrum. The correction amounted to 2.4% of the total coincidence counts. The real-to-random coincidence ratio was determined from a simultaneously accumulated time spectrum, and a correction for random coincidences (5%) was made by subtracting an appropriately normalized singles spectrum from the coincidence spectrum.

The data clearly show the 2086-keV gamma ray corresponding to the main branch from the 4069-keV level, and also a weaker 2541-keV branch to the 1528-keV level. The full curve shown in Fig. 2 represents a least squares fit to the data with line shapes measured for the experimental arrangement described. Allowance was made for summing of cascade gamma rays, assuming isotropic angular distributions. The analysis yielded a branching ratio of (10 ± 3)% for the decay to the 1528-keV level; the quoted error includes allowances for statistical uncertainties, uncertainties in the detector relative efficiencies, and possible gamma-ray angular distribution effects[24].

The present result confirms the existence of a significant branch to the 1528-keV 5^+ level, as reported ty Anttila et al.[18], but the branching ratio obtained is smaller than the value of 21% reported by these authors. Assuming $\tau(4069) \lesssim 4$ fs[18], a 21% branch would require $|M|^2$ (E2) $\gtrsim$ 110 W.u. if $J^\pi(4069) = 3^+$. A branch of (10 ± 3)% would reduce this limit to $|M|^2$ (E2) $\gtrsim$ 36 W.u. which, although large, cannot be rejected[25]. Furthermore, if $J^\pi = 3^+$ is permitted for the 4069-keV level, then a 2^+ assignment for the 1983-keV level would also be permissible. Thus, the restrictions imposed by the branching ratio reported by Anttila et al., i.e. J(4069) = 4 and $J^\pi(1983) = 3^+$, are relaxed by the present result

to $J^{\pi}(4069) = 3^+, 4^{\pm}$ and $J^{\pi}(1983) = 2^+, 3^+$.

II.2. The $^{19}F(\alpha,n)^{22}Na$ reaction

The reaction $^{19}F(\alpha,n)^{22}Na$ (Q = -1950 keV) was used to study weak branches from the 1983-, 2211- and 2572-keV states. In each case singles gamma-ray spectra were obtained at bombarding energies below and above the kinematic threshold for population of the level. Targets consisted of 2 mg/cm^2 SrF_2 evaporated onto 0.25-mm thick tungsten. Both planar and coaxial Ge(Li) detectors were used. Gamma rays were identified from their energies observed at 90° to the beam direction and branching ratios were deduced from spectra taken at 0°, 55°, 90° and 125°. The results obtained are listed in Table 1, together with relevant results of previous workers. Fig. 3 shows spectra taken below and above threshold for the weak gamma rays of energies 1983, 2211, 1915 and 361 keV. The threshold behaviour of these gamma rays confirms their assignment to ^{22}Na levels as proposed by previous workers. Quantitatively the branching ratios obtained are in satisfactory agreement with those reported previously. Contributions to peaks from summing of cascade gamma rays were found to be negligible. The spectra showed no evidence of previously unreported gamma-ray transitions from ^{22}Na levels.

Assuming that the 1983-keV state has $J^{\pi} = 3^+$ and a mean lifetime of (2.40 ± 0.25)ps[20], the present branching ratio for the ground-state transition corresponds to $|M|^2$ (E2) ≤ 0.06 W.u. This is a weak E2 transition, as would be expected if $\Delta K = 3$ in accord with the rotational-band classification of Fig. 1. The shell-model calculations of Preedom and Wildenthal[26] also predict that this E2 transition should be weak ($|M|^2$ (E2) = 0.016 W.u.).

If the 2572-keV level has $J^{\pi} = 2^-$ and a mean lifetime of

(8.8 ± 0.9)ps[20], then the present result for the branching ratio to the 657-keV 0^+ state corresponds to $|M|^2$ (M2) = (0.6 ± 0.3) W.u. This is quite a strong M2 transition for this mass region[25], which supports the $\Delta T = 1$ nature of the transition required by the classification of Fig. 1.

III. ANGULAR DISTRIBUTION OF GAMMA RAYS FROM THE 1983 → 583-keV TRANSITION

The angular distribution of 1400-keV gamma rays emitted in the transition between the 1983-keV state and the 583-keV 1^+ state was measured using the reaction $^{19}F(\alpha,n\gamma)^{22}Na$ at bombarding energies E_α of 5.0, 5.1 and 5.2 MeV, close to the kinematic threshold for population of the 1983-keV state (E_α = 4.76 MeV). A target of approximately 120 μg/cm^2 BaF_2 evaporated onto a 0.25-mm thick tantalum backing was mounted at 45° to the beam direction and bombarded with beams of $^4He^{++}$ ions. The energy loss of the beam in the target was thus about 70 keV. The general arrangement was similar to that described in detail by Bell et al.[27]. Gamma rays were detected in a 40 cm^3 Ge(Li) detector rotatable in an arc of 12-cm radius centred on the target, and in a similar detector fixed at 90° relative to the incident beam direction. Singles gamma-ray spectra were simultaneously accumulated from both detectors. Data were taken with the moving detector at angles of 0°, 15°, 30°, 45°, 60°, 75° and 90° in random order, and several angles were repeated at each energy to check reproducibility. Integrated charges of 500, 400 and 300 μC at each angle were used for E_α = 5.0, 5.1 and 5.2 MeV, respectively.

Angular distributions were extracted by normalizing the yield of the 1400-keV gamma ray in the moving counter to that of the 583-keV gamma ray in the fixed counter. Appropriate corrections, totalling less than 5%,

were made for ADC dead time, attenuation of gamma rays in the target backing and anisotropy of the target-detector geometry. The latter was determined by assuming that the angular distributions of gamma rays from the long-lived 583-keV state (τ = 352 ns[12]) was isotropic. As a check the angular distributions were also extracted by normalizing the 1400-keV yield to the 583-keV yield in the same (moving) counter, which cancels out dead-time and anisotropy effects, requiring only a relative attenuation correction of less than 1.5%.

The average of the angular distributions obtained at the three bombarding energies, 5.0, 5.1 and 5.2 MeV, was compared with the predictions of the computer program MANDY of Sheldon and Van Patter[28], which assumes a statistical compound nucleus reaction mechanism. This program has been applied successfully to a number of (α,n) reactions in the 2s-1d shell (see, for example, Ref.29), and is expected to be applicable to the present case because of the low outgoing neutron energy and the high level density in the compound nucleus. A statistical analysis for the relevant excitation region in the ^{23}Na compound nucleus has been carried out previously by Seaman et al.[30], and further support for the assumption of a statistical compound nucleus reaction in the present case is provided by the similarity of the angular distributions at 5.0, 5.1 and 5.2 MeV bombarding energy (see Table 2), and that at 5.48 MeV, measured using a thick target by Warburton et al.[1].

For the calculation, using MANDY, of magnetic substate populations of ^{22}Na levels, transmission coefficients were calculated from the optical model parameters of Hodgson[31] and Bock et al.[32]. While the majority of previous authors have allowed at most an arbitrary 10% variation of population parameters from the MANDY predictions (see, for example, Ref.29), in the present work more generous allowance was made for the effects of statistical fluctuations. Because the bombarding energy in the

$^{19}F(\alpha,n)^{22}Na$ reaction was, for the levels of interest, not far above the kinematic threshold, only $\ell = 0$, $\ell = 1$ and, to a lesser extent, $\ell = 2$ neutrons should contribute significantly to the reaction cross-section. The relative contributions of these partial waves in the MANDY calculations were varied between the extremes of, on the one hand, zero contribution from $\ell = 0$ outgoing neutrons and, on the other hand, zero contribution from $\ell = 1$ outgoing neutrons; the $\ell = 2$ contribution was allowed to vary from zero to twice the value calculated from the optical model parameters. In addition the effect of varying the relative transmission coefficients for neutrons with total angular momenta $j = \ell + 1/2$ and $j = \ell - 1/2$ was investigated and found not to affect significantly the MANDY predictions.

Fig. 4 shows the averaged angular distribution for the 1983- → 583-keV transition and the best fits to the data for J(1983) = 2 or 3 and J(583) = 1 obtained using the predictions of MANDY for the magnetic substate populations of the 1983-keV level. Clearly the data are consistent only with J(1983) = 3. Also shown in Fig. 4 are the measured angular distributions for the 1952- → 583-keV decay in ^{22}Na, and the MANDY prediction for this $2^+ \rightarrow 1^+$ transition with a mixing ratio of 0.04 ± 0.06 (Ref. 4). It can be seen that the two are in good agreement even though, because of the low yield at 5.0 and 5.1 MeV, experimental angular distributions could not be averaged over bombarding energy as was done for the 1983- → 583-keV transition. The success of the MANDY predictions in the case of the 1952- → 583-keV transition is taken as further support for the validity of applying this analysis to the neighbouring 1983-keV level.

While strong arguments have been advanced above for the applicability of MANDY to the resolution of the J = (2,3) ambiguity for the 1983-keV level, it is not intended to imply that this method of analysis can be

applied indiscriminately to angular distributions from the $^{19}F(\alpha,n\gamma)^{22}Na$ reaction, even when observed close to threshold; for example, the angular distributions for the 2211- (1^-) → 657-keV (0^+) transition were found to be markedly different at 5.1 and 5.2 MeV bombarding energy (A_2 = -0.77 ± 0.07 and -0.36 ± 0.07 respectively), perhaps in part merely reflecting the fact that for a J = 1 level all the substates are substantially populated, and so the nuclear alignment is more sensitive to the precise values of the population parameters.

In summary, it is concluded from the angular distribution results that the 1983-keV level has J = 3, with the mixing ratio of the 1983- → 583-keV transition being given (see Fig. 4) by arctan δ = 0.6° ± 1.1° or arctan δ = 79° ± 1°. The phase convention for mixing ratios is that of Rose and Brink[33] and the standard errors on arctan δ were estimated using the procedures described by Archer et al.[34]. The possibility arctan δ = 79° ± 1° can be rejected since it implies a miraculously large M3 strength when taken in conjunction with branching ratio and lifetime data[20]. A 3^- assignment can also be rejected since it requires $|M|^2$ (M2) ≥ 400 W.u. (assuming a reasonable E3 strength of ≤ 100 W.u.). Thus for the 1983-keV level $J^\pi = 3^+$, and arctan δ = 0.6° ± 1.1° for the 1983- → 583-keV transition.

IV. ANGULAR-CORRELATION STUDIES OF $^{19}F(\alpha,n\gamma)^{22}Na$ IN COLLINEAR GEOMETRY

The reaction $^{19}F(\alpha,n\gamma)^{22}Na$ has been used to study the angular correlations of gamma-ray transitions from the 3708-, 4069-, 4466- and 4522-keV levels of ^{22}Na. A beam of $^4He^{++}$ ions was used to bombard a 2 mg/cm^2 target of SrF_2 evaporated onto a 0.5-mm thick tungsten backing. The target chamber arrangement was similar to that described in Section III.

Neutrons were detected in a 7.5-cm diameter × 10-cm long liquid (NE 213) scintillator placed at 0° to the beam direction and 10 cm from the target. Gamma rays were detected in two Ge(Li) counters of 50 and 30 cm^3 active volume placed 8.0 and 7.5 cm, respectively, from the target. The former counter could be rotated between 90° and 145° relative to the beam direction and was used to measure the angular correlations; the latter was fixed at 90° and served as a monitor of reaction yield.

For each Ge(Li) counter conventional fast/slow coincidence circuitry was used to select and route real and random neutron-gamma coincidence spectra into 2 × 2048 channels. The neutron pulse-shape discrimination circuit gated both coincidence circuits; therefore the fixed-counter spectra accurately monitored any changes in reaction yield, target condition, neutron detection efficiency and count-rate dependent effects. Furthermore, the coincidence-time windows and pulse-shape windows were frequently checked during the measurements.

It is known[12] that the 4708-keV level of ^{22}Na has a 40% branch to the 4069-keV level, which could introduce some population of magnetic substates of the latter level other than those directly populated by the $^{19}F(\alpha,n)^{22}Na$ reaction (for neutron detection at 0°). A preliminary excitation function was measured to find an energy at which the relative populations of the 4069- and 4708-keV levels were favourable. The 4708- → 4069-keV transition (639 keV) is obscured by the 637-keV transition between the 1528- and 891-keV levels. The intensity of the other branch from the 4708-keV level, namely 60% (2725 keV) to the 1983-keV level, was therefore compared with the intensity of the 4069-1983 = 2086-keV gamma ray. The most suitable beam energy was found to be 11.2 MeV, where the relative intensities of the 2086- and 2725-keV transitions were about 10 to 1, and this energy was used for the angular-correlation measurements. The beam current was maintained between 15 and 25 nA to limit count-rate

dependent effects on dead time and resolution. Twenty-five coincidence spectra were taken, in random order, with the movable Ge(Li) detector at angles of 90°, 115°, 125°, 135° and 145°. The typical charge per run was 200 μC.

Fig. 5 shows the sum of all coincidence spectra from the moving Ge(Li) detector. All but one of the major peaks have been identified with established gamma transitions from levels in ^{22}Na up to E_x = 5166 keV. The unidentified gamma ray has an energy of 3375 ± 3 keV. Considering levels of ^{22}Na at excitation energies below the limit imposed by kinematics and the neutron-detection threshold ($E_x \simeq 6$ MeV), the most likely origin is a transition from the level at E_x = 5317 ± 5 keV[12] having an energy of either 3380 ± 5 or 3365 ± 5 keV, corresponding to final states at 1936.9 ± 0.2 or 1951.9 ± 0.2 keV, respectively; the former possibility gives a better match of energies. The gamma-ray energies E_γ were separately obtained from internal calibration of the sum of all 90° spectra in each counter, relying mainly on the reported[12] energies of the intense ground-state transitions from the long-lived (2571.5 ± 0.3)- and (1527.9 ± 0.2)-keV levels. The values obtained from the two counters were in splendid agreement. The gamma-ray energies were averaged and combined with the known[12] excitation energies E_x of the final states to give the excitation energies E_i of the initial states listed in Table 3.

There is a peak in the spectrum of Fig. 5 which is attributed to the 2541-keV γ-ray emitted in the 4069 → 1528-keV transition. It is possible that other γ-rays could contribute to this peak, e.g. if the 5107-keV level[12] decayed to the 2572-keV level, it would produce a γ-ray of energy 2535 keV. However there is no positive evidence for the existence of such competing γ-rays. Assuming that the peak concerned arises entirely from the 4069- → 1528-keV transition, and allowing for a small contribution to the 4069- → 1983-keV peak from the first escape peak of the 2572-keV γ-ray, the 4069- → 1528-keV branch is found to be (12 ± 3)% from the 125°

data, and (12 ± 2)% from consideration of the data summed over all angles. This result provides excellent confirmation of the (10 ± 3)% value obtained in the present work from studies of the $^{23}Na(^{3}He,\alpha\gamma)^{22}Na$ reaction (Section II.1), particularly as it eliminates uncertainties arising from angular-distribution effects; it is in clear disagreement with the 21% result reported by Anttila et al.[18]. Although the present experiment was not specifically designed for lifetime determinations, conventional Doppler shift attenuation analysis of the neutron-gamma coincidence data for the 4069- → 1983-keV transition yielded an upper limit of 30 fs for the lifetime of the 4069-keV level; this result is consistent with the only previously reported value of ≤ 4 fs (Anttila et al.[18]).

Angular correlations were extracted for the 1895-, 2088-, 2177- and 2996-keV gamma rays (Table 3). They are identified with the following transitions in ^{22}Na: 4466 → 2572[22], 4069 → 1983[6], 3708 → 1528[2] and 4522 → 1528 keV[22], respectively. Here again the level energies correspond to those given in Refs. 6 and 12. The angular correlations were normalized to the total counts observed between 620 and 1480 keV in the fixed-counter spectra. Corrections were made for random coincidences (about 5%). Extensive cross checks were made between total neutron yield, integrated charge, total coincidence yields and coincidence yields of the strong 891- and 1369-keV gamma rays in both counters to ensure that all the data were self-consistent. The 2088-keV peak was imperfectly resolved from the first-escape peak of the 2572-keV gamma ray. Uncertainties introduced into determination of the 2088-keV gamma-ray yield by corrections (∿ 10%) for this contamination were estimated to be ≤ 1%.

Corrections for anisotropy in the target-detector geometry were deduced from the following measurements: (a) the angular distribution of gamma rays from the decay of the 2311-keV, $J^{\pi} = 0^{+}$ level of ^{14}N produced via the reaction $^{11}B(\alpha,n)^{14}N$ using a target of natural boron on

tungsten and a beam energy E_α of 11.2 MeV (i.e. beam conditions identical to those for the ^{22}Na observations); (b) as for (a), but with E_α = 8.0 MeV, which gave cleaner spectra; (c) observation of the angular variation in the intensity of gamma rays from a 1-mm diameter ^{60}Co source placed at the position of the beam spot observed on the target; and (d) direct measurement of the geometry. These four procedures gave mutually compatible results. At 90°, the correction relative to 145° was (5.0 ± 2.5)%; it was less at other angles. Corrections to the nominal angle were less than ± 1°.

Fig. 6 shows the measured correlations. The error bars include uncertainties arising from statistical effects, background interpolations under the gamma-ray peaks, and the anisotropy corrections. Fig. 7 shows the results of least-squares fits to the data calculated for various possible spin sequences; χ^2 is plotted against arctan δ, where δ is the multipole mixing ratio. These fits are shown by the full curves in Fig. 6. For neutron detection at 0°, the $^{19}F(\alpha,n)^{22}Na$ reaction can populate directly the m = 0, ± 1 magnetic substates of the final nucleus. Since the effective angle subtended at the target by the liquid scintillator for neutrons corresponding to the levels of interest was about ± 15°, the population of the next higher substate (m = ±2) may be estimated[21] as approximately 7%. The following substate restrictions were therefore adopted:

$$0 \leq P(m = 0) \leq 1$$

$$0 \leq P(m = \pm 1) \leq 1$$

$$0 \leq P(m = \pm 2) \leq 0.1$$

$$\sum_{m=o}^{J} P(m) = 1$$

The P(m) are defined so that, for example, P(m = ±1) is the sum of the equal populations of the m = +1 and m = -1 magnetic substates. Table

presents the results of Legendre-polynomial fits to the distributions, and the mixing ratios permitted by the results of the least-squares fits of Fig. 7 for various spin sequences.

IV.1. The 3708-keV level

From their coincidence studies of the $^{20}Ne(^{3}He,p\gamma)^{22}Na$ reaction, Poletti et al.[2] report that this level decays 65% to the 891-keV 4^+ state and 35% to the 1528-keV 5^+ state. Warburton et al.[35] used Doppler-shift attenuation studies of the 2817-keV transition to the 891-keV level to determine the mean lifetime of the 3708-keV level as 52 ± 17 fs. These two pieces of information together imply that the spin of the level is 3, 4, 5 or 6, and on this basis it has been generally assumed that the 3708-keV level is the 6^+ member of the $K^\pi = 3^+$, T = 0 rotational band. The level is strongly populated[10] in the heavy-ion reaction $^{12}C(^{14}N,\alpha)^{22}Na$, which is consistent with a high-spin assignment. Recently Haas et al.[20] have made further Doppler-shift measurements of the 2817-keV gamma ray, obtaining a value of 80 ± 40 fs for the lifetime; they have re-analysed the data of Warburton et al.[35] to obtain a value of 75 ± 25 fs, and recommend that a lifetime of 77 ± 20 fs be adopted. Freeman et al.[22] have studied the reaction $^{19}F(\alpha,n\gamma)^{22}Na$, and report branching ratios of (75 ± 7)% and (25 ± 7)% to the 891- and 1528-keV levels, respectively. Their angular-correlation measurements of the 3708- → 891-keV transition are consistent with a J = 6 assignment for the 3708-keV level. However their neutron detector at 0° subtended a half-angle of 38°; hence there was little restriction on substate populations, and no rigorous spin assignments could be made.

The excitation energy obtained in the present work from the transition to the 1528-keV level is 3704.4 ± 1.0 keV (Table 3). This is significantly different from the value 3708 ± 1 keV given by Warburton et

al.[6,35]. However, if the gamma ray of energy 2818.0 ± 0.7 keV is ascribed to a transition to the 891-keV level, then the excitation energy obtained is 3708.9 ± 0.8 keV, in good agreement with the result of Warburton et al. But the latter gamma ray could be contaminated by 2818-keV radiation from the 4770- → 1952-keV transition (a 100% branch[6]). For this reason no attempt was made to analyse the angular correlation of the 2818-keV gamma ray. It is not obvious that previous authors who have studied the 3708- → 891-keV transition have considered this possible contamination.

In order to investigate the possibility that the 4770- → 1952-keV transition could cause difficulties in studying the 3708- → 891-keV transition, singles spectra from the reaction $^{19}F(\alpha,n\gamma)^{22}Na$ were taken below and above threshold for population of the 4770-keV state. A 50 cm^3 Ge(Li) detector was located at 90° to the beam direction, and the target consisted of 3 mg/cm^2 SrF_2 on a thick tungsten backing. The kinematic thresholds for population of the 3708- and 4770-keV levels are E_α = 6849- and 8136-keV, respectively. At E_α = 8000 keV, the relevant γ-ray peak was found to have an energy of 2814.8 ± 0.7 keV; at E_α = 9000 keV, i.e. above threshold for the 4770-keV level, the peak energy was found to be 2817.6 ± 0.5 keV. These results indicate that for beam energies above threshold for the 4770-keV level, the 4770- → 1952-keV transition cannot be ignored in studying the 3708- → 891-keV transition. The data obtained at E_α = 8000 keV produce a level excitation energy of 3705.7 ± 0.7 keV; combining this result with the value deduced from the present (n,γ) coincidence data (3704.4 ± 1.0 keV) yields a best value of E_x = 3705.2 ± 0.5 keV.

It follows from these investigations that all previous studies of the 3708- → 891-keV transition using the $^{19}F(\alpha,n\gamma)^{22}Na$ reaction at bombarding energies above the 4770-keV level threshold should be examined to ensure that account was taken of possible competition from the 4770- → 1952-keV transition. This applies, for example, to the excitation

energy and lifetime determinations by Warburton et al.[35], and to the branching-ratio and angular-correlation studies of Freeman et al.[22].

The present angular-correlation data for the 2176-keV gamma ray to the 1528-keV 5^+ state strongly favour J(3708) = 6. The next most likely assignment is J = 4, and this can be rejected at the 3% confidence limit. For J = 6, arctan $\delta = -75° \pm 7°$, i.e. $\delta = -3.7\ ^{+1.4}_{-4.4}$. The $J^\pi = 6^-$ possibility can be rejected because this would imply $|M|^2$ (M2) $\geq$ 325 W.u., assuming a mean lifetime of 77 ± 20 fs[20] and a branching ratio of 35%[2]. For $J^\pi = 6^+$, $|M|^2$ (E2) = 20 ± 6 W.u., and $|M|^2$ (M1) = $(3\ ^{+10}_{-\ 6}) \times 10^{-4}$ W.u.

IV.2. The 4069-keV level

The excitation energy obtained from the present results is 4071.4 ± 0.6 keV (Table 3), which is in good agreement with the value of 4069 ± 2 keV listed by Warburton et al.[6]. Evidence for a $J^\pi = 4^+$ assignment for this level, and for its identification as the 4^+ member of the $K^\pi = 0^+$, T = 1 band, has been discussed in detail in Sections I and II of this paper. The present angular-correlation data for the 2088-keV transition to the 1983-keV level (shown in Section III to have $J^\pi = 3^+$) are consistent with J(4069) = 3 or 4; all other possibilities are excluded by previous lifetime and branching-ratio data. If the lifetime of the 4069-keV level is taken to be $\leq$ 4 fs (Anttila et al.[18]), then the mixing ratio obtained in the present work for J(4069) = 3 corresponds to a minimum quadrupole strength of 500 W.u. if E2, or 2.5×10^4 W.u. if M2. Thus the present results, together with the lifetime value of Anttila et al., show that the spin of the 4069-keV state is 4, and that for the 2088-keV transition arctan $\delta = 0° \pm 4°$. Assuming the branching ratio obtained in the present work (Section II.1), the M1 strength of the 2088-keV transition is found to be $\geq$ 0.75 W.u. This is quite strong, and implies a T-allowed

transition, as required by the classification of Fig. 1. Because the value obtained for δ is consistent with zero, and only an upper limit is available for the lifetime of the state, no limitations can be placed on the E2 strength of the 4069- → 1983-keV transition.

IV.3. The 4466-keV level

On the basis of its selective population in the $^{12}C(^{14}N,\alpha)^{22}Na$ reaction, Hallock et al.[10] tentatively identified the 4466-keV level as the 4^- member of the $K^\pi = 1^-$, T = 0 band based on the 2211-keV 1^- state. The angular-correlation data of Freeman et al.[22] for the 1894-keV transition to the 2572-keV level are consistent with a pure E2 transition from a 4^- to a 2^- state; however, as indicated previously, their experimental geometry did not ensure good definition of nuclear alignments, and hence rigorous spin assignments were not possible. The decay scheme of the 4466-keV level has not yet been investigated in detail; the 1894-keV transition to the 2572-keV state is the only gamma-decay branch yet reported[22]. Gamma-ray singles spectra from the reaction $^{19}F(\alpha,n\gamma)^{22}Na$ taken during the present work confirm that the 1894-keV gamma-ray displays the correct threshold behaviour for its identification with a transition from the 4466-keV level; the kinematic threshold for population of the 4466-keV state is E_α = 7768 keV, and the 1894-keV gamma ray was clearly present at E_α = 8000 keV and higher energies, but absent at E_α = 7500 keV. Freeman et al. measured a mean lifetime for the level of $145\ ^{+65}_{-40}$ fs. If it is assumed that the 1894-keV gamma ray represents a major branch, i.e. $\geq$ 10%, then the spin and parity may be restricted, on the basis of this lifetime value, to 0^-, $1^\pm$, $2^\pm$, $3^\pm$, or 4^-. The present angular correlation for the transition to the 2572-keV level is clearly anisotropic (Fig. 6), which eliminates the 0^- possibility. The mixing ratios obtained for J = 1 and 3 (Table 3) require implausibly strong M2 components for positive

parity ($|M|^2(M2) \geq 12$ W.u. and 36 W.u. respectively, assuming again that $J^\pi(2572) = 2^-$ and that the observed 1894-keV transition represents a branch of greater than 10%). Hence, the combination of lifetime and angular-correlation data restricts $J^\pi(4466)$ to 1^-, $2^\pm$, 3^- or 4^-. If $J^\pi = 4^-$, and if the branching ratio for the 1894-keV transition is assumed to be 50%, then the E2 strength of the transition is $31\ ^{+12}_{-10}$ W.u.

The excitation energy obtained from the present work, 4467.0 ± 0.7 keV, is in good agreement with previous values[6,22].

IV.4. The 4522-keV level

Warburton et al.[6] suggested that the $J^\pi = 7^+$ member of the $K^\pi = 3^+$, T = 0 band based on the ground state of ^{22}Na should lie in the region of excitation energy from 4.4 to 5.3 MeV. Garrett et al.[9] found that the 4522-keV state is weakly populated in one- and two-nucleon transfer reactions, and that it may therefore be a high-spin state. On the basis of its selective population in the $^{12}C(^{14}N,\alpha)^{22}Na$ reaction, Hallock et al.[10] suggested that the 4522-keV state is the 7^+ member of the $K^\pi = 3^+$, T = 0 band. Del Campo et al.[17] found that the 4522-keV state is populated in the $^{10}B(^{16}O,\alpha)^{22}Na$ reaction with a strength and angular distribution consistent with the predictions of Hauser-Feshbach calculations for $J^\pi = 7^+$. Freeman et al.[22] found a 2994-keV transition between the 4522-keV level and the 1528-keV 5^+ state; no other information on the decay scheme of the level has been published. Gamma-ray singles spectra from the reaction $^{19}F(\alpha,n\gamma)^{22}Na$ taken during the present work confirm that the 2994-keV gamma-ray displays the correct behaviour for its identification with a transition from the 4522-keV level; the kinematic threshold for population of the 4522-keV state is E_α = 7836 keV, and the 2994-keV gamma ray was clearly present at E_α = 8000 keV and higher energies, but absent at E_α = 7500 keV. The angular correlation obtained by Freeman et al.[22] for

this transition was consistent with a pure E2 transition between 7^+ and 5^+ states, but a rigorous spin assignment could not be made. They also measured the mean lifetime of the 4522-keV level to be $115\ ^{+50}_{-35}$ fs. On the basis of this lifetime, and assuming conservatively that the transition to the 1528-keV level represents a branch of greater than 2%, the spin and parity of the 4522-keV level may be restricted to $J^\pi = 3^+$, $4^\pm$, $5^\pm$, $6^\pm$ or 7^+. The mixing ratios required by the present angular-correlation data (Table 3) for the transition to the 1528-keV state eliminate $J^\pi = 3^+$, 4^- and 6^-, provided that the transition represents a branch of greater than 0.01%, 14% and 20%, respectively (the requisite transition strengths would be $|M|^2(M3) \gtrsim 30$ W.u., $|M|^2(M2) \gtrsim 3$ W.u. and $|M|^2(M2) \gtrsim 3$ W.u., respectively). In addition J = 3, 4 and 6 assignments can be rejected at 3%, 3% and 1% confidence levels, respectively. Thus, the combined lifetime and angular-correlation data require $J^\pi = 4^+$, $5^\pm$, 6^+ or 7^+, and strongly favour $J^\pi = 5^\pm$ or 7^+. If $J^\pi = 7^+$, then the E2 transition to the 1528-keV 5^+ state has a strength of 8 ± 3 W.u., assuming that the transition is a 100% branch; this is a reasonable assumption, since the only other possibly significant decay mode would be to the 3708-keV 6^+ state, which Freeman et al. find to be less than 3%.

The excitation energy obtained in the present work (4523.4 ± 0.7 keV) is in good agreement with previous values[6,22].

V. CONCLUSIONS

The results reported in this paper may be summarized as follows:

(a) Particle-gamma coincidence studies of the reaction $^{23}Na(^3He,\alpha\gamma)^{22}Na$ show that the 4069-keV level of ^{22}Na has a branch of (10 ± 3)% to the 1528-keV 5^+ state. Investigation of the spectrum of gamma rays emitted in coincidence with neutrons from the reaction $^{19}F(\alpha,n\gamma)^{22}Na$

confirms this result, yielding a value of (12 ± 2)%.

(b) Evidence for the existence of several weak gamma transitions reported by other workers from studies of the reaction $^{19}F(\alpha,n\gamma)^{22}Na$ has been placed on a secure footing by taking data below and above threshold for population of the initial state involved. The results are shown in Table 1.

(c) The angular distribution of 1400-keV gamma rays from the 1983-keV state populated in the reaction $^{19}F(\alpha,n\gamma)^{22}Na$ was studied at energies close to the kinematic threshold; the results resolve the long-standing $J^\pi = 2^+$ or 3^+ ambiguity for the 1983-keV state, which is shown to have $J^\pi = 3^+$.

(d) Angular-correlation studies of the reaction $^{19}F(\alpha,n\gamma)^{22}Na$ were made in collinear geometry. The results, taken in conjunction with other data, impose limitations on spins and parities of several levels, and on the mixing ratios of associated gamma-ray transitions. The spin-parity values are as follows:

$J^\pi(3708) = 6^+$, with $J = 4$ rejected at the 3% confidence level;

$J^\pi(4069) = 4^\pm$;

$J^\pi(4466) = 1^-, 2^\pm, 3^-$ or 4^-;

$J^\pi(4522) = 5^\pm$ or 7^+, with $J^\pi = 4^-$ and 6^+ rejected at the 3% and 1% confidence levels, respectively.

The data obtained on spins and parities provide a more substantial basis than previously existed for the assignments assumed in the rotational-band classification of Fig. 1. It has been shown previously[4,22] that intraband E2 and M1 transition strengths are in reasonable agreement with the predictions of the rotational model. Table 4 lists available information on E2 and M1 transitions within the ground-state band. The data are taken from previous compilations[12,22], except that the results obtained in

the present work are given for the $3708(6^+) \rightarrow 1528(5^+)$ transition. It is assumed for the sake of the present discussion that the spin-parity assignments of Fig. 1 are correct. The intrinsic quadrupole moments Q_o have been deduced from the E2 strengths, and the quantity (g_K-g_R) from the M1 strengths. It is seen that Q_o is approximately constant within the band, implying that the relative E2 strengths are in approximate agreement with the predictions of the rotational model. The internal consistency of the (g_K-g_R) values is only fair, but they are in reasonable agreement with the value of (0.056 ± 0.012) deduced[4] from the measured magnetic moments of the ground state and the 583-keV state. The rotational model predicts[4,22] that the E2/M1 mixing ratios for transitions within the ground-state band should be large and negative, in agreement with the values in Table 4. The picture presented thus far of general agreement between experiment and the predictions of the simple rotational model is marred by the observation of a substantial branch from the 4069-keV state (assumed $J^\pi = 4^+$, $T = 1$) to the 1528-keV state ($J^\pi = 5^+$, $T = 0$). Although the branching ratio obtained in the present work is smaller than that previously reported[18], it still corresponds to an M1 transition of strength $|M|^2(M1) \gtrsim 0.03$ W.u. (assuming $\tau(4069) \lesssim 4$ fs[18] and $|M|^2(E2) \lesssim 10$ W.u.). According to the rotational-model classification, the transition would have $\Delta T = 1$, $\Delta K = 3$, and would be doubly-inhibited by the K-selection rule. But a strength of $|M|^2 \gtrsim 0.03$ W.u. falls within the upper half of the distribution of T-allowed M1 strengths for this mass region[25], and thus the observed transition presents a significant difficulty for the simple rotational model. Probably this difficulty could be overcome by assuming substantial mixing of other K-values in the 4069-keV level, but this would be at the expense of the simplicity, and hence the attractiveness, of the model.

Preedom and Wildenthal[26] found that the shell model was able to

account for the observed "rotational" properties of positive-parity states in ^{22}Na as a consequence of coherent motion among the six extra-core nucleons. Indeed, the shell-model results agreed with data which deviated from the predictions of the simple rotational model; for example, the shell model gave a better description of the J-dependence of excitation energies of levels within a rotational band than did the rotational model. Freeman et al.[22] found that their measurements of M1 and E2 transition strengths in ^{22}Na were in remarkably close agreement with the predictions of Preedom and Wildenthal. From Table 4 it is clear that for the $3708(6^+) \rightarrow 1528(5^+)$ transition, the shell-model predictions are in excellent agreement with the new results reported in this paper.

Although the simple rotational model has had striking success in accounting for the general features of the level scheme and electromagnetic transition rates in ^{22}Na, deficiencies become evident when detailed comparison is made with experiment. Such deficiencies cannot be overcome without increasing the complexity, and hence decreasing the aesthetic appeal, of the model. On the other hand, recent shell-model calculations display impressive agreement with experiment. Freeman et al.[22] point out that the predictions of the shell model and the rotational model diverge more strongly when higher-spin states are considered. It is therefore of great interest to investigate the lifetimes and decay modes of the high-spin members of rotational bands recently suggested by Del Campo et al.[17].

VI. ACKNOWLEDGMENTS

The authors are grateful to Dr. J.V. Thompson, Dr. L.E. Carlson and Mr. K.I. Hong for assistance with some parts of the data acquisition and analysis.

TABLE 1

Branching ratios for some weak gamma-ray transitions in ^{22}Na

Initial State (keV)	Kinematic Threshold in $^{19}F(\alpha,n)^{22}Na$ (keV)	Final State (keV)	E_γ (keV)	Branching Ratio (%)			
				Warburton et al.[1]	Baxter et al.[19]	Haas et al.[20]	Present Work
1983	4761	0	1983	< 2		1.7 ± 0.3	1.9 ± 0.3
		583	1400	100		98.3 ± 0.3	98.1 ± 0.3
2211	5037	0	2211	1 ± 1			1.7 ± 0.5
		657	1554	99 ± 1			98.3 ± 0.5
2572	5474	0	2572	82 ± 5	80 ± 3	75 ± 2	73.0 ± 4.0
		583	1989	18 ± 5	19 ± 3	21 ± 2	23.5 ± 3.0
		657	1915	< 5	1.3 ± 0.4	1.8 ± 0.5	2.5 ± 1.0
		2211	361	< 7		2.4 ± 1.0	1.0 ± 0.3

TABLE 2

Legendre polynomial fits to the angular-distribution data for the 1400-keV gamma ray.

E_α (MeV)	a_2*	a_4*
5.0	0.44 ± 0.03	-0.17 ± 0.04
5.1	0.35 ± 0.04	-0.20 ± 0.04
5.2	0.40 ± 0.04	-0.06 ± 0.04
average	0.40 ± 0.02	-0.14 ± 0.03

* $a_i = A_i/A_o\ Q_i$, where $Q_2 = 0.997$ and $Q_4 = 0.971$.

TABLE 3

Gamma-ray energies and angular-correlation results

E_i [a] (Initial Level) (keV)	E_γ [b] (keV)	E_f [c] (Final Level) (keV)	Legendre Polynomial Coefficients [d] a_2	a_4	$J_i \rightarrow J_f$	arctan δ [e]
3704.4 ± 1.0	2176.5 ± 1.0	1527.9 ± 0.2	0.65 ± 0.15	0.92 ± 0.21	4 → 5	+68° ± 12°
					6 → 5	-75° ± 7°
4071.4 ± 0.6	2088.2 ± 0.5	1983.2 ± 0.3	-0.26 ± 0.10	0.14 ± 0.16	4 → 3	0° ± 4°
					3 → 3	64° ± 24°
4467.0 ± 0.7	1895.5 ± 0.6	2571.5 ± 0.3	0.56 ± 0.26	-0.11 ± 0.31	1 → 2	-55° ± 25°; +35° ± 15°
					2 → 2	-35° ± 40°
					3 → 2	-50° ± 25°
					4 → 2	$-4^{\circ}\ {}^{+16^{\circ}}_{-24^{\circ}}$ [f]
4523.4 ± 0.7	2995.5 ± 0.6	1527.9 ± 0.2	0.40 ± 0.08	-0.17 ± 0.10	3 → 5	+27° ± 18°
					4 → 5	+38° ± 15°
					5 → 5	-41° ± 8°
					6 → 5	-26° ± 5°
					7 → 5	1° ± 4°
3708.9 ± 0.8	2818.0 ± 0.7	890.89 ± 0.17	—	—		

[a] Deduced from $E_i = E_\gamma$ (this work) + E_f (Ref. 12).

[b] This work.

[c] Ref. 12.

[d] $a_i = A_i/A_o\, Q_i$, where $Q_2 = 0.98$, $Q_4 = 0.96$.

[e] Standard errors calculated using the procedure of Ref. 34.

[f] A deeper minimum in the χ^2 plot at arctan $\delta = -60°$ can be rejected on the grounds of excessive octupole enhancement.

TABLE 4

Summary of available information on E2 and M1 transition strengths within the $K^{\pi} = 3^{+}$ rotational band based on the ground state of ^{22}Na. It is assumed that the spin-parity assignments of Fig. 1 are correct. The data for the 3708- → 1528-keV transition are from the present work; other data are taken from the compilations of references 12 and 22. The intrinsic quadrupole moment Q_o and the quantity $(g_K - g_R)$ have been calculated from the data using rotational-model expressions. The shell-model predictions for $|M|^2(E2)$ and $|M|^2(M1)$ are from the calculations of Ref. 26.

Transition (energies in keV)	δ(E2/M1)	$\|M\|^2(E2)$ (W.u.)	Q_o (barns)	$\|M\|^2(M1)$ (W.u.)	$g_K - g_R$	Shell-Model Predictions	
						$\|M\|^2(E2)$ (W.u.)	$\|M\|^2(M1)$ (W.u.)
$891(4^+) \rightarrow 0(3^+)$	$-(3.1 \pm 0.3)$	24.9 ± 1.2	0.512 ± 0.012	$(2.8 \pm 0.3) \times 10^{-4}$	0.035 ± 0.002	24.6	4.2×10^{-4}
$1528(5^+) \rightarrow 0(3^+)$		5.3 ± 0.4	0.48 ± 0.02			5.7	
$1528(5^+) \rightarrow 891(4^+)$	$-(2.00 \pm 0.15)$	15 ± 5	0.42 ± 0.06	$(2.2 \pm 0.7) \times 10^{-4}$	0.025 ± 0.004	21.6	7.8×10^{-4}
$3708(6^+) \rightarrow 891(4^+)$		11 ± 3.5	0.52 ± 0.08			8.7	
$3708(6^+) \rightarrow 1528(5^+)$	$-(3.7\ ^{+\ 4.4}_{-\ 1.4})$	20 ± 6	0.52 ± 0.09	$(9\ ^{+\ 10}_{-\ 6}) \times 10^{-4}$	0.047 ± 0.022	15.6	1.0×10^{-3}
$4522(7^+) \rightarrow 1528(5^+)$		8 ± 3	0.38 ± 0.07			10.4	
$4522(7^+) \rightarrow 3708(6^+)$		< 240		$< 2.3 \times 10^{-2}$		12.8	1.3×10^{-3}

REFERENCES

1. E.K. Warburton, J.W. Olness and A.R. Poletti, Phys. Rev. 160, 938 (1967).

2. A.R. Poletti, E.K. Warburton, J.W. Olness and S. Hechtl, Phys. Rev. 162, 1040 (1967).

3. A.R. Poletti, E.K. Warburton and J.W. Olness, Phys. Rev. 164, 1479 (1967).

4. E.K. Warburton, A.R. Poletti and J.W. Olness, Phys. Rev. 168, 1232 (1968).

5. P. Paul, J.W. Olness and E.K. Warburton, Phys. Rev. 173, 1063 (1968).

6. J.W. Olness, W.R. Harris, P. Paul and E.K. Warburton, Phys. Rev. C1, 958 (1970).

7. J.D. Garrett, R. Middleton, D.J. Pullen, S.A. Andersen, O. Nathan and O. Hansen, Nucl. Phys. A164, 449 (1971).

8. J.D. Garrett, R. Middleton and H.T. Fortune, Phys. Rev. C4, 165 (1971).

9. J.D. Garrett, H.T. Fortune and R. Middleton, Phys. Rev. C4, 1138 (1971).

10. J.N. Hallock, H.A. Enge, A. Sperduto, R. Middleton, J.D. Garrett and H.T. Fortune, Phys. Rev. C6, 2148 (1972).

11. E.C. Halbert, J.B. McGrory, B.H. Wildenthal and S.P. Pandya, Advances in Nuclear Physics 4, 315 (1970).

12. P.M. Endt and C. Van der Leun, Nucl. Phys. A214, 1 (1973).

13. H.C. Lee and R.Y. Cusson, Phys. Lett. 39B, 453 (1972).

14. M.R. Gunye, Phys. Lett. 47B, 219 (1973).

15. S.K.M. Wong and A.P. Zuker, Phys. Lett. 36B, 437 (1971).

16. P. Wasielewski and F.B. Malik, Nucl. Phys. A160, 113 (1971).

17. J.G. del Campo, J.L.C. Ford, R.L. Robinson, P.H. Stelson and S.T. Thornton, Phys. Rev. C9, 1258 (1974).

18. A. Anttila, M. Bister, and E. Arminen, Z. Physik 234, 455 (1970).

19. A.M. Baxter, B.W.J. Gillespie and J.A. Kuehner, Can. J. Phys. 48, 2434 (1970).

20. F. Haas, R.M. Freeman, J.F. Castillo and A. Gallmann, Phys. Rev. C8, 2169 (1973).

21. A.E. Litherland and A.J. Ferguson, Can. J. Phys. 39, 788 (1961).

22. R.M. Freeman, F. Haas, B. Heusch, J.F. Castillo, J.W. Olness and A. Gallmann, Phys. Rev. C8, 2182 (1973).

23. R.V. Elliott, K.W. Carter and R.H. Spear, Nucl. Instr. and Meth. 59, 29 (1968).

24. R.V. Elliott, T.R. Ophel and R.H. Spear, Nucl. Phys. A115, 673 (1968).

25. P.M. Endt and C. Van der Leun, Atomic Data and Nuclear Data Tables 13, 67 (1974).

26. B.M. Preedom and B.H. Wildenthal, Phys. Rev. C7, 1633 (1972).

27. R.A.I. Bell, J.V. Thompson, I.G. Graham and L.E. Carlson, Nucl. Phys. A222, 477 (1974).

28. E. Sheldon and D.M. Van Patter, Rev. Mod. Phys. 38, 143 (1966).

29. D.A. Viggars, P.A. Butler, P.E. Carr, L.L. Gadeken, L.L. Green, A.N. James, P.J. Nolan and J.F. Sharpey-Schafer, Journ. of Phys. A7, 360 (1974).

30. G.G. Seaman, R.B. Leachman and G. Dearnaley, Phys. Rev. 153, 1194 (1967).

31. P.E. Hodgson, Ann. Rev. Nucl. Sci. 17, 1 (1967).

32. R. Bock, P. David, H.H. Duhm, H. Hefele, U. Lynen and R. Stock, Nucl. Phys. A92, 539 (1967).

33. H.J. Rose and D.M. Brink, Rev. Mod. Phys. 39, 306 (1967).

34. N.P. Archer, W.V. Prestwich and G.L. Keech, Nucl. Instr. and Meth. 44, 114 (1966).

35. E.K. Warburton, L.E. Carlson, G.T. Garvey, D.A. Hutcheon and K.P. Jackson, Nucl. Phys. A136, 160 (1969).

FIGURE CAPTIONS

Fig. 1. Rotational band classification of ^{22}Na states for $E_x < 5$ MeV. Excitation energies (in keV) are taken from reference 12 for $E_x < 3.4$ MeV, and from reference 6 for $E_x > 3.4$ MeV. Possible Nilsson configurations are indicated, assuming for each band that an unpaired nucleon in the $3/2^+[211]$ orbit is coupled to an unpaired nucleon in the orbit shown.

Fig. 2. The spectrum of gamma rays in coincidence with alpha particles populating the 4069-keV level of ^{22}Na. The inset shows windows set on the alpha-particle position spectrum. The full curve is a line shape fit obtained as described in the text. All energies are in keV. The 2086- and 1400-keV gamma rays arise from the cascade 4069 → 1983 → 583 keV, and the 2541- and 1528-keV gamma rays from the cascade 4069 → 1528 → 0 keV.

Fig. 3. Ge(Li) spectra showing threshold behaviour of the following weak gamma rays from the reaction $^{19}F(\alpha,n\gamma)^{22}Na$:

(a) $E_\gamma = 1983$ keV, $E_{th} = 4761$ keV;

(b) $E_\gamma = 2211$, $E_{th} = 5037$;

(c) $E_\gamma = 1915$, $E_{th} = 5474$;

(d) $E_\gamma = 361$, $E_{th} = 5474$.

All energies shown in the diagram are in keV. The arrows indicate the positions expected for appropriate gamma rays. The data have been smoothed by a three-point averaging procedure.

Fig. 4. Angular-distribution data and χ^2-analysis for the 1983- → 583-keV transition (data averaged over 5.0, 5.1 and 5.2 MeV bombarding energy) and for the 1952- → 583-keV transition (data obtained at 5.2 MeV only). Magnetic substate populations have been allowed to vary as described in the text. The horizontal error bar on the χ^2 plot for the 1952- → 583-keV transition indicates the mixing-ratio range determined by Warburton et al.[4]

Fig. 5. Portion of Ge(Li) spectrum of gamma rays in coincidence with neutrons emitted at 0° from the reaction $^{19}F(\alpha,n\gamma)^{22}Na$ at E_α = 11.2 MeV. The data shown represent the sum of spectra taken at 90°, 115°, 125°, 135° and 145° with the moving detector during the angular-correlation measurements. To simplify presentation the spectrum has been compressed by adding channel contents in pairs. Transitions between states in ^{22}Na are identified. All energies are in keV.

Fig. 6. Angular correlation data for the reaction $^{19}F(\alpha,n\gamma)^{22}Na$. The full curves represent best fits to the gamma-ray distributions for various spin sequences. For small values of $\cos^2\theta$, the following pairs of curves are very similar, and in each case have been represented by a single curve: (i) 4466 → 2572, J = 2 and 4; (ii) 4522 → 1528, J = 3 and 4; (iii) 4522 → 1528, J = 5 and 7.

Fig. 7. Results of least squares fits to the angular distributions of Fig. 6 for various spin sequences. Confidence levels for the χ^2 statistic are indicated.

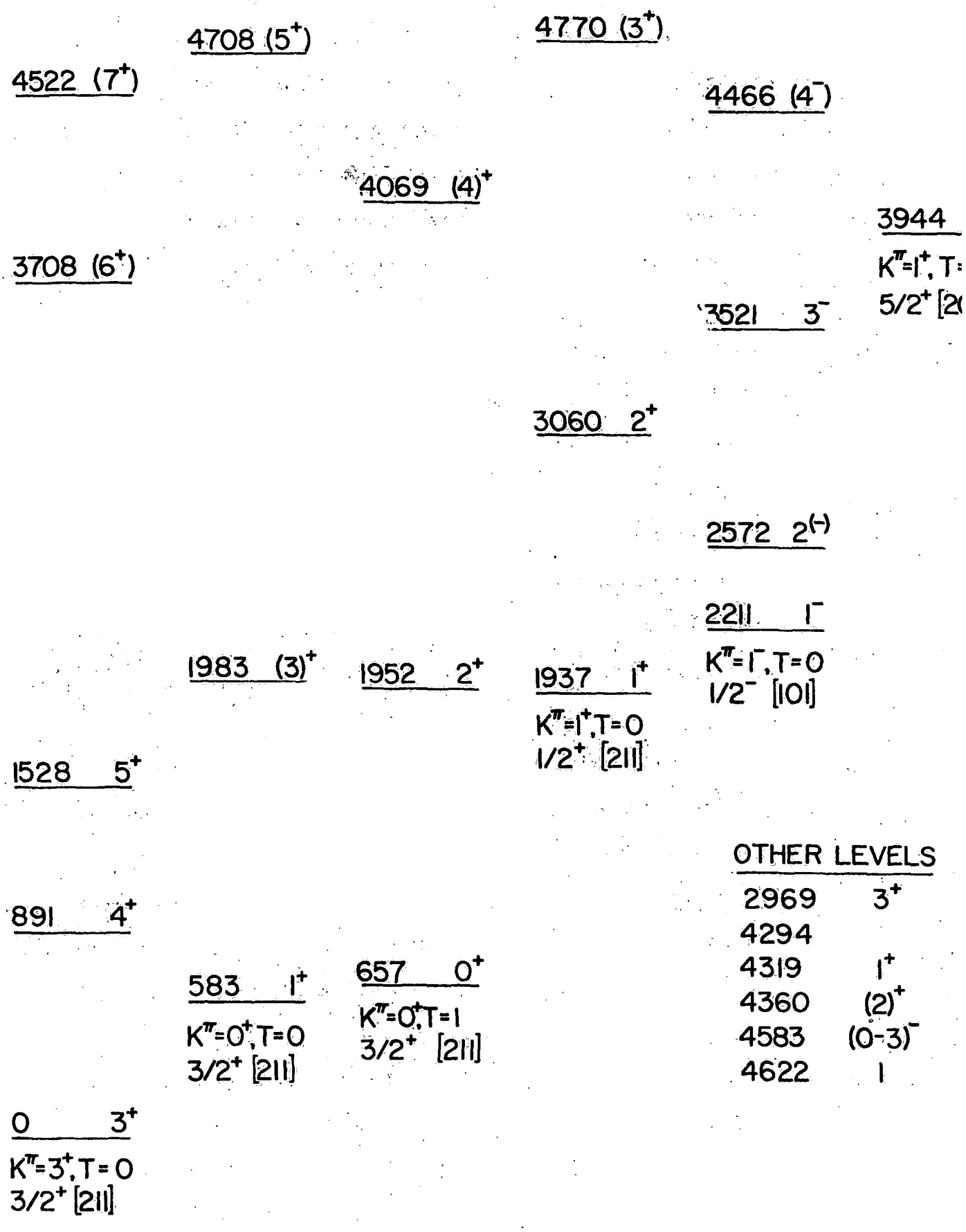
4708 (5+)
4770 (3+)
4522 (7+)
4466 (4−)
4069 (4)+
3944
K=1+, T=
5/2+ [2
3708 (6+)
3521 3−
3060 2+
2572 2(−)
2211 1−
K=1−, T=0
1/2− [101]
1983 (3)+
1952 2+
1937 1+
K=1+, T=0
1/2+ [211]
1528 5+
OTHER LEVELS
2969 3+
4294
4319 1+
4360 (2)+
4583 (0-3)−
4622 1
891 4+
583 1+
K=0+, T=0
3/2+ [211]
657 0+
K=0+, T=1
3/2+ [211]
0 3+
K=3+, T=0
3/2+ [211]

FIG. 1.

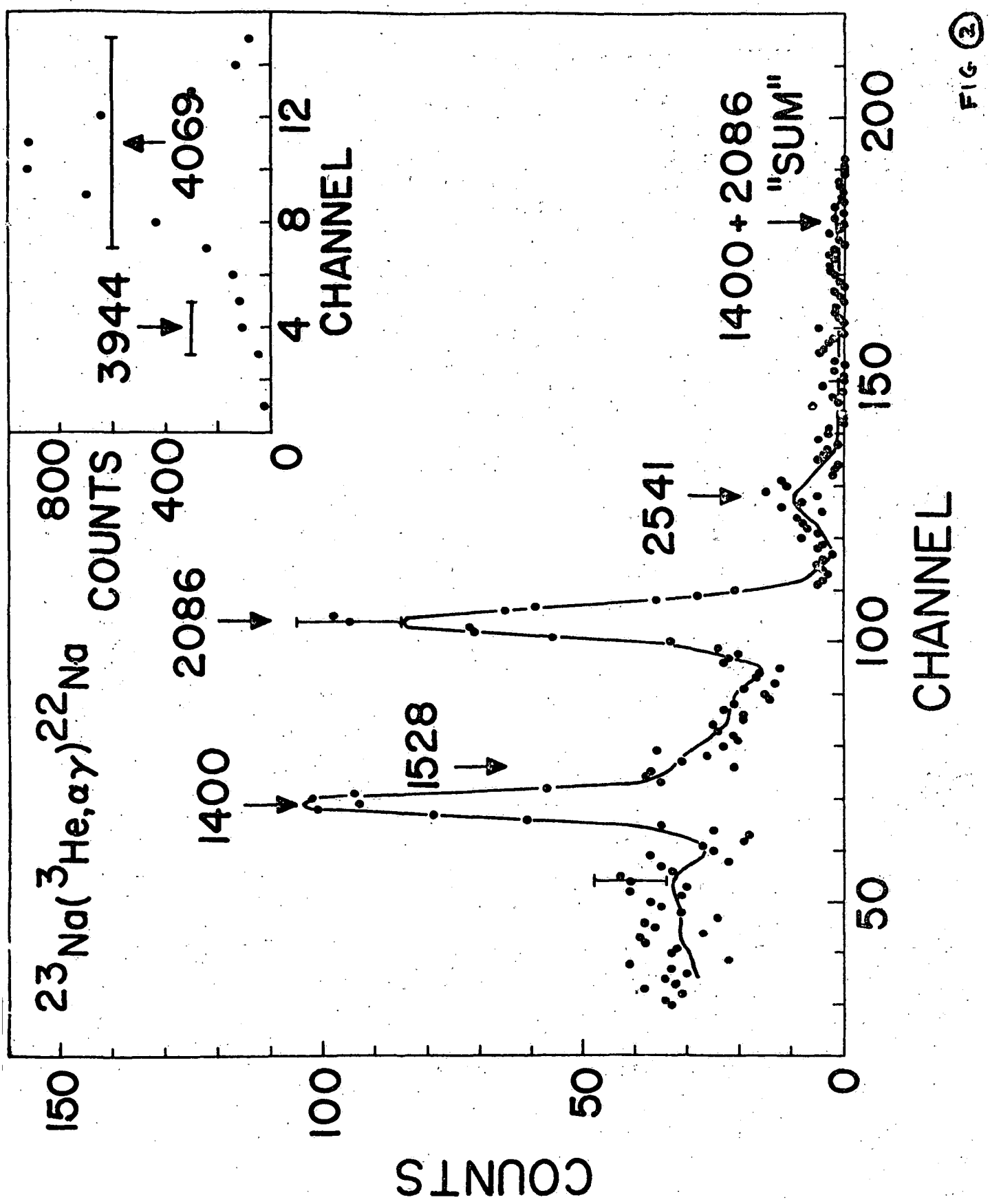
$^{23}Na(^{3}He,\alpha\gamma)^{22}Na$
COUNTS
CHANNEL
1400
1528
2086
2541
1400+2086
"SUM"
3944
4069
4
8
12
0
400
800
50
100
150
200

FIG ②

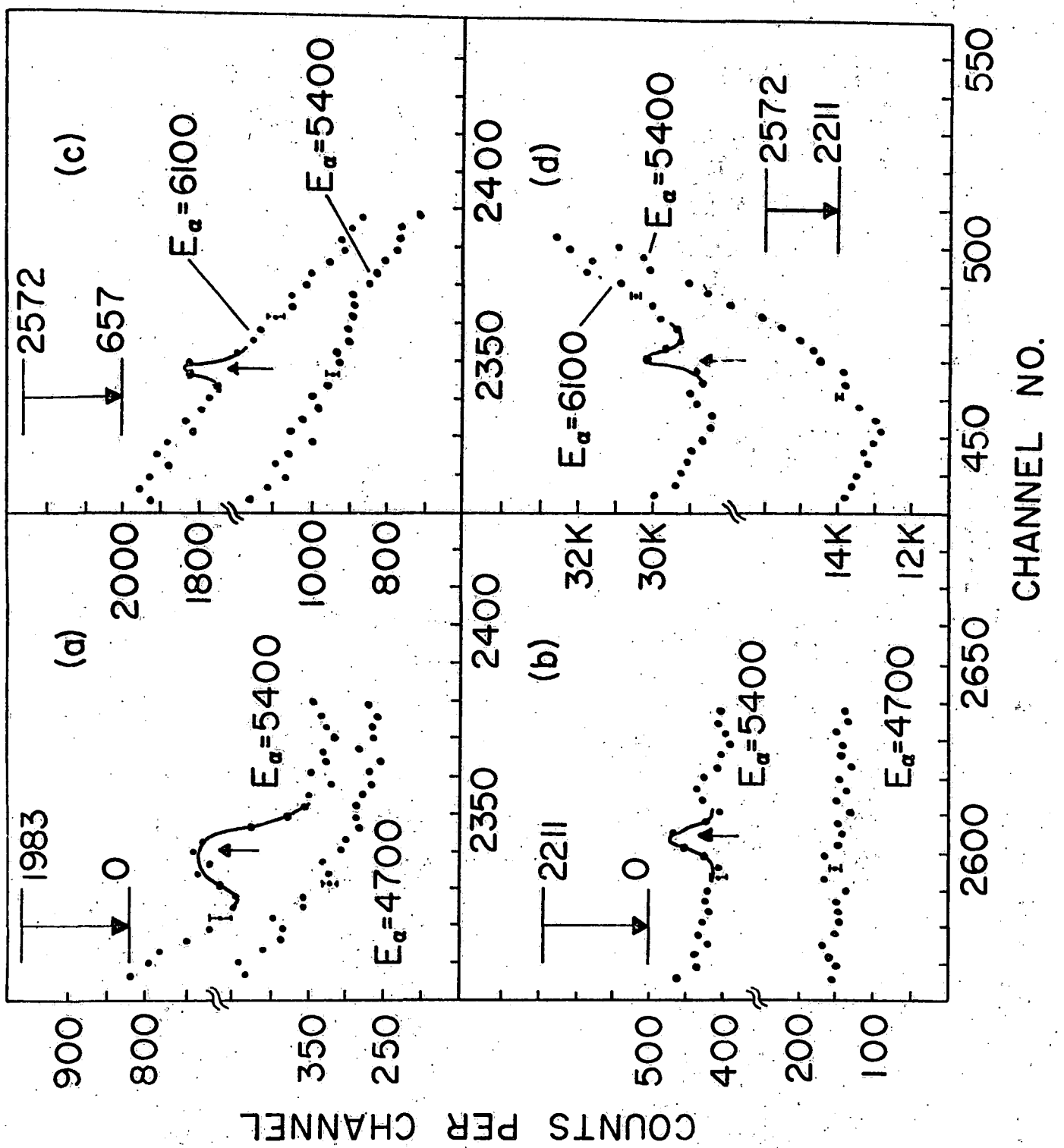
(a)
(b)
(c)
(d)
1983
0
2211
0
2572
657
2572
2211
E_α=5400
E_α=4700
E_α=6100
E_α=5400
E_α=6100
E_α=5400
E_α=5400
E_α=4700
2000
1800
1000
800
32K
30K
14K
12K
900
800
350
250
500
400
200
100
2350
2400
2600
2650
2350
2400
450
500
550
COUNTS PER CHANNEL
CHANNEL NO.

FIG (3)

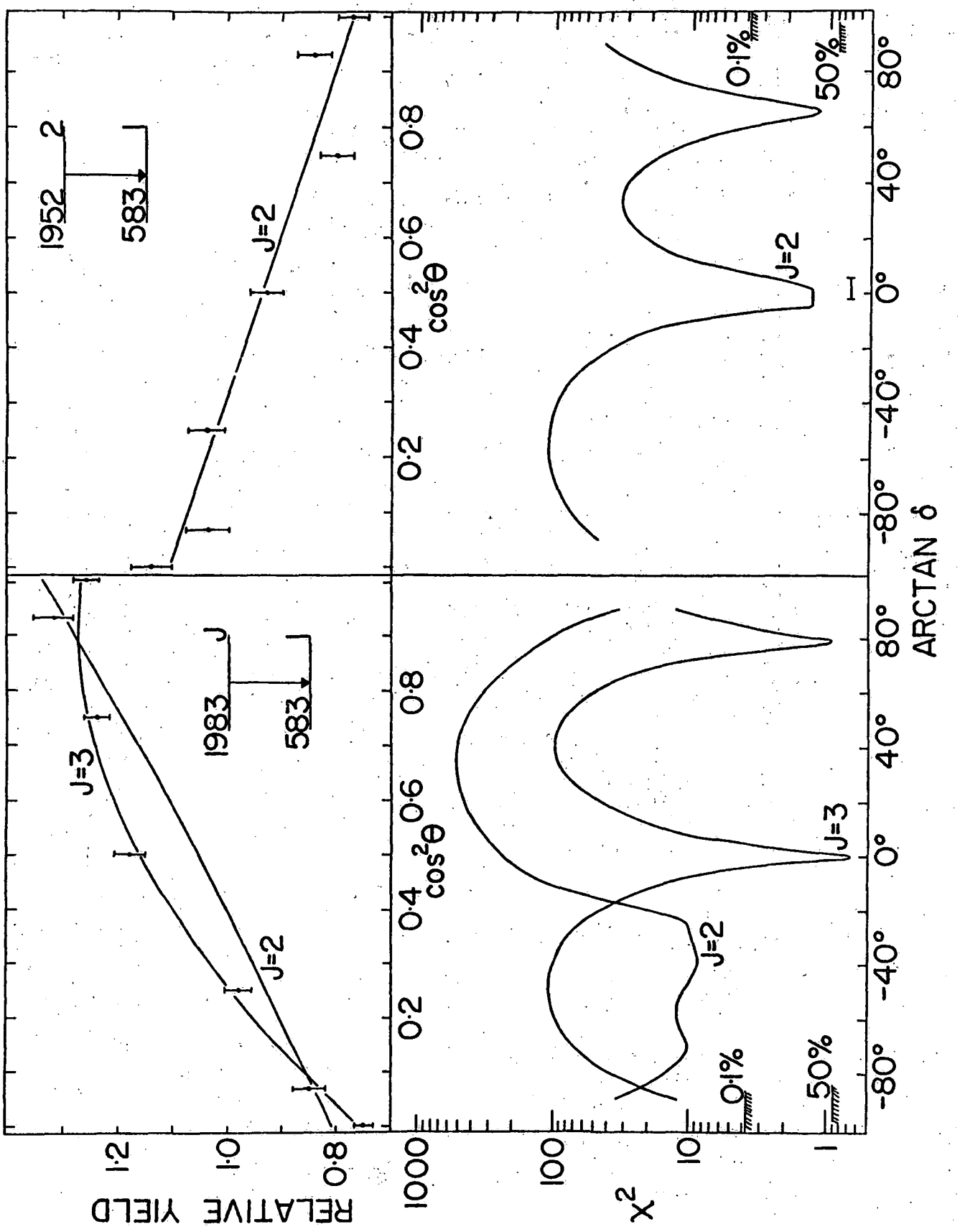
RELATIVE YIELD
1·2
1·0
0·8
1952
2
583
J=2
1983
J
583
J=3
J=2
1000
100
10
1
χ^2
0·2
0·4
0·6
0·8
$\cos^2\theta$
0·1%
50%
J=2
J=3
-80°
-40°
0°
40°
80°
ARCTAN δ
I

Fig 4

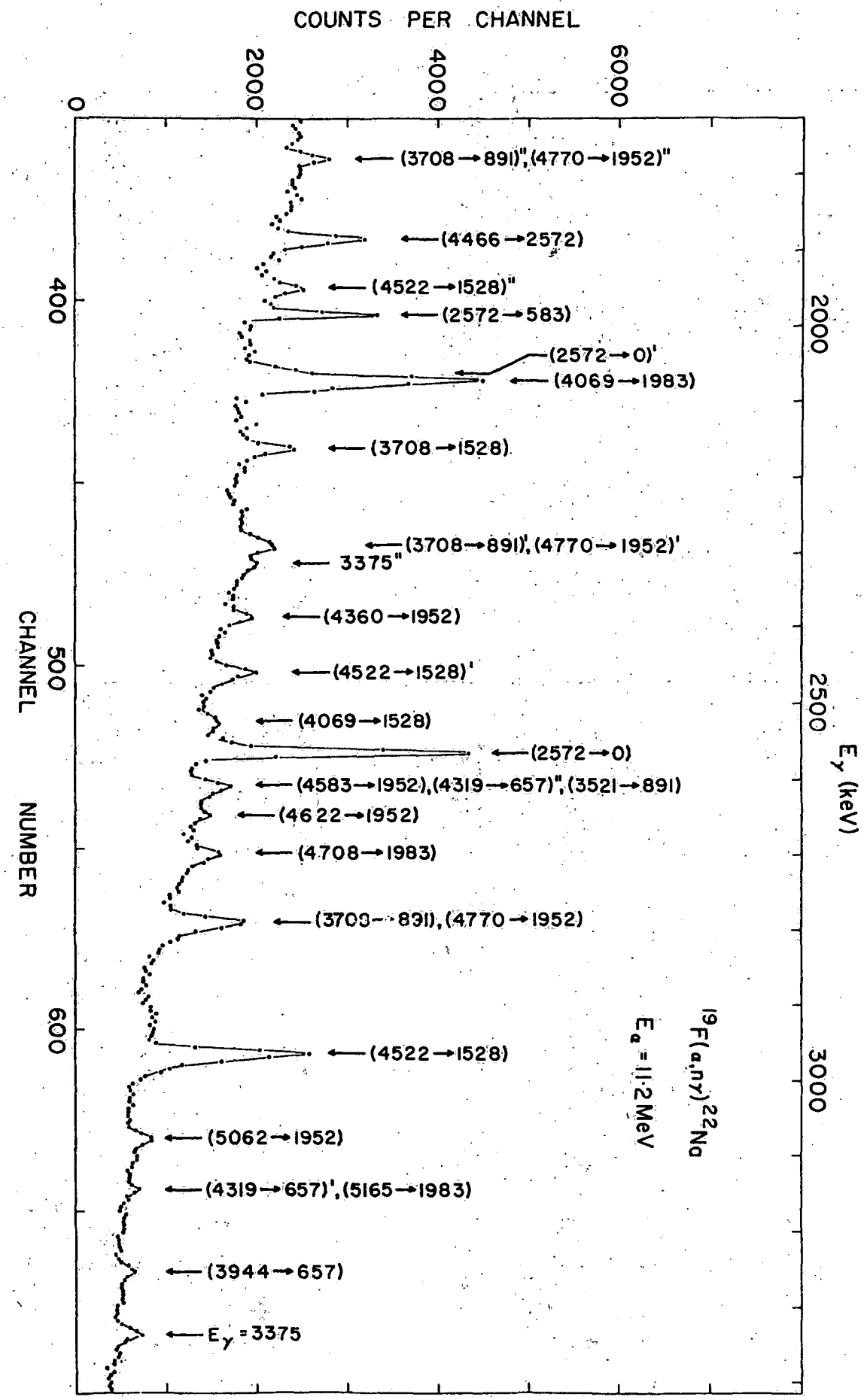
COUNTS PER CHANNEL
0
2000
4000
6000
CHANNEL NUMBER
400
500
600
E_γ (keV)
2000
2500
3000
(3708→891)", (4770→1952)"
(4466→2572)
(4522→1528)"
(2572→583)
(2572→0)'
(4069→1983)
(3708→1528)
(3708→891)', (4770→1952)'
3375"
(4360→1952)
(4522→1528)'
(4069→1528)
(2572→0)
(4583→1952), (4319→657)", (3521→891)
(4622→1952)
(4708→1983)
(3708→891), (4770→1952)
(4522→1528)
(5062→1952)
(4319→657)', (5165→1983)
(3944→657)
E_γ = 3375
E_α = 11·2 MeV
$^{19}F(\alpha,n\gamma)^{22}Na$

FIG (5)

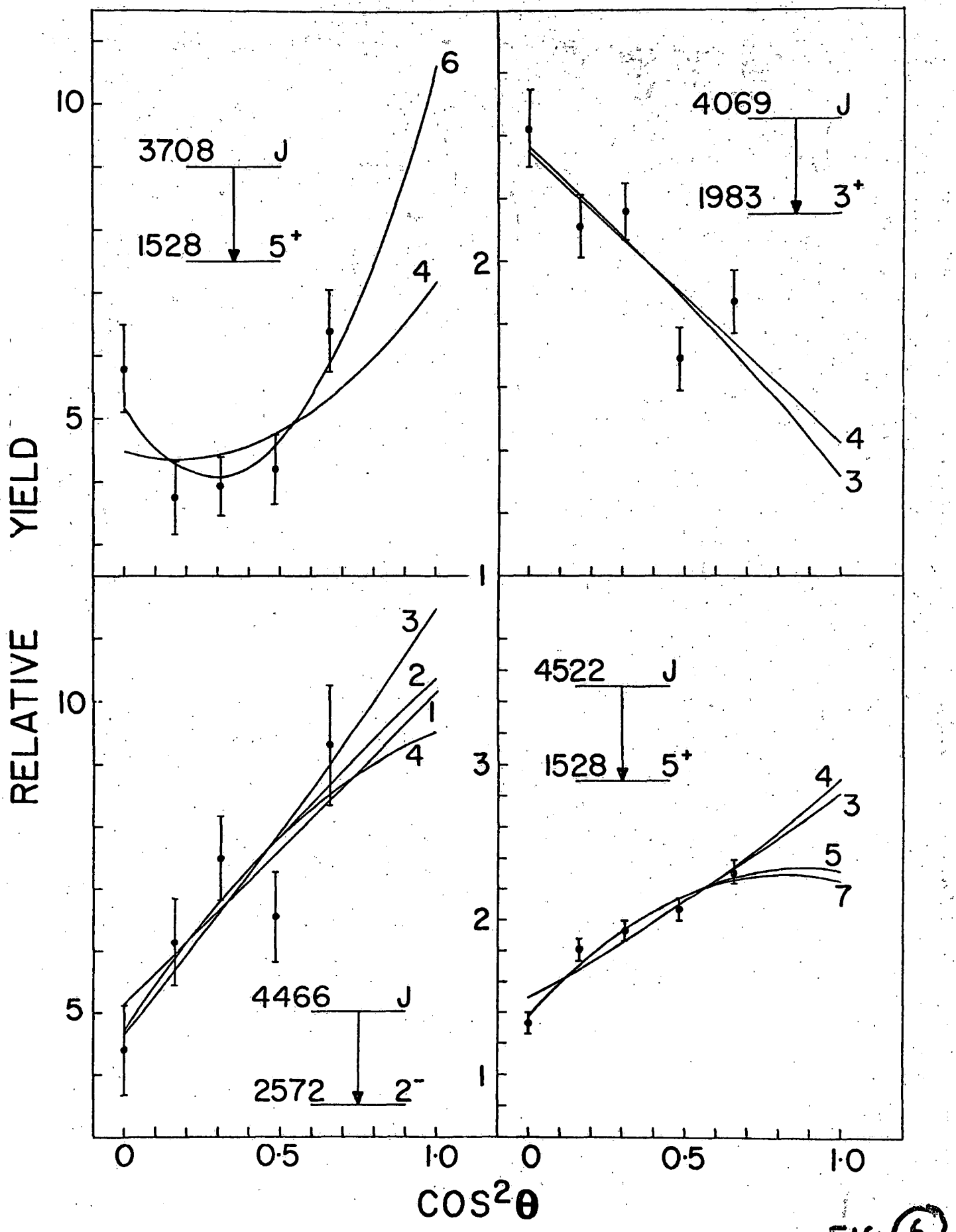
RELATIVE YIELD
10
5
2
3
1
3708 J
1528 5+
6
4
4069 J
1983 3+
4
3
4466 J
2572 2-
3
2
1
4
4522 J
1528 5+
4
3
5
7
0
0·5
1·0
COS²θ

FIG (6)

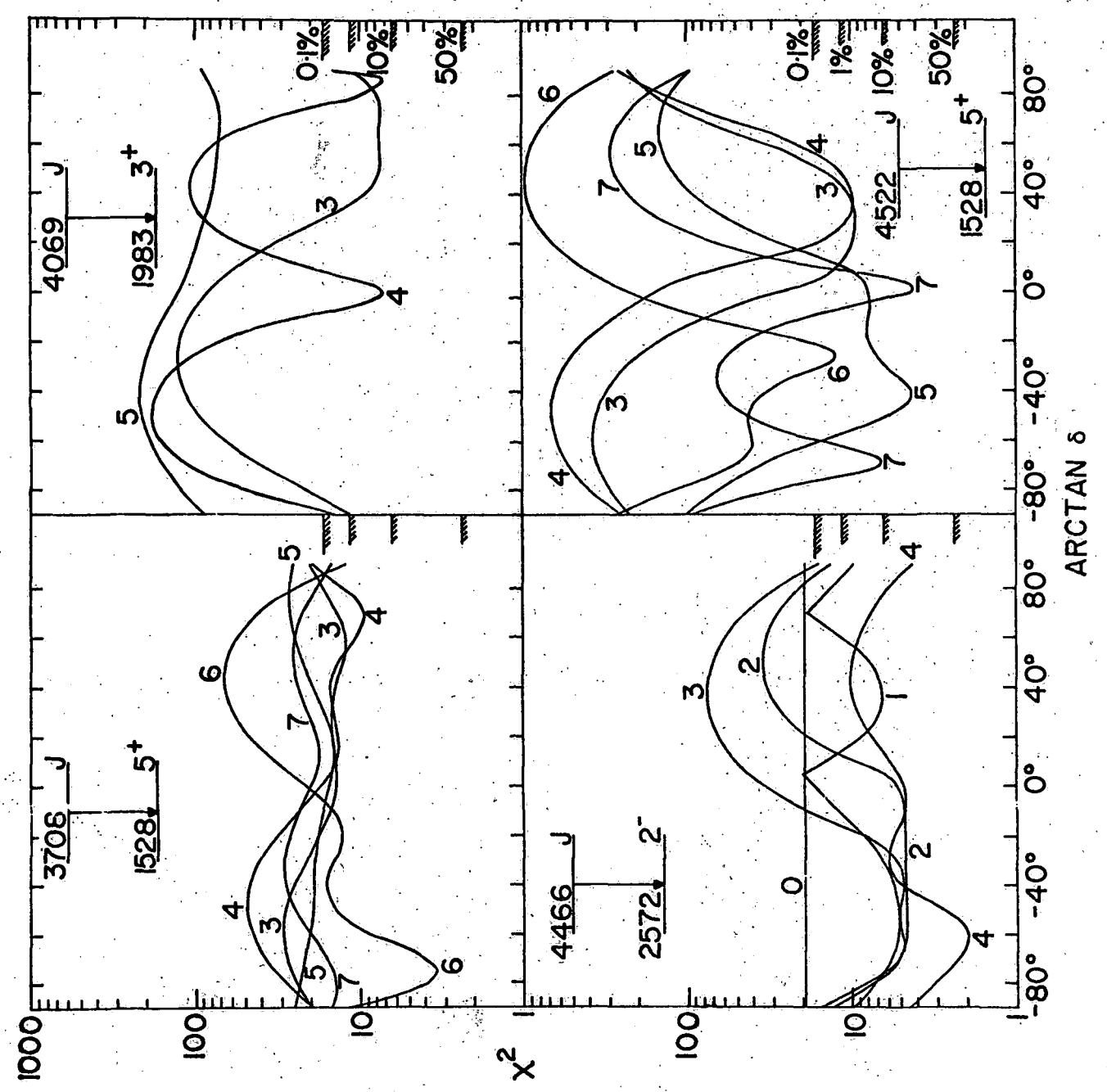
4069 J
1983 3+
3706 J
1528 5+
4466 J
2572 2-
4522 J
1528 5+
0·1%
1%
10%
50%
1000
100
10
1
χ²
-80°
-40°
0°
40°
80°
ARCTAN δ

FIG 7

(p,γ) Resonance Strengths in the s,d Shell

D. G. Sargood University of Melbourne

When we speak of measuring (p,γ) cross sections, what we are normally measuring are the resonance strengths, $(2J+1)\frac{\Gamma_p\Gamma_\gamma}{\Gamma}$, of the resonances in the compound nucleus.

This is generally done by measuring the height of the step in a thick target yield function at each resonance. The resonance strength is related to the thick target step by the formula[1)]

$$(2J+1)\frac{\Gamma_p\Gamma_\gamma}{\Gamma} = 2\left(\frac{A}{A+1}\right)^2 (2J_A+1)\,\frac{M_p E_r \varepsilon_{E_r}}{\pi^2\hbar^2}\, y(\infty\,\infty)$$

where $y(\infty\infty) = \frac{N_\gamma}{N_p} = \frac{N_\gamma'/\eta_\gamma}{Q'/e}$ is the thick target step.

In this formula, the 2 is the statistical weight of the proton,

$\left(\frac{A}{A+1}\right)^2$ is a centre of mass factor

J_A is the spin of the target nucleus

M_p is the mass of the proton

E_r is the resonance energy in the laboratory

ε_{E_r} is the atomic stopping power of the target at the resonance energy

$\frac{N_\gamma}{N_p}$ is the number of resonance decays per incident proton

N_γ' is the number of decays actually detected

η_γ is the total detection efficiency of the gamma detector

Q' is the total charge incident on the target

e is the electronics charge.

There are three quantities here which are crucially important in deducing the resonance strength from the experimentally measured step: the atomic stopping power, the detection efficiency, and the beam current integration.

An alternative method of determining resonance strengths which avoids dependence on knowledge of these three quantities has been developed by

workers at Utrecht. By means of a resonance absorption technique[2], they determine Γ and Γ_γ separately, and with the proton channel the only particle channel open put $\Gamma_p = \Gamma - \Gamma_\gamma$. The resonance strength is then built up from its separate factors, assuming the spin J is already known.

They have used the resonance absorption technique to determine the strength of the 621 keV resonance in $^{30}Si(p,\gamma)^{31}P$[3]. The method consists of bombarding a ^{30}Si target at resonance and observing the ground state gamma transition at an angle α to the incident beam, using a very finely collimated NaI detector, with a sample of ^{31}P in the collimator to act as absorber, (see figure 1 of reference[2]). After account is taken of recoil of the emitting and absorbing nuclei, and Doppler shift due to emission from a moving source, there is just one value of α for which the ^{31}P will resonantly absorb the ground state gamma ray.

The detection of gamma rays as a function of α (see figures 1 and 2 of reference[3]) shows a sharp dip, the width of which is sufficiently greater than the instrumental width for the resonance width, Γ, to be determined. (The instrumental width had been previously determined by making a similar measurement on the 771 keV resonance in $^{27}Al(p,\gamma)^{28}Si$, for which the resonance width is only 9 eV.)

This dip in the gamma ray transmission of the collimator was converted to an absorption peak, the area of which gives the ground state gamma width, Γ_{γ_o}, of the resonance, through the formula

$$A_\alpha = \int_o^\pi A(\alpha)d\alpha = \frac{\pi}{2} \frac{\Gamma}{\left(\frac{dE_\gamma}{d\alpha}\right)_r} F(n\sigma_o)$$

where A_α, the absorption integral, is the peak area

σ_o (the resonant cross section) $= 2\pi\lambda^2 \frac{2J+1}{2J_o+1} \frac{\Gamma_{\gamma_o}}{\Gamma}$

$$F(n\sigma_o) = \frac{1}{\pi} \int_{-\infty}^{\infty} \left(1 - \exp \frac{-n\sigma_o}{1+x^2}\right) dx$$

n is the number of absorber atoms per cm^2 in the collimator.

Since Γ is already found, measurement of A_α is effectively measurement of $F(n\sigma_o)$. A graph of $F(n\sigma_o)$ against $n\sigma_o$ is given in figure 3 of reference[3], using which one can then find $n\sigma_o$, and hence Γ_{γ_o}. From known branching ratios one then gets Γ_γ and the determination of resonance strength is complete, without recourse to a knowledge of any of the three quantities on which the thick target step method depends

This method is very limited in its applicability, since it requires a resonance with measurable width and a strong ground state gamma decay mode. It has been applied to only two resonances: at 621 keV in $^{30}Si(p,\gamma)^{31}P$ and at 1966 keV in $^{26}Mg(p,\gamma)^{27}Al$[4], both measurements being made by the Utrecht group.

To enable the use of the $^{30}Si(p,\gamma)^{31}P$ measurement as a standard, the Utrecht workers have determined a set of relative strengths across 16 nuclei in the s,d shell by comparing thin target yields from chemical compounds targets containing two of the nuclei to be compared[5], a method for which an accurate knowledge of the chemical composition of the targets is crucial. Their network of comparisons (see figure 3 of reference[3]) is overdetermined and shows a high degree of internal consistency, and excellent agreement with the resonant absorption measurement on $^{26}Mg(p,\gamma)^{27}Al$.

However, the Untrecht values are in general disagreement with very careful work on thick target step yields made with elemental targets at Caltech[6] and similar measurements either made with elemental targets or referred to measurements on elemental targets at Melbourne[7,8]. These results are shown below.

$(2J+1)\frac{\Gamma_p\Gamma_\gamma}{\Gamma}$ (eV): Comparison of Results

Reaction	Resonance Energy (keV)	Utrecht	Caltech	Melbourne	Toronto
$^{23}Na(p,\gamma)^{24}Mg$	512	1.05±0.16		0.85±0.18	
$^{27}Al(p,\gamma)^{28}Si$	633	5.3 ±0.8	3.1±0.4	3.16±0.33	
$^{31}P\ (p,\gamma)^{32}S$	642	0.52±0.08	0.23[b]	0.25±0.03	
$^{30}Si(p,\gamma)^{31}P$	621	3.10±0.26[a]	3.93±0.40		
$^{26}Mg(p,\gamma)^{27}Al$	1966	5.7 ±0.8 5.6 ±1.8[a]	9.7 ±1.6		
$^{24}Mg(p,\gamma)^{25}Al$	823	0.52±0.08	0.89±0.13[c]		0.98±0.15

a) Resonance absorption measurements

b) Unpublished

c) Deduced from $^{26}Mg(p,\gamma)^{27}Al$ result, using Utrecht value for ratio

Recently a new measurement of the strength of the 823 keV resonance in $^{24}Mg(p,\gamma)^{25}Al$ has been made at Toronto[9] by comparing the step in a thick target yield function with the yield of protons in Rutherford scattering. The effect of referring the measurement to the Rutherford scattering yield is essentially to remove the atomic stopping power from the calculation, and it also reduces the dependence on absolute beam current integration by requiring only the ratio of the charges collected in the two measurements, as shown by the second of the two following formulae.

Rutherford scattering gives

$$\epsilon_{E_r} = \frac{\Delta_{E_r} \frac{Q}{e} \left(\frac{d\sigma_R}{d\Omega}\right)_{E_p\theta}}{\left(\frac{dN_{scatt}}{d\Omega}\right)_{E_p\theta}}$$

where ϵ_{E_r} is the stopping power at the (p,γ) resonance energy

Δ_{E_r} is the target thickness in energy units at the (p,γ) resonance energy.

Q is the total incident charge in the Rutherford scattering measurement, which is made off resonance

$\frac{d\sigma_R}{d\Omega}$ is the calculated Rutherford scattering cross section

$\frac{dN_{scatt}}{d\Omega}$ is the observed yield of scattered protons

The thick target step expression then becomes

$$(2J+1)\frac{\Gamma_p\Gamma_\gamma}{\Gamma} = 2\left(\frac{A}{A+1}\right)^2 (2J+1) \frac{M_p E_r}{\pi^2\hbar^2} \frac{N'_\gamma}{\gamma} \Delta_{E_r} \frac{Q}{Q'} \frac{\left(\frac{d\sigma_R}{d\Omega}\right)_{E_p,\theta}}{\left(\frac{dN_{scatt}}{d\Omega}\right)_{E_p,\theta}}$$

The Toronto value is in agreement within quoted errors with the Caltech result, but in serious disagreement with Utrecht.

Since the Caltech, Melbourne, and Toronto values are all the result of thick target yield measurements, and are all in good agreement, the possibility is very real that the disagreements are not just disagreements between different laboratories but are disagreements between two basically different methods of measuring the same thing. If this be the case, then, until the differences are resolved, I think we must regard all (p,γ) resonance strengths as suspect.

REFERENCES

1) H.E. Gove, Nuclear Reactions, Vol. 1, Ch. VI; ed. P.M. Endt and M. Demeur (North-Holland Publ. Co. Amsterdam, 1959).

2) P.B. Smith and P.M. Endt, Phys. Rev. 110 (1957), 397.

3) P.B. Smith and P.M. Endt, Phys. Rev. 110 (1958), 1442.

4) C. Van der Leun and N.C. Burhoven Jaspers, Nuc. Phys. 88 (1966), 235.

5) G.A.P. Engelbertink and P.M. Endt, Nuc. Phys. 88 (1966), 12.

6) P.B. Lyons, J.W. Toevs and D.G. Sargood, Nuc. Phys. A130 (1969), 1.

7) Z.E. Switkowski, R. O'Brien, A.K. Smith and D.G. Sargood, University of Melbourne internal report UM-P-74/24.

8) R. O'Brien, Z.E. Switkowski, A.K. Smith, and D.G. Sargood, University of Melbourne internal report UM-P-74/25.

9) H. Trautvetter, Ph.D. Thesis, Toronto, (1973).

De-excitation gamma rays following Photo-disintegration of ^{27}Al and ^{19}F.

J. E. M. Thomson
School of Physics, Melbourne University

This paper presents the results of experiments in which de-excitation gamma rays following photo-disintegration have been observed. The giant resonance of the target nucleus is excited with E1 photons and decays by emitting a nucleon. The residual nucleus is left in either the ground state or low lying excited state. It is the prompt de-excitation gamma rays from these low lying excited states that we have been observing with high resolution germonium detectors.

We wanted to determine the change in the population of a residual state as a function of energy of the giant resonance state in the target nucleus. To obtain this information, measurements of the de-excitation spectrum were made for a series of different bremsstrahlung tip energies. From the relevant peak areas the strength or "yield" of a given de-excitation gamma ray was determined as a function of bremsstrahlung tip energy. The cross section for neutron reaction leading to this residual state was then computed from this yield data by using the Penfold-Leiss yield curve analysis technique. Because of the relatively poor statics and very limited number of yield points the resulting cross sections have rather poor resolutions. None the less, our results indicate the general shape of the true cross sections as a function of excitation energy.

Aluminium

Figure 1 shows the de-excitation gamma ray spectrum following photo-disintegration of ^{27}Al. Table 1 lists the deduced energy integrated cross sections. It should be noted that whenever a level in ^{26}Mg is populated so is its T=1 analogue in ^{26}Al. The cross section for veaction to the 3.587 MeV and 6.129 MeV levels in ^{26}Mg have been shown in brackets. This is because both these levels have cascade gamma rays of the same energy. Hence it cannot be established which of these levels is being populated or whether both are. Note also that in general the (γ,p) cross sections are larger than the corresponding (γ,n) cross sections. This appears to be a general property of the light nuclei. Attempts have been made to explain this phenomena in self conjugate nuclei by allowing isospin mixing in the Giant resonant states. However, there appears to be no satisfactory explanation for this phenomena for the light nuclei in general.

In the shell model discription of the ^{27}Al ground state the major component has 11 nucleon in the $d_{5/2}$ shell. This is born out experimentally by the fact that pickup reactions attribute nearly all their strength to the transfer of an $l=2$ nucleon. (Refs. 1 & 2).

Direct nucleon pickup neutrons on ^{27}Al result in states of ^{26}Mg and ^{26}Al. The results of these experiments tell us the population of residual states when a $d_{5/2}$ nucleon is plucked out of ^{27}Al. If we propose a giant resonance excitation mechanism which involves the excitation of a single nucleon, it will be a $d_{5/2}$ nucleon which is excited. Furthermore, if the excited nucleon is emitted with little further interaction with the nucleus the population of residual states following the photo-neutron should be similar to the $d_{5/2}$ nucleon pickup spectroscopic factor.

Table 2 shows a comparison between our results and the spectroscopic factors for levels in ^{26}Mg. Note that not only are the same levels populated but there is also a fair agreement in magnitude. The one exception is the weak population of the 3.587 MeV level, but as pointed out, an ambiguity exists in our assignment here. The pickup work[1] could not resolve which of the levels at 4.3 MeV were being populated. We would suggest that it is the 4+ level at 4.320 MeV that has the major portion of the pickup strength.

On the right of the table we have the spectroscopic factors from the shell model calculation of Wildenthal et al (ref. 3.). The calculation works quite well for the strongly populated levels. It is quite specific about predicting a large spectroscopic factor for a 4+ level at about 4.3 MeV in ^{26}Mg. This is in agreement with our results insofar as it is a 4+ level at this energy that we see most strongly populated.

Table 3 shows a comparison between our results and the spectroscopic factors from neutron pickup. Again the correlation is quite good with the exception of the level at 1.76 MeV. Why we get disagreement solely for this level is not at all clear. Note the reasonably strong population of the 4+ level at 4.711 MeV in ^{26}Al, this state being the analogue of the 4+ level at 4.32 MeV in ^{26}Mg. The shell model calculation[3] again predicts a large spectroscopic factor for a 4+ level at about this energy in ^{26}Al.

Overall it would appear that we have established fairly good correlation between the reported integrated cross sections and the spectroscopic factors determined from nucleon pickup.

Figure 2 shows the deduced cross sections as a function of energy. A smoothed version of the total (γ,n) cross section is shown for comparison in the top right. The most significant feature about the cross sections to various residual states is that they do not differ dramatically from that of the total (γ,n) reaction. This is consistent with the proposed model in so far as any gaint resonance state is formed via the excitation of a single $d_{5/2}$ nucleon and that the population of residual states is solely by the spectroscopic break-up of the additional $d_{5/2}$ hole amongst the residual states.

Fluorine

The study of ^{19}F is interesting because of the fairly strong photo-alpha reactions leading to the positive parity states at 5.3 MeV in ^{15}N. Table 4 shows the integrated cross section for neutrons to various residual states. The the left is shown the results of other experiments.

The integrated cross section up to 29 MeV the ratio of (γ,p) reaction to (γ,α) reaction is about 10 to 1. In contrast, the integrated cross section to 14 MeV of Shikazono et al[5] gives the (γ,p) and (γ,α) reaction roughly equal strengths. This suggests that whereas the (γ,α) reaction is small compared to the total (γ,p) reaction, integrated up to 29 MeV, at lower energies they become comparable in size.

Figure 3 shows the deduced cross section as a function of excitation energy. As anticipated the (γ,p) cross sections to states in ^{18}O have their strength spread throughout the whole giant resonance region whereas (γ,α) reaction have their strength limited to a fairly narrow resonance accuring at 16 MeV.

The overall large size of these (γ,α) reactions suggests an electric dipole phenomena. One possible process would be the direct excitation of an alpha particle cluster present in the ^{19}F ground state. In other words the photon is absorbed through the dipole moment set up by the effective charge of the alpha cluster. The effective charge of the alpha particle is given by $\varepsilon = \frac{2(N-Z)}{A}$. An order of magnitude calculation using this effective charge would suggest that this process is far too weak to account for the observed (γ,α) strength.

An alternative mechanism that should be considered is that the reaction proceedes via the excitation of a single nucleon. The particle-hole state so formed is sufficiently long lived so as to allow further interactions within the nucleus and the subsequent emission of an alpha particle.

To zero order ^{19}F may be considered as a closed ^{16}O core with an additional 3 nucleons in the $d_{5/2}$ orbital. The reaction may proceed by the promotion of a single nucleon from the $1p_{1/2}$ shell to the 2s-1d shells. Before the excited nucleon can be emitted it interacts strongly with the 3 remaining nuclei in the $1p_{1/2}$ shell. An alpha group is formed and emitted. The residual nuclei is left having a configuration of four holes in the $1p_{1/2}$ shell and 3 particles in the $1d_{5/2}$ shell. Such a 3-particle-4 hole configuration is required to describe the positive parity states in ^{15}N which are seen to be strongly populated following the photo-alpha neutron (ref. 6.). Detailed calculations on the basis of this model are underway in this department, but as yet no conclusions can be drawn as to its validity.

References

1. R.R. Betts and H.T. Fortuna, Phys. Rev. C8 (1973) 670.

2. G.J. Wagner, G. Mairle, U. Schmidt-Rohr and P. Turoek, Nuc. Phys. A125 (1969) 97.

3. B.H. Wildenthal, J.B. McGrony, E.C. Halbert, and P.W.M. Glaudemans, Phys. Letts. 26B (1968) 692.

4. B.J. Thomas, A. Buchnea, J.P. Irish and K.G. McNeil, Canadian Jour. Phys. 50 (1972) 3085.

5. N. Shikozono and Y Kawaraski, Nuc. Instr. and Meth. 92 (1971(349.

6. A.P. Zuker, B. Buch and J.B. McGrony, Phys. Rev. Letts. 21 (1968) 39.

INTEGRATED CROSS SECTIONS FOR REACTIONS LEADING TO VARIOUS RESIDUALS IN ^{26}Al AND ^{26}Mg.

^{26}Mg T=1			^{26}Al		
E_x	J^π	$\int^{24}\sigma(\gamma p\gamma')dE$ Mev-mb/sr	E_x	$J^\pi;T$	$\int^{24}\sigma(\gamma,n,\gamma')dE$ Mev.-mb/sr.
			1.759	2^+	0.36±0.07
			1.850	1^+	0.05
			2.069	3	0.17
1.809	2^+	2.00±0.3	2.070	$2^+T=1$	0.92±0.3
			2.072	1	N.O.
			2.365	3^+	0.50±0.1
			2.545	3^+	0.60±0.1
			2.661	$2^+,3^+$	0.17±0.04
2.939	2^+	0.74±0.15	3.159	$2^+T=1$	0.38±0.05
			3.405	5^+	0.09±0.04
3.587	0^+	(0.32±0.1)	3.745	$0^+T=1$	N.O.
4.320	4^+	1.47±0.2	4.710	$(4^+T=1)$	0.32±0.05
4.333	(2^+)	< 0.25			
4.350	(3^+)	0.74±0.2			
4.835	(2^+)	0.63±0.1			
4.901	$(2,3,4)^+$	0.23			
6.129	(2^+)	(0.37±0.13)			

All cascades from observed states have been taken into account.

TABLE 1.

A COMPARISON BETWEEN LEVELS POPULATED IN ^{26}Mg FOLLOWING PHOTO-PROTON EMISSION FROM ^{27}Al AND SPECTROSCOPIC FACTORS FROM PROTON PICKUP ON ^{27}Al.

^{26}Mg (T=1) E_x MeV. (a)	J^π	$\int^{24} \sigma(\gamma p \gamma')dE$		C^2S $^{27}Al(d,^3He)$ (b)	C^2S Shell Model (c) (d5/2 -2s½)
1.809	2^+	.92 **		.92	.75
2.939	2^+	.32		.19	.29
3.587	0^+	(.15)		.01	-
3.942	3^+	N.O.		.01	-
4.320	4^+	.69	1.15	1.92	1.8 (4^+)
4.333	(2^+)	.12			
4.350	(3^+)	.34			
4.835	2^+	.28	.37	.36	.02
4.910		.09			
5.292	(2^+)	N.O.		—	
6.125	(2^+)	(.18)		.12	

(a) Selin & Hardell $^{25}Mg(n,\gamma)$ Nuc. Phys. A139 (1969) 375.

(b) Wagner et al. Nuc. Phys. A125 (1969) 97

(c) Wildenthal et al. Phys. Lett. B26 (1968) 692

** Normalized Here.

TABLE 2.

A COMPARISON BETWEEN LEVELS POPULATED IN ^{26}Al FOLLOWING PHOTO-NEUTRON EMISSION FROM ^{27}Al AND SPECTROSCOPIC FACTORS FROM NEUTRON PICKUP ON ^{27}Al.

^{26}Al E_x (a)	J^π	$\int\sigma(\gamma,\gamma')dE$ Not Observable	C^2S (a) ^{27}Al (^3He,) L=2	L=0	C^2S (a) Nilsson	C^2S (b) Shell Model
0.228	0^+ T=1		0.14			
0.418	3^+			0.12		
1.058	1^+		0.31			
1.759	2^+	0.19	0.02	0.01		
1.850	1^+	0.03	0.02			
2.069	4^+	0.09				
2.070	2^+ T=1	0.50**	0.50		0.30	0.38
2.072	1^+	-				
2.365	3^+	0.27	0.26		0.13	
2.545	3^+	0.32	0.30			
2.661	$(2,3)^+$	0.09	-			
2.740	1^+	-	-			
2.913		-	-			
3.074		-	-			
3.159	2^+ T=1	0.21	0.10			0.14
3.405		0.05	0.08			
3.507		-	-			
3.594	$(2,3)^+$	-	-			
3.675	$(2,3)^+$	-	0.14	0.01		
3.719		-	-	-		
3.745	0^+ T=1	-	0.02	0.02		
3.918		-	-	-		
3.960		-	0.08	0.03		
⋮						
4.711	(4^+)T=1	0.17	0.86		0.04	0.90

(a) Betts, Fortuna and Pullen. Phys. Rev. C8(1973) 670

(b) Wildenthal *et al*

** Normalized here.

TABLE 3.

INTEGRATED CROSS SECTIONS FOR PHOTO-DISINTEGRATIONS OF ^{19}F LEADING TO EXCITED RESIDUAL STATES

^{19}F (γ,n) $^{18}F^*$ E_x	J^π	$^{29}\int \frac{d\sigma}{d\Omega} dE$ MeV-mb/sr. This Work	$^{25}\int \frac{d\sigma}{d\Omega} dE$ MeV-mb/sr. Thomas et al	$^{14}\int \frac{d\sigma}{d\Omega}$ Rel.Unit Shikazono Kawarsak
0.936	3^+	1.17 ±0.4	1.25	
1.04	0^+	1.0±0.3	0.45	
1.08	0^-	0.28±0.15	-	
3.059	2^+	weak	-	
3.135	1^-	weak	-	
^{19}F (γ,p) $^{18}O^*$				
1.98	2^+	1.8±0.2	1.75	158±10
3.63	0^+	0.93±0.2	0.90	38±11
3.92	2^+	weak	-	20±10
4.448	3^-	<0.2	-	
^{19}F (γ,α) $^{15}N^*$				
5.27	$(5/2)^+$	$0.095^{+0.03}_{-0.06}$	-	71±2
5.27+5.29	$(\frac{1}{2}^+ + 5/2^+)$	0.333±0.13	0.75	184±6

All observed cascades taken into account.

TABLE 4.

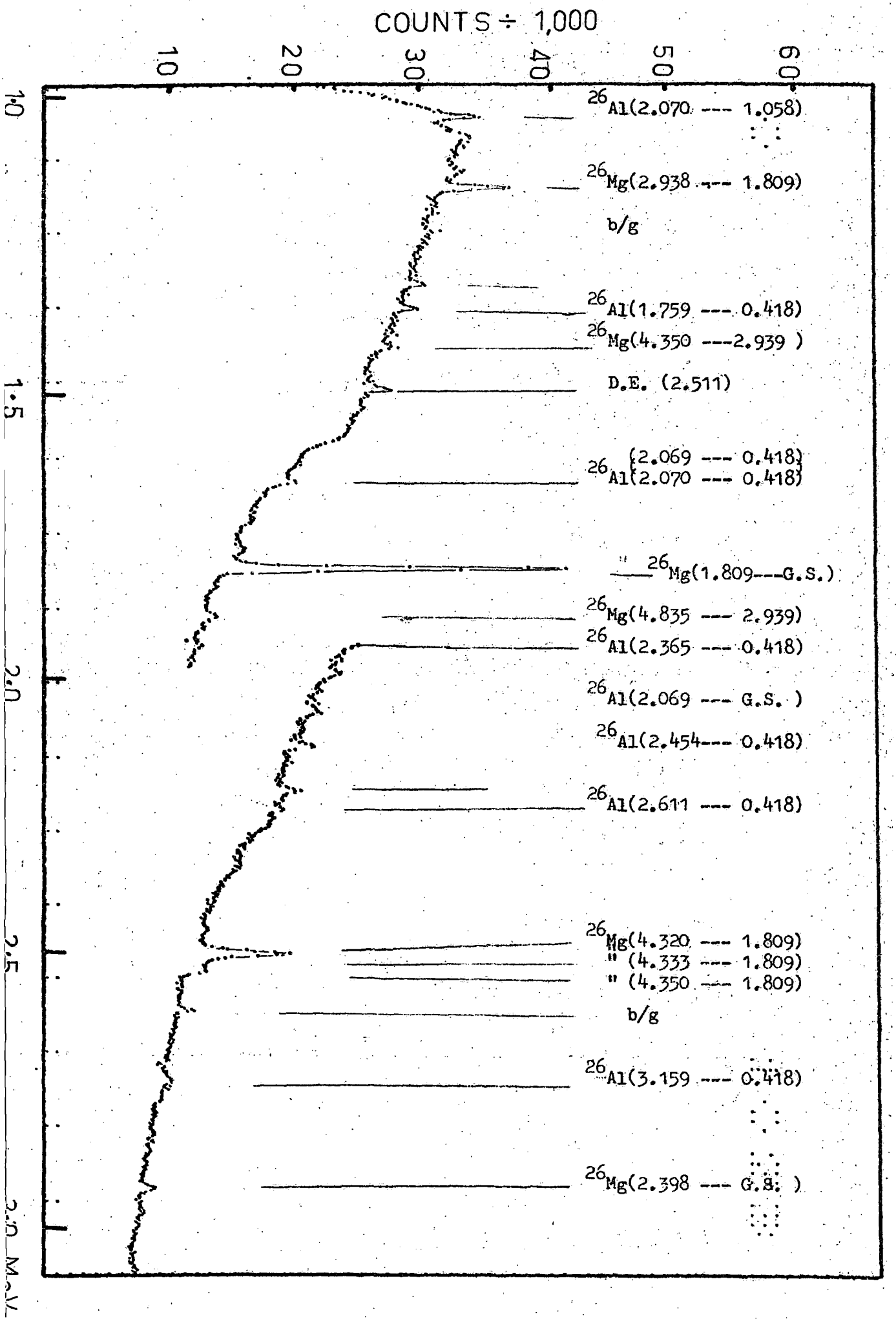
COUNTS ÷ 1,000
10
20
30
40
50
60
1.0
1.5
2.0
2.5
3.0 MeV
^{26}Al(2.070 --- 1.058)
^{26}Mg(2.938 --- 1.809)
b/g
^{26}Al(1.759 --- 0.418)
^{26}Mg(4.350 ---2.939)
D.E. (2.511)
(2.069 --- 0.418)
^{26}Al(2.070 --- 0.418)
" ^{26}Mg(1.809---G.S.)
^{26}Mg(4.835 --- 2.939)
^{26}Al(2.365 --- 0.418)
^{26}Al(2.069 --- G.S.)
^{26}Al(2.454--- 0.418)
^{26}Al(2.611 --- 0.418)
^{26}Mg(4.320 --- 1.809)
" (4.333 --- 1.809)
" (4.350 --- 1.809)
b/g
^{26}Al(3.159 --- 0.418)
^{26}Mg(2.398 --- G.S.)

FIGURE 1.

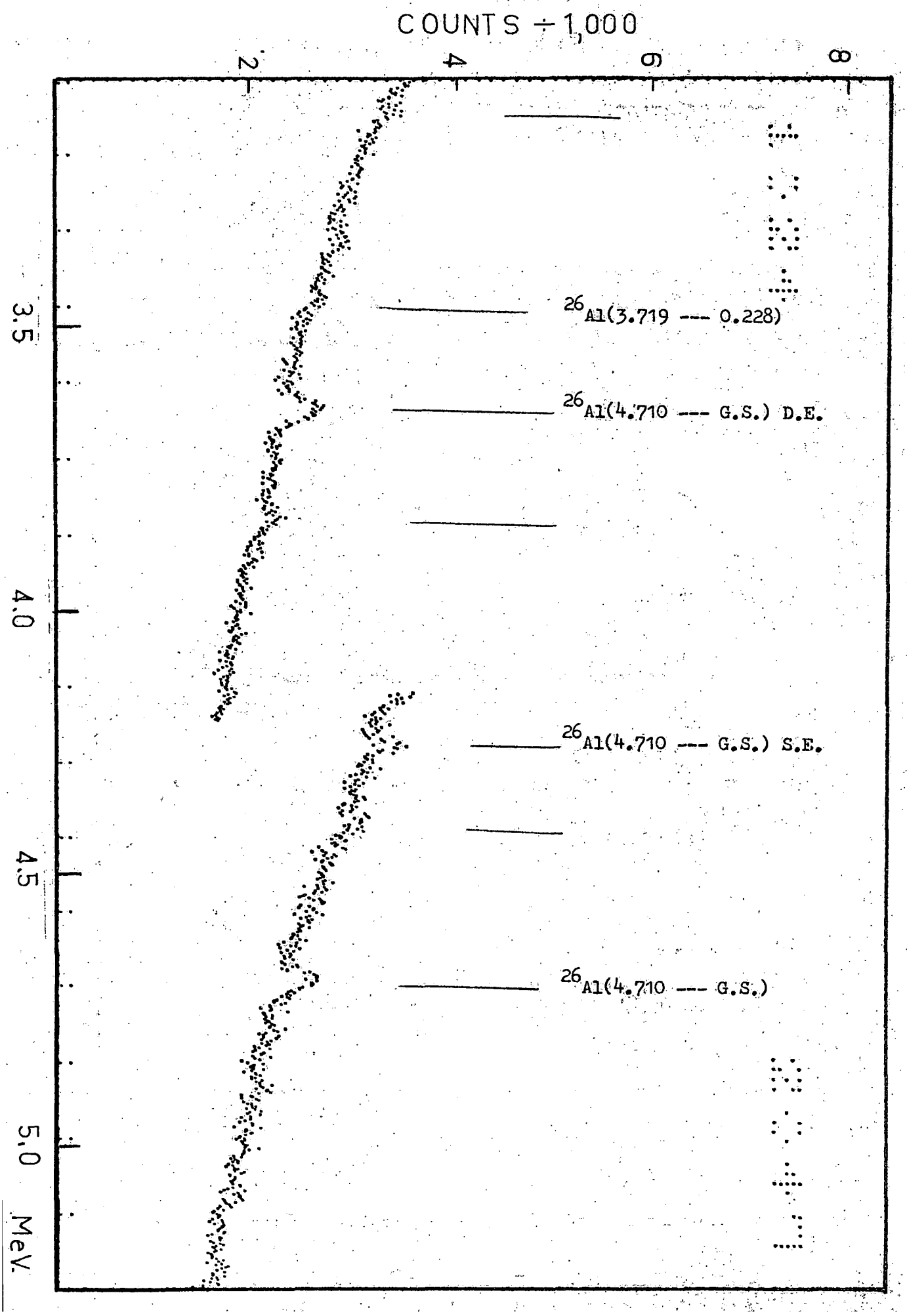

FIGURE 1 (contd.)

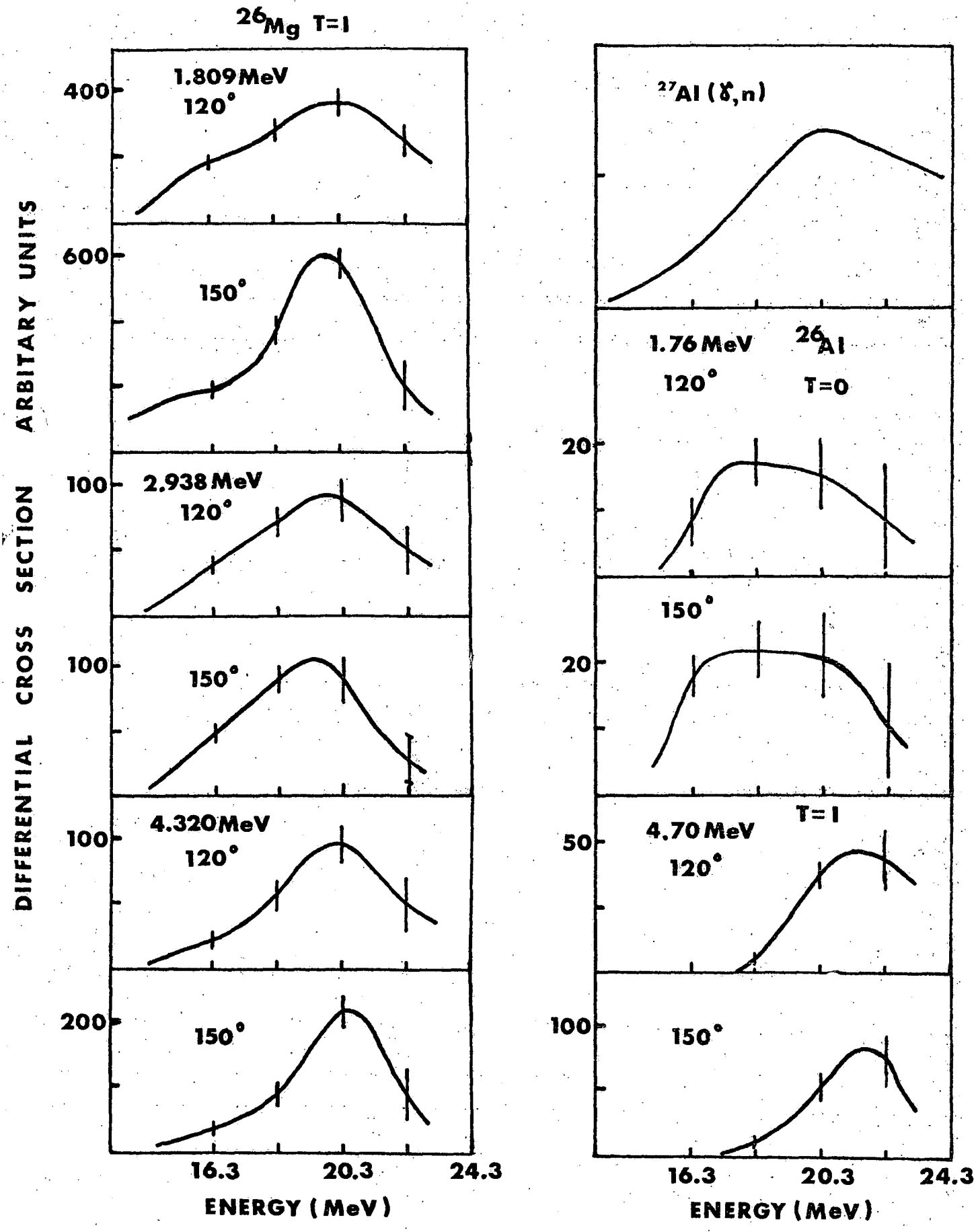
^{26}Mg T=1
1.809MeV
120°
400
150°
600
2.938MeV
120°
100
150°
100
4.320MeV
120°
100
150°
200
^{27}Al (δ,n)
1.76MeV ^{26}Al
120°
T=0
20
150°
20
T=1
4.70MeV
120°
50
150°
100
DIFFERENTIAL CROSS SECTION ARBITARY UNITS
16.3
20.3
24.3
ENERGY (MeV)
16.3
20.3
24.3
ENERGY (MeV)

FIGURE 2.

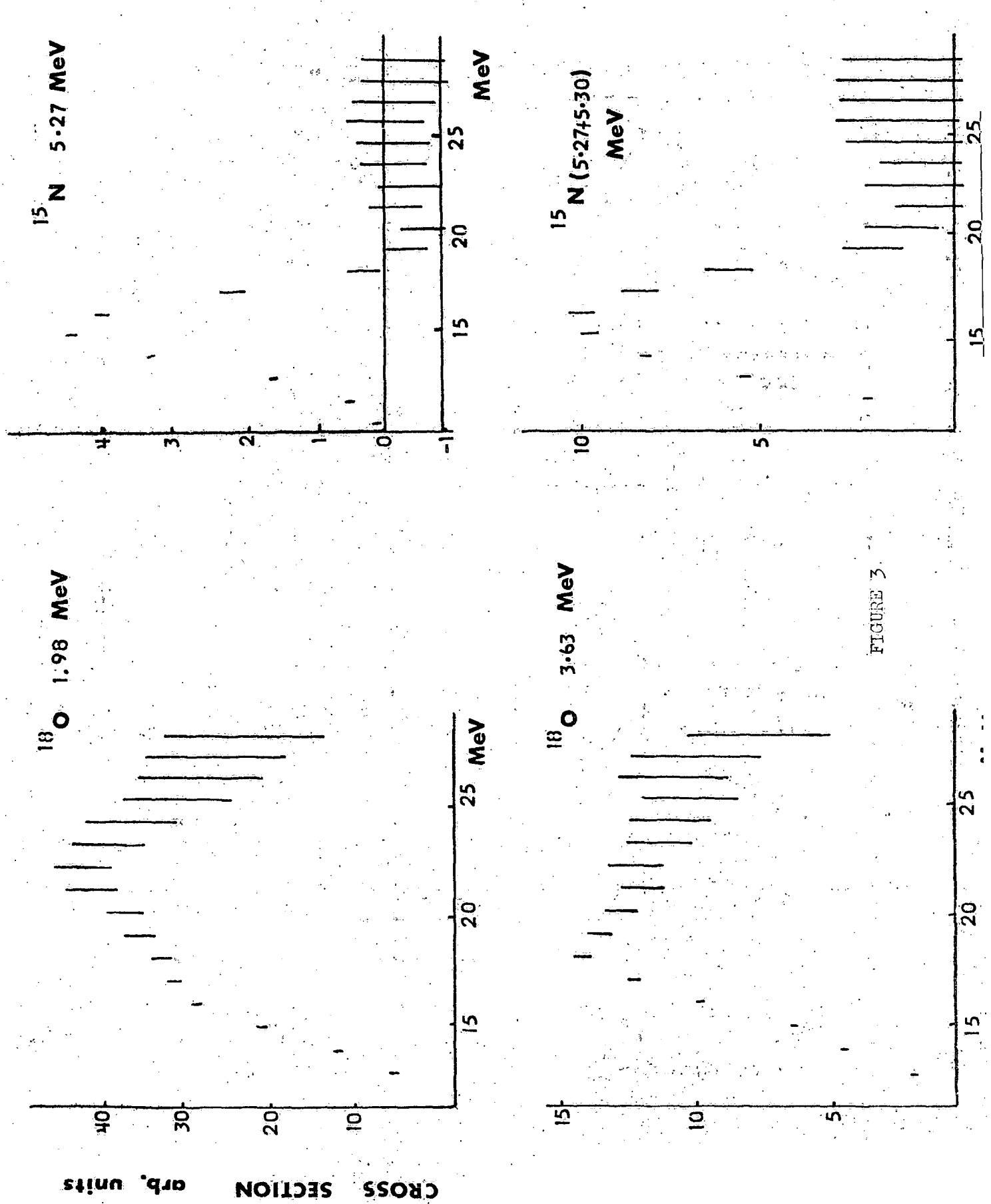
^{15}N 5·27 MeV
^{15}N (5·27+5·30) MeV
^{18}O 1·98 MeV
^{18}O 3·63 MeV
CROSS SECTION arb. units
MeV

FIGURE 3

ABSTRACTS

G. B. YANKOV (Kurchatove Atomic Energy Institute, USSR)

- Secondary Gamma-rays Emitted after Interaction of Neutrons with Air

A number of reactions such as $(n,n'\gamma)$, $(n,\alpha\gamma)$, $(n,d\gamma)$ can occur as neutrons interact with nitrogen, oxygen and hydrogen in air. Inconsistencies exist in the various cross sections leading to errors of between 50 and 100 per cent in calculation of the secondary gamma ray spectra.

B. M. SPICER (Melbourne University)

- Recent Photoneutron Cross Section Measurements

Recent precision measurements of the photoneutron cross sections of ^{45}Sc, ^{181}Ta and ^{208}Pb. Their relationship to, and interpretation in terms of inelastic scattering experiments with electrons, protons and deuterons on ^{181}Ta and ^{208}Pb targets will be discussed. The ^{45}Sc results will be discussed in terms of isospin effects.

B. ROSE, (UKAEA, Harwell)

- Non-statistical Effects in Neutron Capture in ^{93}Nb and ^{103}Rh

A search has been made by T. Haste and B. Thomas at Harwell for non-statistical effects in partial radiation widths following neutron capture in ^{93}Nb and ^{103}Rh in the neutron energy range up to about 5 keV. The only significant correlations observed have been with the widths of d-p transitions to the same final states.